PLANNING AND PROTECTING CRITICAL INFRASTRUCTURE: THREE APPLICATIONS OF OPTIMIZATION UNDER UNCERTAINTY OR VARIABILITY

A Dissertation
Presented to
The Academic Faculty

By

Amelia E. Musselman

In Partial Fulfillment
of the Requirements for the Degree
Doctor of Philosophy in the
School of Industrial and Systems Engineering

Georgia Institute of Technology

August 2017

PLANNING AND PROTECTING CRITICAL INFRASTRUCTURE: THREE APPLICATIONS OF OPTIMIZATION UNDER UNCERTAINTY OR VARIABILITY

Approved by:

Dr. Valerie M. Thomas, Advisor
School of Industrial and Systems Engineering
Georgia Institute of Technology

Dr. Dima Nazzal, Advisor
School of Industrial and Systems Engineering
Georgia Institute of Technology
Fortna R&D

Dr. Richard Li-Yang Chen
Research Science
Amazon Research

Dr. Natashia Boland
School of Industrial and Systems Engineering
Georgia Institute of Technology

Dr. Xu Andy Sun
School of Industrial and Systems Engineering
Georgia Institute of Technology

Date Approved: May 30, 2017

For my parents who have supported me throughout my education.

ACKNOWLEDGEMENTS

I would like to thank my advisors, Valerie Thomas and Dima Nazzal, without whose support and encouragement I would not have been able to complete my doctorate. They have not only been dedicated and knowledgable research advisors but also great professional mentors. I would also like to thank my committee for their helpful suggestions and ideas.

I would like to thank Richard Chen and Janson Wu, who provided the initial ideas and motivation for the network interdiction chapter of this thesis during my summer internship at Sandia National Laboratories. Janson and Richard also continued to work with me and guide me throughout my research on this problem, long after my internship was completed.

I would like to thank Natashia Boland, for her suggestions on how to improve the formulation for the wind multi-objective integer program. Additionally, I would like to thank Perry Ellis who helped convert the implementation of the wind heuristic from R to C and pointed out an error in my original way of handling the demand data.

Finally, I would like to thank Yassine Ridouane, who helped run the tests and create some of the figures for the Africa chapter of this dissertation.

TABLE OF CONTENTS

LIST OF TABLES

LIST OF FIGURES

SUMMARY

This dissertation presents the study of three strategic planning problems in the area of critical infrastructure planning and protection. Each of these problems involves real-world data that is uncertain or stochastic, and we use a range of methods to accommodate such data.

First, we consider a network interdiction problem in which an adversary seeks to maximize the damage of transporting illicit nuclear material to a selected target while the defender seeks to minimize this damage. We model the problem as a bi-level program where the adversary's goal is to maximize damage to the system while the defender seeks to minimize damage under a limited budget. Furthermore, since effectiveness of mitigation options is often difficult to assess, we take a robust optimization approach to allow for parametric uncertainty. In order to account for the combined impact of mitigation options, we consider multiple attributes: situational awareness, detection, and interdiction. We test our method on a synthetic example of the U.S. supply chain network that includes rail, air, and maritime transportation between both domestic and international locations. For this test example, we are able to achieve a large decrease in damage with a mitigation budget that is only a small percent of the cost to implement all mitigation options. This approach allows consideration of joint strengths of complementary mitigation options and can be applied to any situation in which a defender has multiple options for defending a network.

Second, we consider the problem of electrification in sub-Saharan Africa. Many people across Africa are without sufficient access to electricity. The unavailability and unreliability of electricity resources in Africa contribute to developmental challenges in many areas including business, education, and healthcare. In this research, we develop a multi-period optimization model for power generation and transmission system expansion planning in sub-Saharan Africa. Although optimization models have been developed to address power generation expansion planning in Africa they largely neglect the restricted budget for elec-

tricity development, assuming 100% of demand will be met in the near future. In order to advise development decisions under budgetary restrictions we consider a variety of electrification policies and analyze the impact of varying the fraction of demand met on the cost of power system expansion. We test our model on a case study of Rwanda and find that the electrification goals affect the cost, transmission system, and timing of construction decisions. This comprehensive approach provides richer insight into electrification choices and their consequences than existing electricity production planning models for developing countries by considering both strategic and operational planning decisions under a variety of electrification policy options.

Finally, we present a multi-objective optimization model to strategically locate wind farms to reduce the negative impact of wind variability on the rest of the power system. In order to model the impact of wind variability without explicitly modeling the highly complex structure of the full electricity generation and transmission system, we develop a metric, which we call demand deficit, that measures the load that the remainder of the system would need to account for under wind fluctuations. We aim to select a complementary set of wind sites to minimize both demand deficit and the variability in this deficit. To approach this problem we first develop two heuristics to find an approximate solution using the complete dataset and then solve the exact optimization problem for a well-selected subset of the data. We solve our model using demand data and potential wind sites for the Southwest Power Pool. We find that though demand deficit decreases monotonically as more sites are added, the variability across time initially increases then decreases. For a fixed number of sites, demand deficit and variability in this deficit are competing objectives. Unlike previous work, this framework allows us to compare demand deficit and variability trade-offs when an integer number of sites is selected.

CHAPTER 1
INTRODUCTION

Applications of optimization arise across many areas of critical infrastructure planning and protection. Furthermore, when planning for the future there is always some level of uncertainty involved and perhaps variability as well. This dissertation presents the study of three critical infrastructure planning and protection problems under an optimization framework. Two of the problems relate to power system planning. The third, although motivated by nuclear smuggling interdiction, could be adapted to electricity transmission network security. Additionally, each of these problems exhibit some level of uncertainty or variability in the real-world data used. The following sections introduce each of the three problems and contributions made in this work.

1.1 Chapter 2: Robust Network Interdiction Considering Multi-Attribute Defense Options

Despite many beneficial uses of radiological and nuclear materials, advances in this area have carried a specter of dangerous and evolving risks. Rapid globalization in a multipolar world has fostered persistent threats of radiological and nuclear terrorism that are real but difficult to quantify. As reiterated by President Obama in the recent 2016 Nuclear Security Summit, a serious and sustained global effort is required to counter nuclear terrorism. The United States Government has taken a multi-pronged approach to developing international awareness and cooperation in the area of nuclear security through programs such as Global Threat Reduction Initiatives and Nuclear Security Summits in conjunction with systems such as the Global Nuclear Detection Architecture (GNDA). According to U.S. Department of Homeland Security [1], "The Global Nuclear Detection Architecture is a framework for detecting (through technical and non-technical means), analyzing, and reporting

on nuclear and other radioactive materials that are out of regulatory control. Homeland Security Presidential Directive 14 and the SAFE Port Act of 2006 mandated the creation of the Global Nuclear Detection Architecture and charged the Domestic Nuclear Detection Office (DNDO) with coordinating its development and implementing its domestic component." The GNDA affects the full spectrum of transshipment modes (air, land, and sea) and includes both domestic and international controls.

To continue to combat evolving radiological and nuclear threats, the sustainment of the GNDA requires periodic evaluation of investment, policy, and operational decisions that encompass the set of potential mitigation options. However, making these decisions is non-trivial, in part because it is difficult to assess and communicate the combined benefits of different sets of mitigation options across sectors.

In this research we develop a method for selecting an optimal combination of mitigation options, using only the effectiveness metrics of each mitigation option evaluated in isolation, to strengthen the GNDA with a limited investment budget. In order to directly account for the combined impact of multiple mitigation options, we consider multiple defense attributes: situational awareness, detection, and interdiction. We develop a bi-level programming model, where the adversary's goal is to maximize damage to the system while the defender's goal is to minimize this damage. Furthermore, since effectiveness of various mitigation options may be uncertain or difficult to assess, we use a robust optimization approach to allow for uncertainty in the model parameters.

We test our method on a large synthetic example of the U.S. supply chain network that includes rail, air, and maritime transportation between both domestic and international locations. We consider an intelligent adversary whose goal is to use this network to smuggle radiological or nuclear material into and across the U.S.

1.2 Chapter 3: The Impact of Development Priorities on Power Generation Expansion Planning in Sub-Saharan Africa

It is well known that energy systems in sub-Saharan Africa are underdeveloped. Many countries in sub-Saharan Africa have electrification rates below 30%, some far below [2]. Wood and charcoal are the primary cooking fuels, most of the rural population does not have electric grid access, and the urban population has unreliable electricity service. When electricity from the centralized system is unreliable or unavailable, businesses [3] and critical industries such as healthcare and government services are forced to rely on diesel generators and other individual power sources for backup generation. Such barriers severely limit economic growth and development throughout many areas of sub-Saharan Africa.

There are a few key factors that make sub-Saharan Africa unique compared to other regions when considering power generation expansion planning. For one, unlike many recently developed regions in which electrification has occurred largely through urbanization, both rural and urban populations in sub-Saharan Africa continue to grow [4]. Thus, it is important to consider distributed as well as centralized electrification options. Additionally, although many countries have set lofty goals of reaching complete or near complete electrification within the next 10-15 years [5, 4], the funds to reach these goals are limited, and it is important to consider how to optimally allocate these funds if 100% electrification cannot be reached in the near future.

In this research, we develop a multi-period linear optimization model for power generation and transmission system expansion planning in sub-Saharan Africa. Rather than focusing on minimizing the cost to reach 100% electrification by a fixed year, we analyze the costs and system development decisions across four different electrification policies and a range of electrification rates. We also consider the impact of varying CO_2-equivalent emissions limits, solar home system costs, and transmission costs through sensitivity analysis. This framework allows decision makers to compare the costs over time of various

electrification policies and can thus help advise decisions for a development budget. We test our model on a case study of Rwanda over a thirty-year time horizon.

1.3 Chapter 4: Optimizing Wind Farm Siting Decisions to Reduce the Negative Impacts of Wind Variability

It is widely agreed upon that wind is an important resource to consider for a sustainable energy future. In the U.S., wind power accounted for 4.7% of electricity generation in 2015 and was the second most used renewable energy resource after hydropower [6]. As many countries seek to decrease their reliance on fossil fuels, wind power will become increasingly more important.

A well known challenge to wind integration is the fact that wind is uncontrollable and highly variable. An increased reliance on wind power can burden the rest of the system by making power balance more difficult. To ensure system reliability, generators that can ramp up and down quickly are required to account for fluctuations in wind power. When wind variability is high, some of these systems may need to be left on to meet reserve requirements, potentially negating the benefit of wind power. In this research, we aim to strategically select wind farm locations during the capacity planning stage of power system planning so as to minimize the burden of wind variability on the rest of the power generation system.

We develop a metric, which we call demand deficit, to indirectly measure the impact from wind power on the rest of the power generation system. We seek to minimize demand deficit as well as the change in demand deficit over time. We approach the problem in two ways: first we develop two heuristics to give an approximate solution based on the full data set, then we solve the exact optimization problem on a well-chosen subset of the data.

CHAPTER 2
ROBUST NETWORK INTERDICTION CONSIDERING MULTI-ATTRIBUTE DEFENSE OPTIONS

2.1 Background and Modeling Approach

2.1.1 Network Interdiction Framework

From its initial establishment for military operations, operations research has been widely used across defense applications. Although some researchers have taken the approach of assuming the adversary's decision is random [7, 8], oftentimes a game-theoretic framework is useful in such applications. In strengthening the GNDA, our goal is to defend against a malicious attack, more specifically, an intelligent adversary who strategically selects an attack plan in order to maximize the damage inflicted on the defender. To capture both the defender and the adversary's decisions, we employ a Stackelberg game framework [9], in which the defender first selects which mitigation options to add and the adversary then decides which path to take given the network. We assume that the adversary is aware of the defender's decision because the decision is static and the adversary may reconnoiter the system before attacking.

In our problem of interest, the adversary's goal is to circumvent the GNDA in order to cause maximal damage to a selected target, while the defender seeks to minimize this damage given a limited defensive budget. We model the system as a network flow problem. The adversary sends an initial flow of 1 from the source node, and this flow is diminished by the probabilities along each arc that the adversary takes. The adversary's objective is to maximize damage, and the adversary achieves this goal by selecting a target and path to reach that target. The defender seeks to minimize damage by selecting a set of mitigation options - a combination of technology, operations, and policies to detect and interdict the

adversary - to install throughout the network.

Although some authors [10, 11, 12] have considered defense or infrastructure protection problems in which the adversary and defender do not have diametrically opposed objectives, it is most common to consider settings in which the defender and adversary are in direct competition, as is the case in our problem. A bi-level program is considered an interdiction problem if the attacker's objective is directly opposed to the defender's objective [13]. Network interdiction problems arise across a broad range of applications from preventing drug smuggling [14] to strengthening the power grid against potential attacks [15].

The basic interdiction model structure is as follows,

$$\min_{x \in X} \max_{y \in Y} f(x, y),$$
$$\text{s.t.} \quad g(x, y) \leq 0.$$

The upper level decision x is the defender's decision, and the lower level decision y is the adversary's decision. In our case these decisions represent the mitigation options selected and the adversary's path, respectively. The objective $f(x, y)$ depends not only on the chosen defense x but also on the adversary's chosen action y against the defense. Typically (and in our problem), the objective is the damage incurred if the adversary is successful. In our problem, the set X of options available to the defender is constrained by the mitigation budget, and Y is the set of paths that the adversary may take. Finally, $g(x, y) \leq 0$ is the set of constraints imposed on the smuggler by the defender.

A number of researchers have considered defense and smuggling applications of network interdiction or other game theoretic models. In his 1993 article, Wood lays the basic groundwork for a mathematical approach to network interdiction, presenting various formulations and complexity results [14]. In another early study, Washburn and Wood [16]

consider the problem of placing an inspection point along a path to interdict an adversary who attempts to smuggle drugs from a given source to sink. Paté-Cornell [17] gives an overview of three counterterrorism and nuclear non-proliferation applications of game theory. Haphuriwat *et al.* [11] use a game theoretic approach to assess the level of inspection required to deter an adversary from attempting to smuggle nuclear material into the U.S. with and without retaliation measures. Shan and Zhuang [18] extend this work by considering non-credible threats in addition to credible threats. Brown *et al.* [15] present three types of interdiction models: an attacker-defender model, a defender-attacker model, and a defender-attacker-defender model, along with examples for each of them. Israeli and Wood [19] consider the problem of interdicting arcs on a directed network to maximize the minimum path length on that network. Scaparra and Church [20] and Aksen *et al.* [10] have done work extending the p-median problem, in which a supplier aims to minimize the median distance to a set of demand nodes, to account for potential attacks. These studies consider the decision of where to place a pre-specified defense mechanism or, in some cases, simply whether or not to defend the system at all or how many defense resources to use. Our model is more general in that it allows us to select a set of mitigation options to work in collaboration, where these mitigation options may affect a subset of the arcs in the network. The value of this will be discussed further in Section 2.1.3.

Some authors [21, 22, 23, 24] have considered multi-period models for defense and deterrence. While our model could be run multiple times to continually strengthen the GNDA as the resource options and adversary's abilities change, a direct multi-period analysis is beyond the scope of this work. However, such an extension may be interesting to consider in future work.

2.1.2 Robust Optimization Framework

Besides selecting from a set of multiple mitigation resources, another key distinction of our work is that we take a robust optimization approach in order to account for the fact that

the adversary's probability of success cannot be known with certainty. Some authors have considered stochastic variants of network interdiction or, more generally, bi-level programming problems. Cormican *et al.* [25] consider a network interdiction problem in which the arc capacities and the defender's success in interdicting an arc are stochastic, and they develop an approximation algorithm for solving this problem. Janjarassuk and Linderoth [26] extend this work by developing an efficient algorithm to obtain approximate solutions to the deterministic reformulation of the problem. Michalopoulos *et al.* [27] use a tabu search to find approximate solutions to a network interdiction problem in which the adversary's origin and destination are random and the budget is initially unknown to the defender. Pan and Morton [28] solve the problem of placing sensors on a network to minimize the probability that an adversary successfully traverses the network from a random source to a random sink. Dimitrov *et al.* [29] develop a model for placing radiation detectors along border crossings to prevent the smuggling of nuclear material, where the sensor effectiveness depends on the scenario, which is partially determined by the stochastic origin and destination pair. Alizadeh *et al.* [30] develop a stochastic bi-level programming model to select tariffs for a transportation system, which they solve in two stages. Wang and Bier [12] also consider a two-stage problem in which a defender determines how to allocate defense resources amongst a set of targets in two stages, between which additional information about the adversary type is gained.

These authors all capture uncertainty in their models through considering random source and sink nodes or other stochastic parameters. However, their focus is often on solving the problem in expectation or in two stages such that the defender and adversary have different information. We capture uncertainty in the effectiveness of each mitigation option by considering a range for the adversary's probability of successfully traversing each arc. Rather than optimizing for the average case, we take a robust optimization approach, which allows the decision maker to control the conservativeness of the solution. We loosely follow the method presented in Bertsimas and Sim [31], a widely used framework for robust optimiza-

tion. Details on this are discussed in Section 2.3.3. In addition to selecting an optimal path, we allow the adversary to select the weapon origin and target in order to cause maximal damage. We believe that the choice of the source and sink node is important to include in the adversary's decision in order to more completely model the adversary's options.

A common approach to solving bi-level programs is to reformulate the problem into a single level program by taking the dual of the lower level problem, as is done in Wood [14], Brown *et al.* [15], and Israeli and Wood [19]. However, this approach requires the lower-level program to be convex, which is not the case in our robust model due to the presence of binary decision variables (see Section 2.4 for more details). Because our model cannot be solved by standard reformulation techniques, we develop a new cutting plane algorithm using a bounded penalty reformulation, discussed in Section 2.4. This new algorithm is applicable to a more general class of bi-level integer programs.

2.1.3 Combined Benefits of Multiple Mitigation Options

Perhaps the most significant distinction between our work and previous network interdiction research is that we are interested in selecting a set (combination) of mitigation options holistically rather than simply deciding whether or not to defend a given arc. Some of the key network interdiction work [32, 28, 29] has been motivated by the Second Line of Defense Program for which the main focus is installing radiation detection equipment at points of exit in key countries [33]. In this case, it makes sense to limit the decision to whether or not to defend an arc. The scope of the GNDA, however, covers a broader range of systems for monitoring nuclear material across multiple domains (i.e. land, air and sea). Our approach models the collaborative impact of many different types of programs, technologies, policies, and operations by estimating and combining security and defense attribute parameters across the full GNDA system architecture. The prevailing binary selection model of defending/not defending an arc is thus a special case of our model.

To more accurately model the varying strengths of different mitigation options we con-

sider three stages of defense: situational awareness, detection, and interdiction. It is the combined effect across these three parameters that creates a mutual benefit when implementing multiple mitigation options. Situational awareness describes how cognizant the defender is of the security surroundings. For example, in a maritime port, is the Coast Guard aware of every boat entering and leaving the port? Detection describes how effective a mitigation option is at detecting a radiological nuclear source that is present. For example, if a maritime cargo container carrying nuclear material is scanned with a radiation portal monitor upon entering a port, how likely is it that the source will be detected? Finally, interdiction describes how effective a mitigation option is at apprehending a source that is detected. For example, if the radiation portal monitor detects a mobile source, will a defender be able to capture the source?

As a simplification, we assume that the success of the three mitigation components are independent. For many of the mitigation options the effectiveness is not known with certainty and requires expert opinion even to estimate. Since there are exponentially many potential combinations of mitigation options, soliciting expert opinion for every possible combination is unreasonable. By assuming the three components are independent we can still capture the joint impact of implementing multiple mitigation options while only requiring an expert to evaluate each of the components of each mitigation option once.

Assuming independence, the total probability that the adversary successfully traverses the three components is the product of the three probabilities. However, we don't simply combine these three probabilities for each mitigation option individually. Rather, for every mitigation option, we create a separate arc for each of the three components, which allows us to use the lowest probability for each of the three components across all mitigation options in place. This approach allows us to jointly consider mitigation options that are strong in different areas. For example, small vessel capable radar may be most effective in the area of situational awareness, while vessel boarding security teams are more effective for interdiction. If both of these mitigation options (and no others) are in place we will use

the situational awareness probability from small vessel capable radar, the interdiction probability from vessel boarding security teams, and whichever detection (adversary success) probability is lower between the two options, to calculate the overall probability that the attacker will evade capture via maritime transportation at the affected location.

In general, among the mitigation options selected, we use the probability for the mitigation option with the strongest defense in each of the three areas. That is, we use the lowest probability of adversary success across mitigation options, considering situational awareness, detection, and interdiction, independently to calculate the combined benefit. Note, however, that capabilities can only be combined in this way among mitigation options affecting the same mode of transportation. An example is shown in Figure 2.1. The details of how we implement this probability selection are discussed in Section 2.2.2.

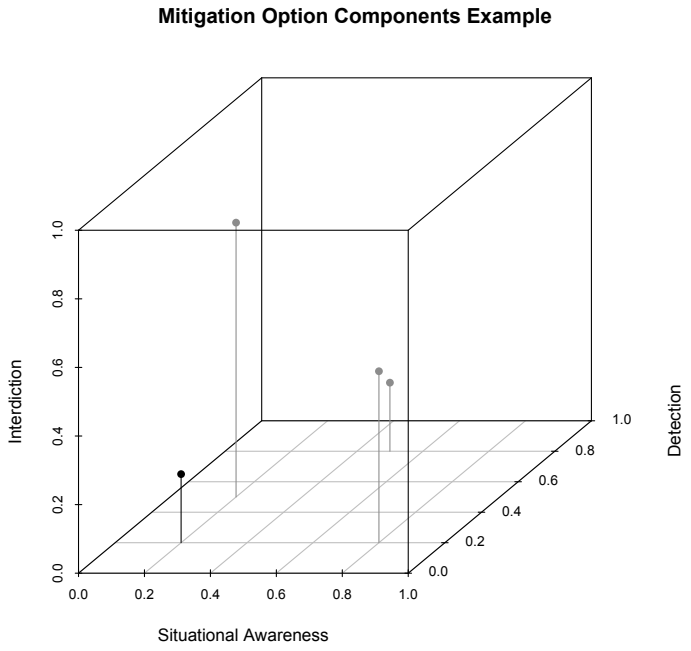

Figure 2.1: Shows the combined benefit of implementing multiple mitigation options. The three mitigation options, shown in gray, have probabilities (0.2, 0.5, 0.8), (0.5, 0.8, 0.2) and (0.8, 0.2, 0.5) for (situational awareness, detection, interdiction). The combined impact of these three mitigation options, shown in black, is (0.2, 0.2, 0.2) since we take the best (lowest adversary success) probability for each component. The lines are for visualization purposes only.

There are some limitations to assuming the probabilities of the three components are independent, primarily when the defender has no capability in one of the three components. In this case, the adversary's probability of success should be 1 because all three components are needed to stop the adversary, but the probability from taking the product of the three component probabilities would be less than 1 (unless there was no capability in any area). Ideally, we would like to use the joint probabilities of each component, but, as discussed, such data is beyond what can reasonably be obtained from expert opinion. Another alternative would be to use the highest probability across the three components. However, this method does not capture the benefit of the three components working together. Instead, to avoid these extreme cases, we assume that there is always a small probability that the adversary will be caught, even if just by serendipity.

2.2 Network Model

To solve our problem of interest we use a network flow model, allowing for multiple arcs between nodes and the option to shut off arcs that are unavailable due to the mitigation options in place.

2.2.1 Baseline Network Structure

We model the set of possible nuclear smuggling routes on digraph $\mathcal{D}(\mathcal{N}, \mathcal{A})$, where $\mathcal{N}$ is the set of nodes and $\mathcal{A}$ is the set of arcs. In the baseline network, $\mathcal{N}$ represents physical locations, both foreign and domestic. These nodes include potential origins of smuggling activities, destinations of smuggling activities (targets), and transshipment points. $\mathcal{A}$ represents transit options, specifically air, train, and sea. This network is augmented with additional nodes and arcs to represent various weapon types, defense types, and auxiliary source and sink nodes. A small example of the baseline network structure for a single nuclear weapon type is shown in Figure 2.2.

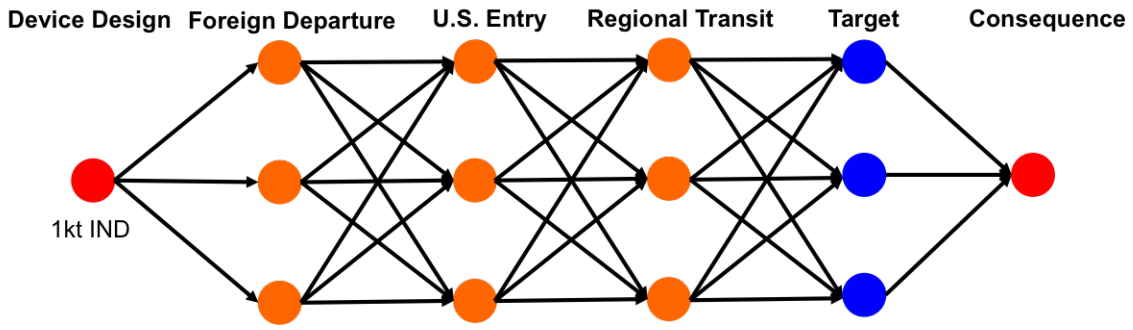

Figure 2.2: Basic interdiction network for a single (1 kiloton improvised nuclear device) nuclear weapon.

A pair of nodes may have multiple connecting arcs if there are multiple transit options between the two nodes. We call the set of all arcs connecting a given pair of nodes a *corridor*. We also model each mitigation option that affects a given transit option with a separate arc. The weight on each arc is the probability that an adversary will successfully evade capture if the given arc is traversed. When a given mitigation option is in place all arcs with a higher probability are "shut off," so the adversary may not take them. The method for shutting off arcs is discussed in detail in Appendix A.

Since mitigation options may vary in effectiveness depending on the weapon type smuggled we replicate the network for each possible weapon type, with one modification: we have a single source (s) and sink (t) node connecting the networks across all weapon types. The source node is adjacent to the foreign departure nodes across all weapon types. The weights on arcs originating at s are 1 since these arcs do not represent actual transit options and cannot lower the probability of an adversary's success. The sink node is adjacent to the target nodes across all weapon types. The probability of successfully traversing these arcs is also 1. However, here we use the expected damage if the arc is traversed as the arc weight, accounting for both the target chosen and the weapon type used.

An example of a possible network structure for three weapon types is shown in Figure 2.3.

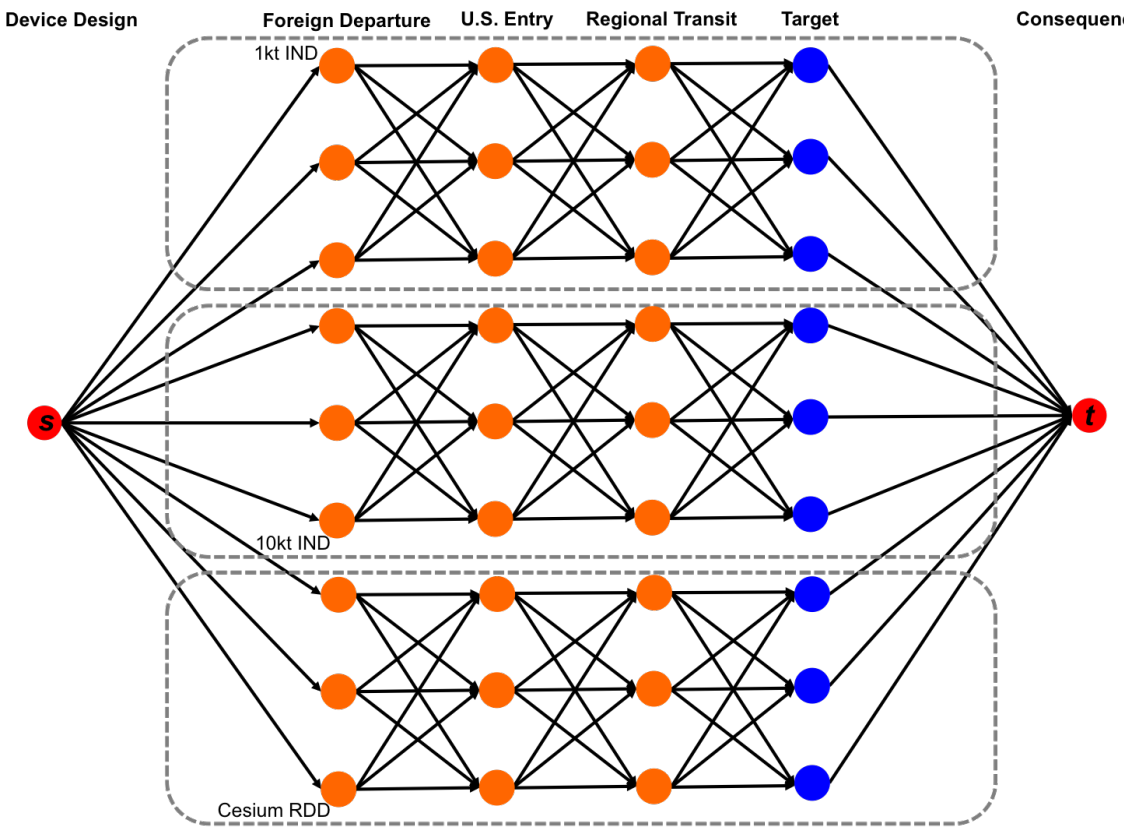

Figure 2.3: Basic interdiction network for a three nuclear weapon configuration.

2.2.2 Components of Mitigation Impact

In order to evaluate the effectiveness of various mitigation options in more detail, we make one additional modification to the network framework described in Section 2.2.1. As discussed in Section 2.1.3, we consider three components of defense: situational awareness, detection, and interdiction. We expand the network to include an arc for each of these components by adding two auxiliary nodes to each corridor for each transportation mode. From the original start node to the first of these auxiliary nodes (for the appropriate transportation mode) we add an arc for each mitigation option representing situational awareness. Between the first and the second auxiliary nodes we add an arc for each mitigation option representing detection, and between the second auxiliary node and original end node we add an arc for each mitigation option representing interdiction. The weight on each of these

arcs is the probability that the adversary will evade the situational awareness, detection, and interdiction capabilities, respectively, if the given arc is taken with the corresponding mitigation option in place. An example is shown for a single corridor with two transportation modes in Figure 2.4, where Figure 2.4(a) is the original corridor and Figure 2.4(b) is the augmented corridor. In this example there are three mitigation options that affect the original air arc and two that affect the maritime arc, so we have three arcs between each node pair for the air option and two between each node pair for the maritime option.

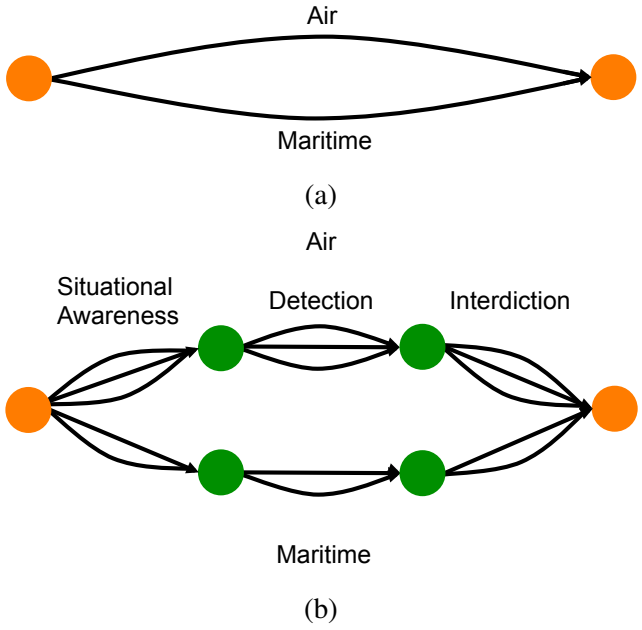

Figure 2.4: Shows how the network is expanded to include situational awareness, detection, and interdiction components. (a) Shows the original corridor, which includes air and maritime arcs. (b) Shows the augmented corridor with arcs added for situational awareness, detection, and interdiction for each mitigation option. We have three mitigation options for the air arc and two for the maritime arc (including the baseline, i.e. no additional mitigation options).

Augmenting the baseline network in this way allows us to apply the best defense on each of the three components of each arc given the set of mitigation options selected and, more importantly, yields a linear network flow representation of the adversary's evasion model. This linear network flow model relies on the introduction of arc shut-off constraints

that restrict flows on arcs with higher probabilities, as prescribed by the set of mitigation options selected (details of this network augmentation and shut-off constraints are described in Appendix A).

2.3 Mathematical Formulation

We first describe the deterministic model, in which the adversary's probability of success is known for every arc. We then extend this model to the robust variation, in which the adversary's probability of success is unknown.

2.3.1 Nomenclature

The following summarizes the nomenclature that will be used for both the deterministic and robust optimization models.

Index sets:

- $\mathcal{A}$: set of arcs, indexed by $a = (i, j, k)$, where i and j are indices of the arc's origin and destination nodes, respectively, and k is an additional ordering index to allow for the definition of multiple arcs for each node pair (i, j)
- $\mathcal{M}$: set of mitigation options that the adversary may select from, indexed by m
- $\mathcal{N}$: set of nodes, indexed by i. s and t denote the source and sink nodes, respectively.

Decision Variables:

- f_a : continuous variable corresponding to flow on arc a
- x_m : binary variable that takes value 1 if mitigation option m is implemented and 0 otherwise

Parameters:

- c_m : the cost of mitigation option m
- d_a: damage incurred by the defender if smuggler successfully traverses arc a. Note, if traversing arc a results in no damage to the defender, as is the case until the sink node is reached, then $d_a = 0$.
- $\delta(i)^+$: the set of arcs $(i, j, k) \in \mathcal{A}$ directed out of node i
- $\delta(i)^-$: the set of arcs $(j, i, k) \in \mathcal{A}$ directed into node i
- γ_a^m: binary parameter that is 1 if mitigation option m shuts off arc a and 0 otherwise
- Γ: mitigation budget
- Γ^U: uncertainty budget
- p_a: probability that a smuggler who attempts to traverse arc a is successful

2.3.2 Deterministic Optimization Model

We formulate the problem of selecting a set of mitigation options to minimize the expected damage from an attack as a bi-level program. The adversary seeks to maximize the damage done, while the defender seeks to minimize this damage. To simultaneously optimize these two conflicting objectives we solve the following bi-level program,

$$\min_{\boldsymbol{x}\in\mathcal{X}} \max_{\boldsymbol{f}\geq 0} \quad \sum_{a\in\delta^-(t)} d_a f_a, \tag{2.1a}$$

$$\text{s.t.} \quad \sum_{a\in\delta^+(s)} f_a = 1, \tag{2.1b}$$

$$\sum_{a\in\delta^-(i)} p_a f_a = \sum_{a\in\delta^+(i)} f_a \quad \forall\, i \in \mathcal{N} \setminus \{s, t\}, \tag{2.1c}$$

$$f_a \leq 1 - x_m \quad \forall\, a \in \mathcal{A}, m \in \mathcal{M} | \gamma_a^m = 1, \tag{2.1d}$$

where $\mathcal{X} = \left\{ \boldsymbol{x} \in \{0,1\}^{|\mathcal{M}|} : \sum_{m \in \mathcal{M}} c_m x_m \leq \Gamma \right\}$. The upper-level decisions $\boldsymbol{x}$ correspond to the defender's selection of a subset of the available mitigation options $\mathcal{M}$. c_m is the cost of mitigation option m, and Γ is the defender's mitigation budget. The lower-level decisions $\boldsymbol{f}$ represent the adversary's selection of flow along arcs in the network, which in aggregate prescribe the adversary's chosen path. Along each arc that flow is sent, f_a is scaled by the probability that the adversary successfully traverses that arc.

$\delta^+(i)$ and $\delta^-(i)$ are the sets of arcs exiting and entering node i, respectively. γ_a^m is a binary parameter that is 1 if mitigation option m shuts off arc a and 0 otherwise. d_a is the damage caused if the adversary successfully traverses arc a. Damage is 0 for all arcs except those entering the sink node. For arcs entering the sink node, the damage is the damage from hitting the target node at the start of the arc scaled by the *weapon factor*, a value that adjusts the damage for the weapon type used. p_a is the probability that the adversary will be successful in an attempt to traverse arc a. Thus, the objective (2.1a) represents the expected damage with a given set of mitigation options and adversary flow decisions.

Constraints (2.1b) and (2.1c) are a variation of the standard flow-balance constraints. Here, rather than requiring 1 unit of flow travels from the source to the sink we scale the flow at each arc it traverses by the probability of successfully traversing that arc. The scaling of the arc flow by the associated arc probability enables the computation of the full path evasion probability, which corresponds to the flow on the arc taken into terminal node t. Constraints (2.1d) are used to shut off arcs that are made unavailable by the mitigation options selected, as described in Appendix A. Finally, $\mathcal{X}$ constrains the total cost of the mitigation options selected to be within the budget Γ.

2.3.3 Robust Optimization Model

The deterministic model assumes that the adversary's probability of success is known. Realistically, we may only have an estimate for the effectiveness of various mitigation options

or a range in which the probability may fall. As an example, consider the effectiveness of radiological sensors. These sensors are well known for having both false positives and false negatives [34] and the effectiveness of these sensors depends heavily on external factors such as shielding, the evader's travel speed, and the amount of ambient radiation. A natural approach that has been used when model parameters are uncertain is to plan for the worst case scenario as shown in Soyster [35]. However, planning for the worst case outcome for all uncertain parameters may be overly conservative, as the probability of such a realization is extremely small. Bertsimas and Sim [31] develop a robust optimization approach that uses an "uncertainty budget" to constrain the number of variables for which the worst case is considered. This method allows the decision maker to control how conservative the solution is by an appropriate selection of the uncertainty budget Γ^U, which governs the number of uncertain parameters (e.g. detection probability) that may deviate from the average.

We take a slightly different approach to account for uncertainty, while still using Bertsimas and Sim's main idea of constraining the number of parameters that may vary with an uncertainty budget. Rather than employing interval uncertainty, we assume that each uncertain parameter can only take on the nominal probability or the worst-case probability. To achieve this, we duplicate the original arcs such that we have two choices for each original arc: one with the original probability and one with the worst case probability in the parameter range. This approach of considering the nominal probability and the worst-case probability for each arc is a less conservative approach, compared to interval uncertainty, and permits the reformulation of the lower-level program as a mixed-integer linear program instead of a mixed-integer non-linear program, which is key to computational tractability. Of these two arcs, only one may be selected, and we limit the number of worst case probability arcs that may be selected via the uncertainty budget. For this reason, we require the uncertainty budget to be integral. Notice that since the adversary's goal is to maximize damage, the worst case for the defender will always be when the probability of the

adversary's success is at its upper bound.

Let $\mathcal{A}^0$ be the set of nominal arcs and $\mathcal{A}^U$ be the set of uncertain arcs (i.e. arcs with the worst case probability). Then the complete set of arcs is $\mathcal{A} = \mathcal{A}^0 \cup \mathcal{A}^U$.

The robust model is as follows,

$$\min_{\boldsymbol{x}\in\mathcal{X}} \max_{\boldsymbol{f}\geq 0, \boldsymbol{z}\in\{0,1\}^{|\mathcal{A}^U|}} \quad \sum_{a\in\delta^-(t)} d_a f_a, \tag{2.2a}$$

$$\text{s.t.} \quad \sum_{a\in\delta^+(s)} f_a = 1, \tag{2.2b}$$

$$\sum_{a\in\delta^-(i)} p_a f_a = \sum_{a\in\delta^+(i)} f_a \quad \forall\, i \in \mathcal{N}\setminus\{s,t\}, \tag{2.2c}$$

$$f_a \leq 1 - x_m \quad \forall\, a \in \mathcal{A}, m \in \mathcal{M} | \gamma_a^m = 1, \tag{2.2d}$$

$$f_a \leq z_a \quad \forall\, a \in \mathcal{A}^U, \tag{2.2e}$$

$$\sum_{a\in\mathcal{A}^U} z^a \leq \Gamma^U, \tag{2.2f}$$

In defining γ_a^m for the worst case model, we require that if a mitigation option shuts off the nominal arc it also shuts off the corresponding worst case arc. Constraint (2.2f) states that at most Γ^U of the robust (uncertain) arcs may be used by the adversary. Constraints (2.2e) enforce that no flow is sent along robust arcs that are not used. When $\Gamma^U = 0$, none of the uncertain parameters may deviate from their nominal values and (2.2) is equivalent to (2.1).

2.4 Solution Method

The standard approach of reformulating the bi-level program as a single level program by taking the dual of the inner problem cannot be applied to our problem since the inner problem includes binary $\boldsymbol{z}$ variables. We instead partition our problem and solve via a

cutting plane approach.

2.4.1 Penalty-Based Reformulation

We propose a penalty-based reformulation of the inner maximization problem following the work of Cormican *et al.* [25]. Observe that shut-off constraints (2.2d) can be removed and replaced by appropriately chosen penalty terms in the objective (2.3a). Non-zero flows are permitted on arcs that have been shut off by the selected set of mitigation options but at a cost of M per unit flow. If M is selected to be sufficiently large, it becomes uneconomical to used these arcs.

The robust optimization problem in (2.2) can be reformulated as follows,

$$\min_{\boldsymbol{x}\in\mathcal{X}} \max_{0\leq \boldsymbol{f}\leq 1, \boldsymbol{z}\in\{0,1\}^{|\mathcal{A}^U|}} \quad \sum_{a\in\delta^-(t)} d_a f_a - M \sum_{a\in\mathcal{A}} \sum_{m\in\mathcal{M}|\gamma_a^m=1} f_a x_m, \tag{2.3a}$$

$$\text{s.t.} \quad \sum_{a\in\delta^+(s)} f_a = 1, \tag{2.3b}$$

$$\sum_{a\in\delta^-(i)} p_a f_a = \sum_{a\in\delta^+(i)} f_a \quad \forall\, i \in \mathcal{N}\setminus\{s,t\}, \tag{2.3c}$$

$$f_a \leq z_a \quad \forall\, a \in \mathcal{A}^U, \tag{2.3d}$$

$$\sum_{a\in\mathcal{A}^U} z_a \leq \Gamma^U, \tag{2.3e}$$

To see that (2.3) is equivalent to (2.2) first consider when $x_m = 0$. In this case Constraints (2.2d) become $f_a \leq 1$, which is redundant. Also, $M \sum_{a\in\mathcal{A}} \sum_{m\in\mathcal{M}|\gamma_a^m=1} f_a x_m = 0$, so no penalty is added. When $x_m = 1$, Constraints (2.2d) become $f_a \leq 0$, so $f_a = 0$. In this case, the penalty will force $f_a = 0$ in the optimal solution of (2.3) as the objective penalty M makes it uneconomical for the adversary to traverse these arcs. Since x_m is binary these are the only two cases we must consider. Thus, the two problems are equivalent.

Observe that, by employing this penalty-based reformulation, the feasible region of

lower level problem in (2.3) becomes invariant to $\boldsymbol{x}$.

Define $\mathcal{K} = \{\boldsymbol{z} \in \{0,1\}^{|\mathcal{A}^U|} | \mathbf{1}^\top \boldsymbol{z} \leq \Gamma^U\}$. $\mathcal{K}$ is the set of all feasible $\boldsymbol{z}$. Since this set is finite, we can solve (2.3) by enumerating over these values and solving,

$$\begin{aligned} &\min_{\boldsymbol{x} \in \mathcal{X}, \alpha} \ \alpha, \\ &\text{s.t. } \mathcal{R}(\boldsymbol{x}, \boldsymbol{z}^k) \leq \alpha \quad \forall\, \boldsymbol{z}^k \in \mathcal{K}, \end{aligned} \tag{2.4}$$

where $\mathcal{R}(\boldsymbol{x}, \boldsymbol{z}^k)$ is the following linear maximization problem,

$$\begin{aligned} \mathcal{R}(\boldsymbol{x}, \boldsymbol{z}^k) \ = \ \max_{0 \leq \boldsymbol{f} \leq 1} \quad & \sum_{a \in \delta^-(t)} d_a f_a - M \sum_{a \in \mathcal{A}} \sum_{m \in \mathcal{M} | \gamma_a^m = 1} f_a x_m, \\ \text{s.t.} \quad & \sum_{a \in \delta^+(s)} f_a = 1, \\ & \sum_{a \in \delta^-(i)} p_a f_a = \sum_{a \in \delta^+(i)} f_a \quad \forall\, i \in \mathcal{N} \setminus \{s,t\}, \\ & f_a \leq z_a^k \quad \forall\, a \in \mathcal{A}^U. \end{aligned}$$

2.4.2 Cutting Plane Algorithm

We develop a custom cutting-plane algorithm for solving bi-level integer program (2.4). Let the master problem (MP) be defined as follows,

$$\begin{aligned} &\min_{\boldsymbol{x} \in \mathcal{X}, \alpha} \ \alpha, \\ &\text{s.t. } \mathcal{R}(\boldsymbol{x}, \mathbf{0}) \leq \alpha, \end{aligned} \tag{2.5}$$

Rather than attempting to solve (2.4), which has exponentially many constraints, di-

rectly, we iteratively solve (2.5), generating constraints as needed until we have reached an optimal solution. We choose $\boldsymbol{z}^k = \mathbf{0}$ for our starting constraint because we know that there exists a feasible solution where no robust arcs are used (since every robust arc has an associated nominal arc). We generate the remainder of the constraints as needed with the following mixed-integer linear programming separation oracle $\mathcal{S}(\boldsymbol{x})$,

$$\mathcal{S}(\boldsymbol{x}) = \max_{0 \leq \boldsymbol{f} \leq 1, \boldsymbol{z} \in \{0,1\}^{|\mathcal{A}^U|}} \quad \sum_{a \in \delta^-(t)} d_a f_a - M \sum_{a \in \mathcal{A}} \sum_{m \in \mathcal{M} | \gamma_a^m = 1} f_a x_m, \tag{2.6a}$$

$$\text{s.t.} \quad \sum_{a \in \delta^+(s)} f_a = 1, \tag{2.6b}$$

$$\sum_{a \in \delta^-(i)} p_a f_a = \sum_{a \in \delta^+(i)} f_a \quad \forall\, i \in \mathcal{N} \setminus \{s, t\}, \tag{2.6c}$$

$$f_a \leq z_a \quad \forall\, a \in \mathcal{A}^U, \tag{2.6d}$$

$$\sum_{a \in \mathcal{A}^U} z_a \leq \Gamma^U. \tag{2.6e}$$

The complete algorithm is outlined below.

Algorithm 1:

Input: Initialize MP (2.5)

1 Solve MP $\rightarrow \boldsymbol{x}^*, \alpha^*$;
2 Solve $\mathcal{S}(\boldsymbol{x}^*)$ (2.6) $\rightarrow \boldsymbol{f}^*, \boldsymbol{z}^*$;
3 **if** $\mathcal{S}(\boldsymbol{x}^*) > \alpha^*$ **then**
4 Add $\sum_{a \in \delta^-(t)} d_a f_a^* - M \sum_{a \in \mathcal{A}} \sum_{m \in \mathcal{M} | \gamma_a^m = 1} f_a^* x_m \leq \alpha$ to MP (2.5) ;
5 Go to step 1 ;
6 **end**
7 **return** $\boldsymbol{x}^*$ ▷ optimal mitigation allocation

Algorithm 1 solves (2.3) to optimality in a finite number of iterations. We program this algorithm in Python and run the optimization at each iteration using Gurobi.

2.5 U.S. Bulk Transportation Network Application

We develop a large synthetic example of the U.S. supply chain to demonstrate our methodology. For this case study we focus on cargo shipment, though passenger travel is also monitored by the GNDA. We consider air, maritime, and train shipment routes and various mitigation options affecting each of these transportation modes. Although we aim to create an example that is somewhat realistic it should be noted that the network structure and target damages as well as the mitigation options and associated probabilities were developed by the authors for illustrative purposes only and are not based on any actual GNDA data provided by the DNDO.

2.5.1 Network Structure

In the case study, we consider international airports and maritime ports across 32 different countries as well as rail transshipment points/intermodal terminals in Canada and Mexico as potential origins. For targets, we use the top 50 most populated cities in the U.S. based on the 2010 Census estimates for 2014 U.S. Census Bureau, Population Division [36], shown in Figure 2.5. We exclude target cities that do not have any of the air, maritime, or train ports/terminals passing through, which leaves the 39 target cities. For transshipment points, we use airports, maritime ports, and intermodal terminals in the U.S.

The airports used in our case study are the top 30 worldwide airports by cargo volume according to Airports Council International [37]. Of these, 22 are outside of the U.S. and 8 are within the U.S. Two of these airports are in Tokyo and two are in Dubai, but we only consider each of these once, to make for a total of 20 air nodes outside of the U.S. We assume that cargo may be shipped directly from any airport outside of the U.S. to any airport in the U.S., but we do not consider air freight between U.S. airports or between international airports. Airports considered are shown in Figure 2.6. From airports within the U.S., we may transport cargo via rail to adjacent intermodal terminals if the airport is

co-located with an intermodal terminal.

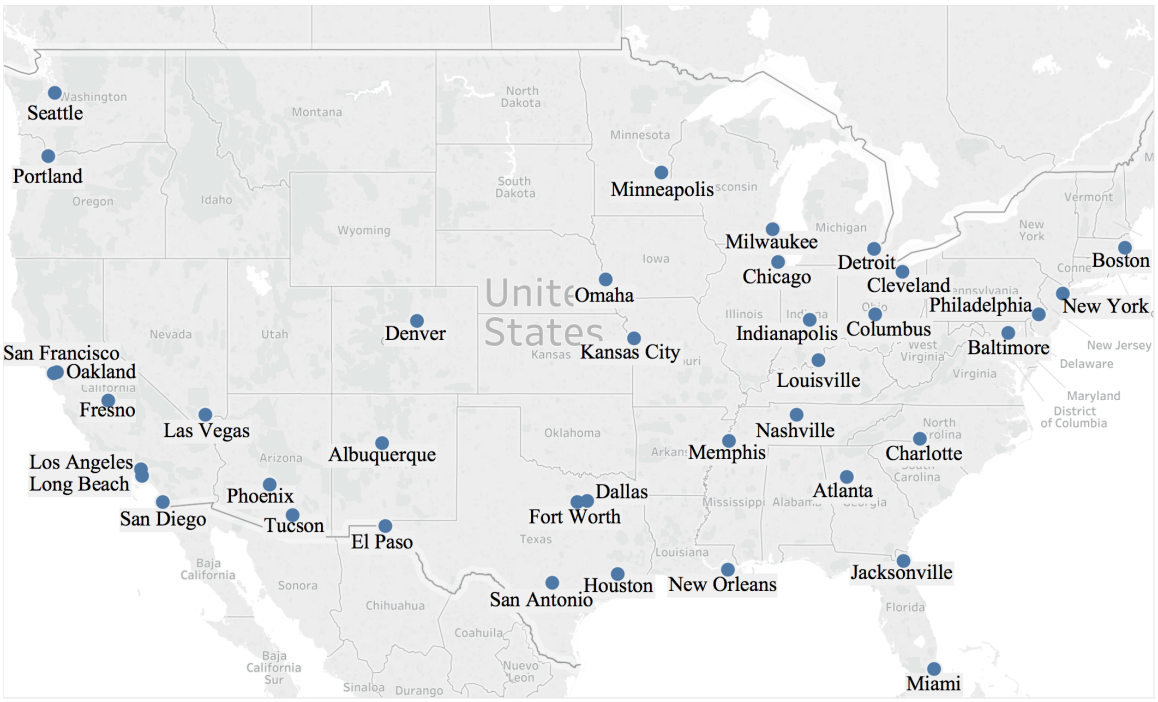

Figure 2.5: The 39 target cities considered in the case study.

Figure 2.6: The 28 airports considered in the case study.

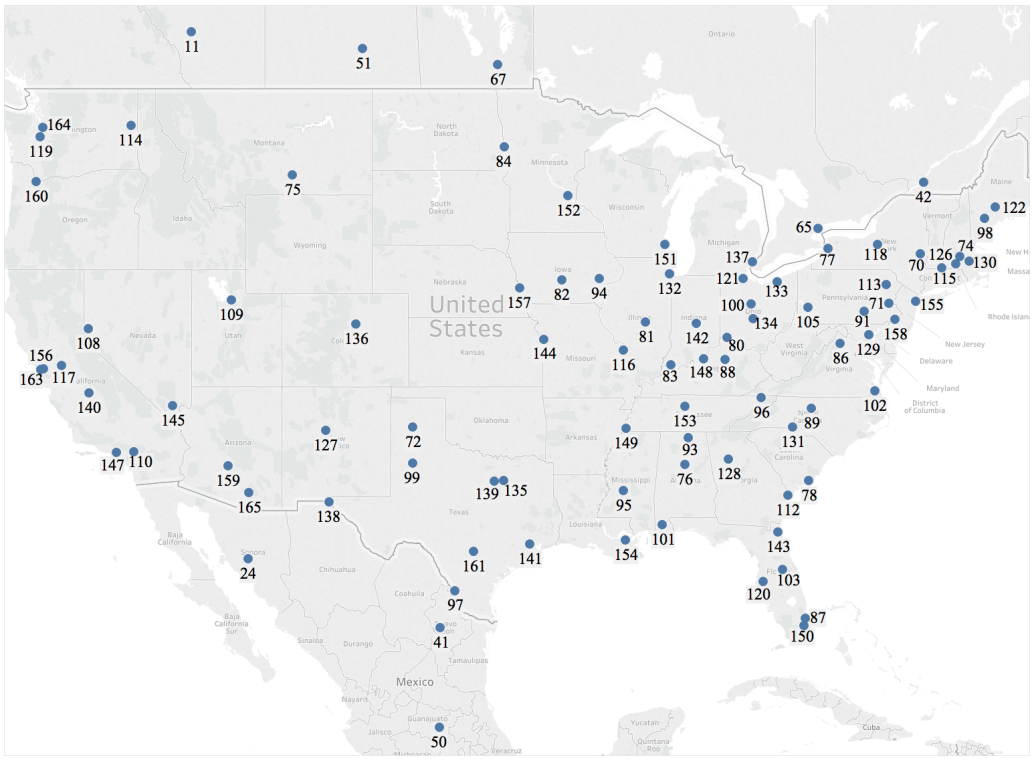

Figure 2.7: The 90 train terminals considered in the case study. Cities corresponding to the labels on the map are given in Appendix C.

We consider direct rail transport between adjacent intermodal terminals, where rail connections are extracted from the map shown in Integrated Distribution Services [38]. Similarly to airports, we do not consider train transportation between international intermodal terminals because anywhere where there was an international transfer the adversary would have the option of simply starting at the end node, which would never decrease the probability that the adversary is successful. We do, however, consider intermodal terminals in Canada and Mexico that are adjacent to intermodal terminals in the U.S. Intermodal terminals considered are shown in Figure 2.7. The key for the node indices is given in Appendix C.

For international maritime nodes we use the top 50 international ports by volume throughput in 2013 according to the World Shipping Council [39]. Of these, 4 are in the U.S. We augment this list with the top 30 U.S. ports by inbound volume [40]. We only

allow ports from outside the U.S. to ship to U.S. ports, with the exception of Hawaii, which can receive shipments from international ports and ship to other ports within the U.S. We only allow maritime arcs from Europe to go to the U.S. East Coast and from Asia to the U.S. West Coast. With other countries (e.g. in Central and South America) it varies, but we only allow each international port to ship to one of the U.S. coasts. Maritime ports considered are shown in Figure 2.8.

For maritime, we consider six different vessel types: containerized cargo, roll on/roll off, bulk, break bulk, cruise ship, and small vessel. Each maritime port is able to process some subset of these options.

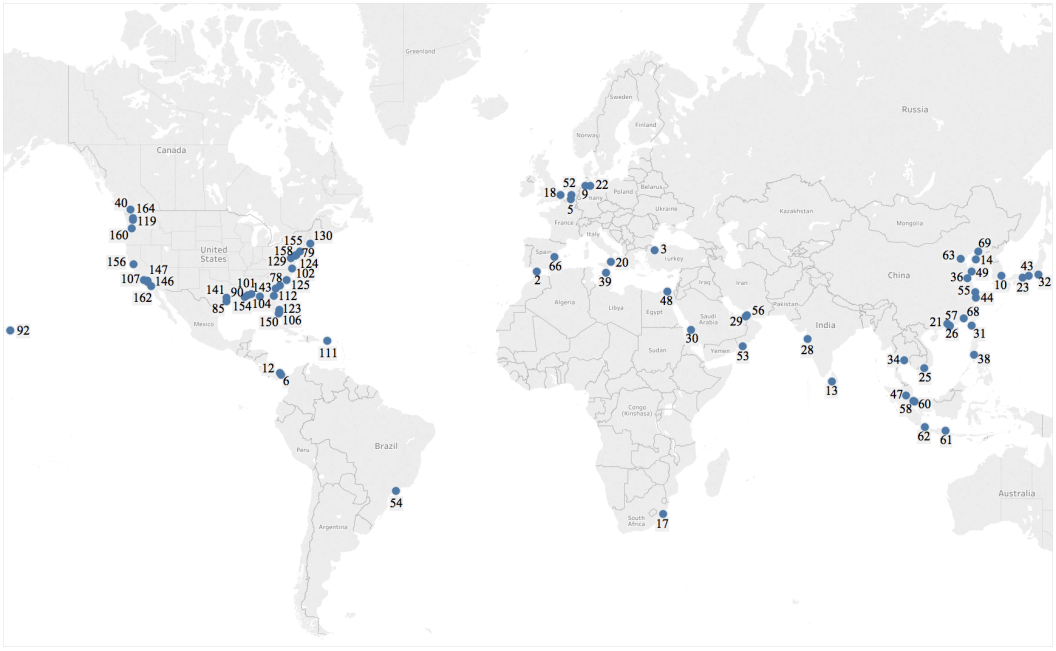

Figure 2.8: The 76 maritime ports considered in the case study. Cities corresponding to the labels on the map are given in Appendix C.

2.5.2 Weapon Types

We consider three nuclear weapon types: 1 kt improvised nuclear device (IND), 10kt IND, and a cesium radiological dispersal device (RDD). Rather than developing an absolute damage metric we consider the relative damage if each weapon type is detonated. 1kt

IND is our baseline with a damage factor of 1. The relative damage factor for 10kt IND is 1000 and for RDD is 0.1.

2.5.3 Mitigation Options

We develop an exemplar set of mitigation options for each of the three transportation types (air, train, and maritime, with maritime further divided by the six cargo conveyance types) based on our own devising. We assume that when a mitigation option is selected it is implemented at every node to which it applies (depending on the transportation type it affects).

For each mitigation option we postulate a probability for situational awareness, detection, and interdiction for each of the three weapon types. This probability is the nominal probability that the adversary will successfully traverse a single arc that is affected by the given mitigation option, if that arc is taken. We assume that the detection probability varies by weapon type, but the situational awareness and interdiction probabilities do not. Mitigation options considered as well as the nominal probabilities for each mitigation component are shown in Appendix B.

We determine the worst case (uncertain) probabilities as follows: Let p^0 be the nominal probability that the adversary is successful. Then the worst case probability is given by $p^U = \min\{p^0 + \eta(0.999 - p^0), 0.999\}$, where η is distributed uniformly at random between 0 and 1. We restrict both the nominal and robust probabilities to be at most 0.999 because even without any mitigation options in place the adversary could be intercepted just by coincidence or the attack may fail due to other unexpected barriers. Similarly, we do not set any of the probabilities to 0 because the adversary always has some small chance of avoiding detection.

2.5.4 Results

We test our method over a range of values for both the mitigation budget and uncertainty budget. We begin by testing mitigation budgets from 0 to 100% of the cost to implement all mitigation options, with uncertainty budgets from 0 to 5. These results are shown in Figure 2.9.

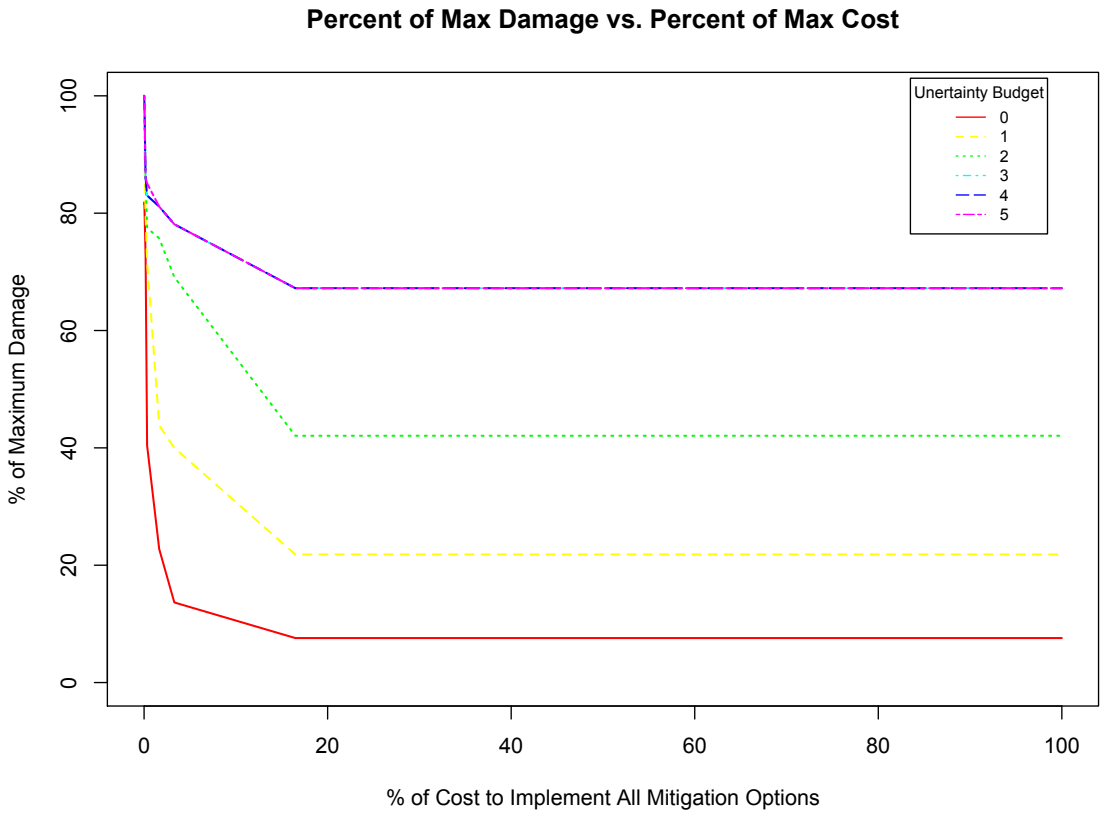

Figure 2.9: Percent of maximum possible damage vs. percent of mitigation budget required to implement all mitigation options for uncertainty budgets 1 to 5 and mitigation budget percents from 0 to 100.

The damage values are proportional to the population at each target node scaled by the weapon factor. These values represent the relative severity of the threat rather than an absolute measure of damage. Thus, rather than focusing on the actual damage values, we analyze the change in percent of the maximum possible damage as the budget is increased.

The maximum possible damage is the damage value we get with a mitigation budget of 0 and uncertainty budget of 20, which is the highest uncertainty value we test. We do not test uncertainty budgets higher than 20 because between 10 and 20 the results are identical for the cases tested, so it appears that increasing the mitigation budget beyond 10 does not affect the solution to our case study (thus, the max damage is also the damage value for an uncertainty budget of 10 and mitigation budget of 0).

As expected, the percent of maximum damage is generally decreasing as the mitigation budget increases and increasing as the uncertainty budget increases. We see increasing the mitigation budget ceases to be beneficial once the budget is around 17% of the maximum. It is reasonable that increasing the mitigation budget will only decrease the damage up to a certain point. Once stronger mitigation options are in effect it is not beneficial to implement the weaker mitigation options as well. For example, we consider the baseline (i.e. implementing no new defenses) as one "mitigation option" in our model. However, once a mitigation option with additional defenses is selected, it does not make sense to select the baseline option as well. Although the baseline has zero cost, there are other mitigation options with non-zero cost that may be superseded by more costly but stronger mitigation options. With a sufficient budget, these weaker options no longer contribute to the effectiveness of the solution. The solutions found give us a range of values over which varying the mitigation budget is most effective.

Following our observations from Figure 2.9, we test mitigation budgets from 0 to 17% on smaller intervals for uncertainty budgets of 0, 1, 2, 3, 4, 5, 10, 15, and 20. Since the initial results decreased the most between 0-2%, we run tests over a finer resolution of mitigation budgets in this region. We test mitigation budgets from 0-2% on increments of 0.1 percent points, and 2-17% on increments of 0.5 percent points. We also include test results for 0.05% of the max mitigation budget to gain additional insight in the 0-0.1% region since there is a sharp decline in this region before a small plateau followed by another decline. We observe this behavior because there is a large cost difference between the 9 cheapest

mitigation options and the 10^{th} cheapest. 0.05% of the max possible mitigation budget is sufficient to add enough of the cheapest group to bring the damage down to the value at the first plateau, but after this point there is a jump in cost to further decrease the damage. The results are shown in Figure 2.10. We exclude results for uncertainty budgets 15 and 20 from the figure because they are identical to the results for uncertainty budget 10.

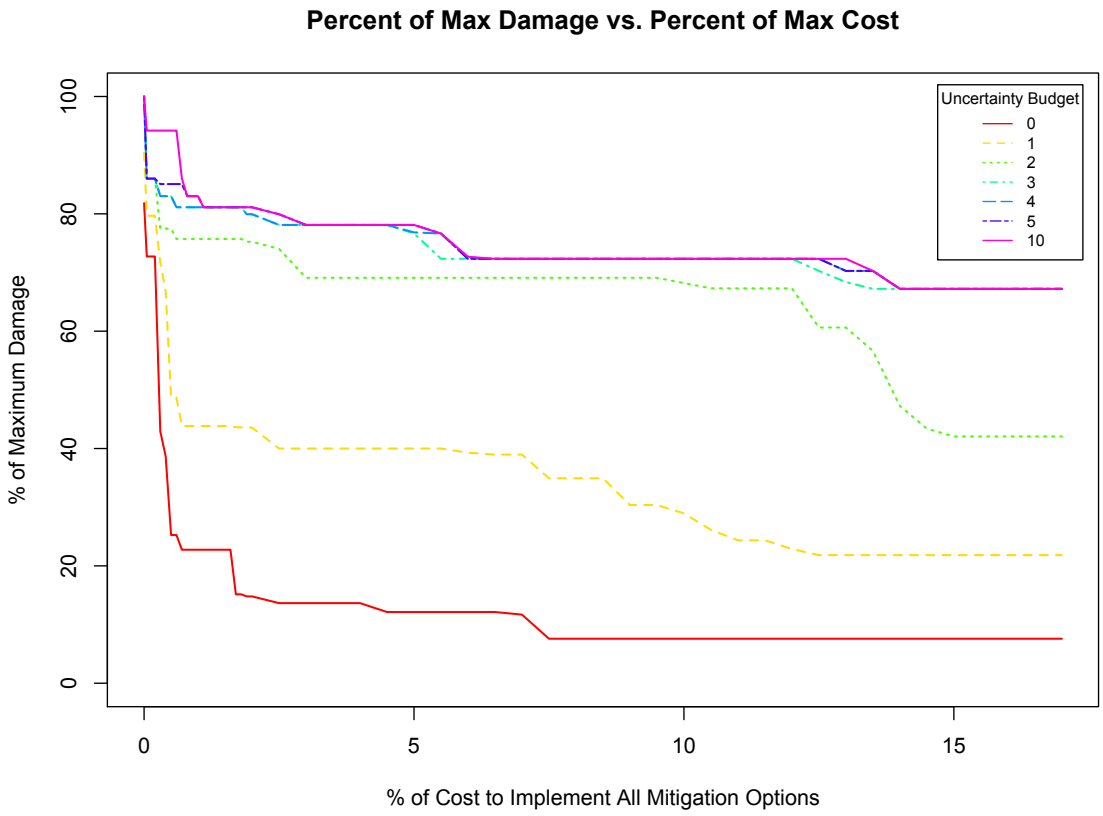

Figure 2.10: Percent of maximum possible damage vs. percent of mitigation budget required to implement all mitigation options for 0 to 17 percent.

We are also interested in the mitigation options selected under each scenario. Figure 2.11 shows the number of times each mitigation option is selected across the same set of scenarios for which the damage is shown in Figure 2.10. The corresponding mitigation options are shown in Appendix B. Options 1-9 affect air transit, 10-18 affect train transit, and 19-42 affect maritime transit. We see that a subset of 28 out of 42 mitigation options

were selected across all of the cases tested. Options 29-33, which affect maritime transit, are selected the most frequently because these five options have a cost of 0.

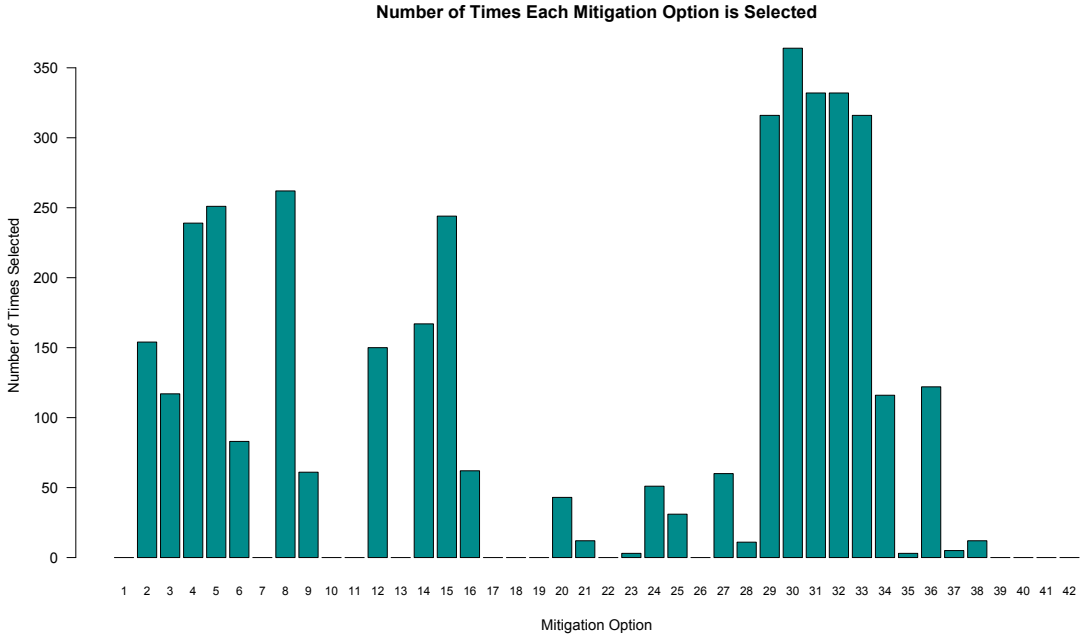

Figure 2.11: Number of times each mitigation option is selected across the scenarios tested. Corresponding mitigation options are shown in Appendix B.

We also compare the mitigation options selected across different uncertainty budgets. These results are shown in Figure 2.12. We see that the aggregate number of times each mitigation option is selected is similar for uncertainty budgets 1, 2, 3, 4, and 5. However, there is a big difference in the charts from uncertainty budget 0 to 1 as well as from 5 to 10. Although it's possible that some solutions are not unique, these results suggest that considering robustness has an impact not only on the optimal objective value but also on the optimal mitigation options to select.

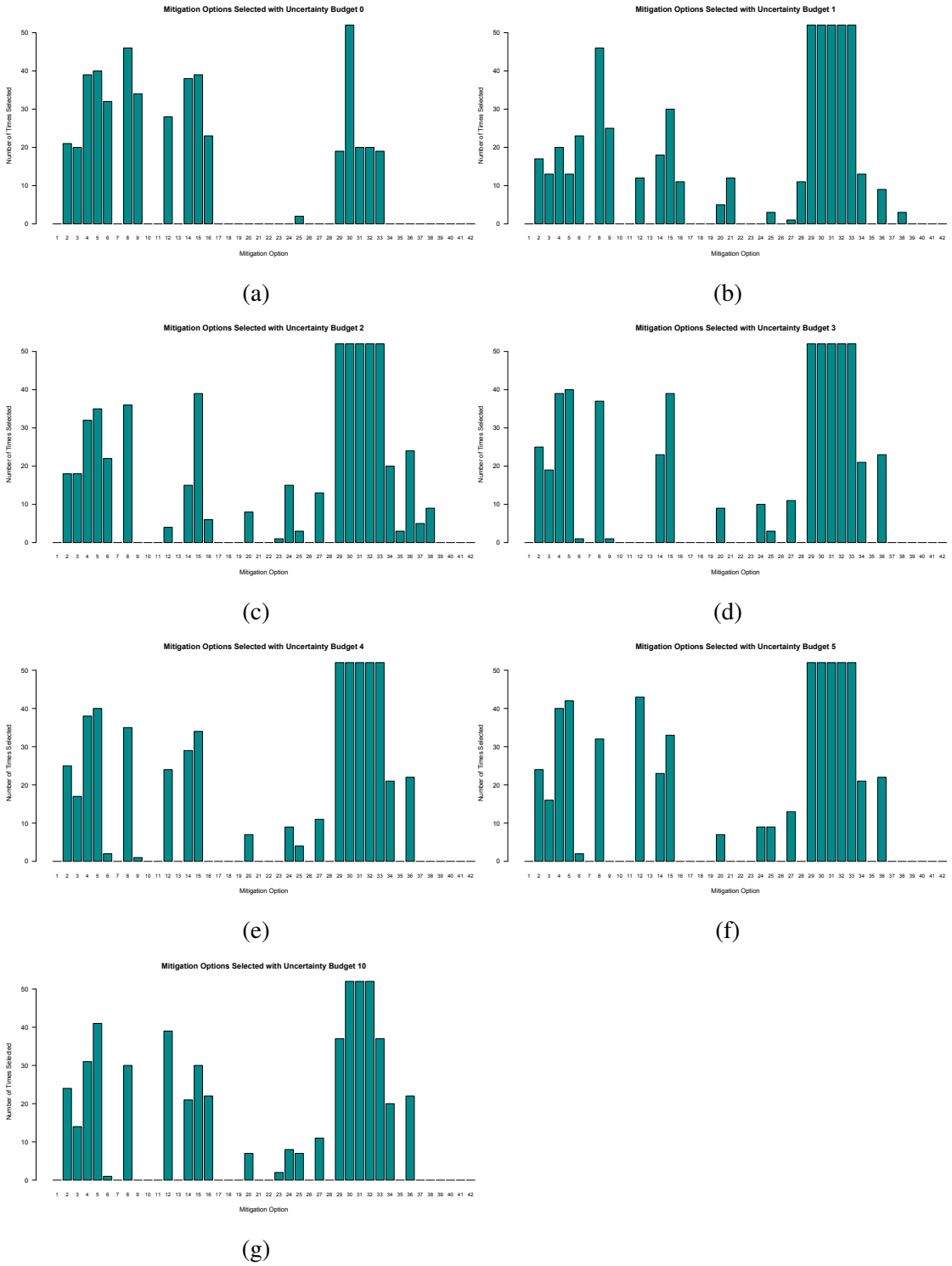

Figure 2.12: Shows the number of times each mitigation option is selected broken down by uncertainty budget, where the graphs correspond to uncertainty budgets as follows: (a) 0, (b) 1, (c) 2, (d) 3, (e) 4, (f) 5, and (g) 10.

Looking at the paths and weapon type that the adversary selects, we see that in all cases tested, New York is selected as the final target and the 10kt IND weapon is used. This behavior is understandable because, in our example, New York has the highest population - over twice that of the city of Los Angeles, which is the second highest - and the damage factor for the 10kt IND weapon is 1,000 times that of the 1kt IND weapon and 10,000 times the RDD weapon option. Since the population, weapon factor, and flow determine the overall damage, it makes sense that the model would choose the target with the highest population and weapon with the highest weapon factor. However, this may not be the case in an example in which the population and weapon factors do not vary as widely. We constructed our example in attempt to be as realistic as possible using open source data (again, no data was provided by the DNDO). If we were to construct an example with targets of more similar population sizes and weapons of more similar weapon factors we would expect to see more variability in the targets and weapon types selected by the adversary.

We also find that all paths selected are either length 5 or length 8. The arcs going from the source and to the sink comprise two arcs in every path. Each geographic arc is also split into three arcs for situational awareness, detection, and interdiction, so these paths correspond to only one or two geographic movements. This observation is, again, reasonable because there are direct flights to New York from many international locations, as well as direct maritime options. We do not consider any train option to New York directly from international ports. However, it is possible to take the train from Montreal to Albany or Toronto to Buffalo and then from either of these locations to New York, and this sequence is what we observe in the paths of length 8.

The short path lengths explain why the results are the same for all uncertainty budgets 10 and higher tested. Since mitigation options that affect air transportation will apply to all air arcs, and mitigation options that affect train transportation will apply to all train arcs, all paths of the same length that exclusively use the same single transportation type and

the same weapon type will have the same probability, and the damage will only depend on the target selected. Thus, since either a direct flight or a two legged train journey to New York is best for the adversary, the adversary need only pick one of each of these path possibilities for the defender to select the best mitigation options to use. If the adversary uses one unit of the uncertainty budget for the each of the situational awareness, detection, and interdiction arcs on these two paths, a total uncertainty budget of 9 will be used (since there are two paths, one with one transitional arc and the other with two). Thus, in this case, an uncertainty budget of only 9 is needed in order for the adversary to cause the worst case damage.

Although it is likely that the origin selected is not unique, we observe that the origin selected varies as we vary the mitigation budget and uncertainty budget and that every possible origin is selected at some point across the tests run. Figure 2.13 shows the number of times each origin is selected across the tests run for 1-17% of the maximum possible cost. The cities corresponding to the origin indices in Figure 2.13 are listed in Appendix C.

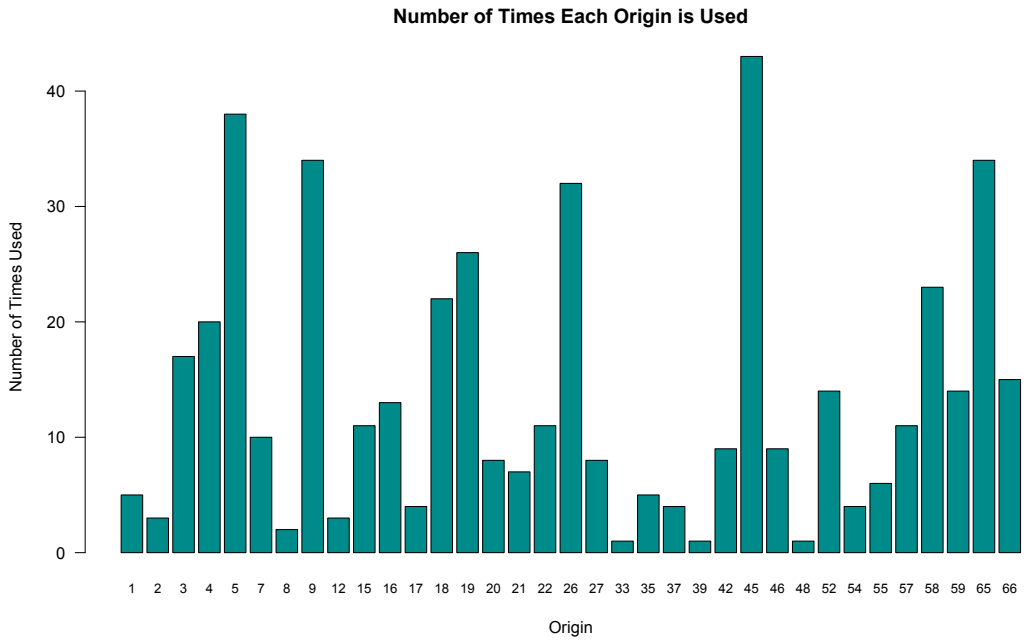

Figure 2.13: Number of times each origin is selected by the adversary across the scenarios tested. Corresponding origin cities are shown in Appendix C.

Figure 2.14 shows the path selected for five different mitigation budgets (0, 1, 5, 10, and 15% of the max cost) and uncertainty budgets 0 and 5. In these figures we only include the arcs that represent a geographic movement and exclude arcs going from/to the source/sink and the arc extensions for situational awareness, detection, and interdiction. The probability on each arc is the probability that the adversary successfully reaches the target when the given path is selected with the corresponding mitigation options in place. Figure 2.14(a) shows the paths selected with an uncertainty budget of 0. The path from Taipei to New York is taken when the mitigation budget is 0% and 5% of the max cost, where the higher probability is associated with the 0% path. The path from Hong Kong to New York is taken when the mitigation budget is 10% and 15% of the max cost. The path from Amsterdam to New York is taken when the mitigation budget is 1% of the max cost. Figure 2.14(b) shows the paths selected with an uncertainty budget of 5. The path from Montreal to Albany to New York is taken when the mitigation budget is 0% of the max cost, Paris to New York when the budget is 1% of the max cost, Singapore to New York when the budget is 5% of the max cost, Antwerp to New York when the budget is 10% of the max cost, and Felixtowe to New York when the budget is 15% of the max cost.

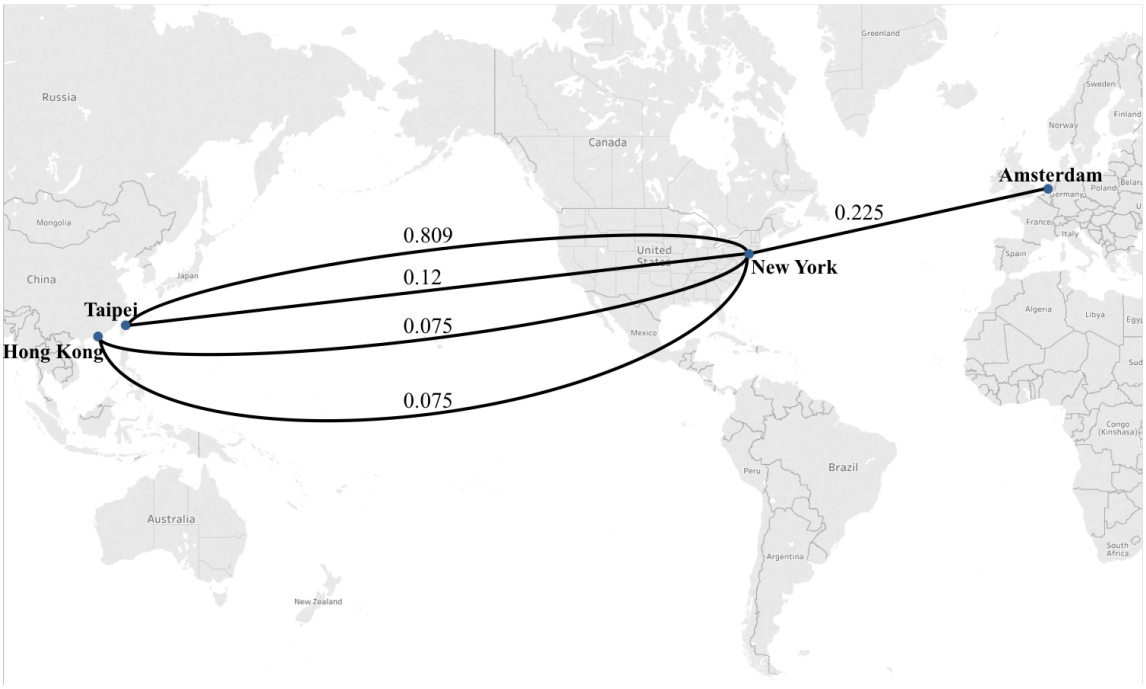

(a)

(b)

Figure 2.14: Shows the path selected for five different mitigation budgets (0, 1, 5, 10, and 15% of the max cost) and uncertainty budgets (a) 0 and (b) 5. The probability on each arc is the probability that the adversary successfully traverses the arc with the selected mitigation options in place.

2.6 Discussion

Overall we observe that uncertainty in the adversary's probability of success can have a large impact on both the damage inflicted and the mitigation options selected. In fact, for the example tested, the decrease in damage from decreasing the uncertainty budget is much greater than the decrease in damage from increasing the mitigation budget. Although the damage is greater with a higher uncertainty budget, we see a similar pattern across all uncertainty budgets in how the damage changes as the budget is increased. In particular, the decrease in damage is greatest for the first 1-2% increase in mitigation budget from 0, and then decreases at a slower rate as the mitigation budget continues to increase, with one exception between around 13-14% of the max cost with an uncertainty budget of 2.

Our results indicate that when optimizing a defense investment portfolio it is important to consider not only which mitigation options to select but also ways to better understand the option parameters. In certain cases, it may be prudent to invest fewer funds in adding mitigation resources and instead invest in reducing uncertainty in the effectiveness of these options. For example, we might be able to reduce uncertainty through increasing intelligence about the adversary's abilities or through research and development to improve our understanding of how effective each sensor type is against each weapon type. Our method gives a framework for determining how to allocate monetary resources between these two areas (selecting mitigation options and research to improve understanding of the option capabilities). Our model allows the decision maker to control how conservative to be in accounting for uncertainty via the uncertainty budget. By varying both the uncertainty budget and the defense budget, the decision maker can observe key inflection points that show where changing the budget will have the biggest impact. In the case we tested, for example, the defender may decide to invest 2% of the cost to implement all mitigation options in adding mitigation resources and use the remainder of the budget for improving understanding of the adversary's probability of success along each arc.

We also observe that the mitigation options selected throughout the instances tested are well spread across the three different transportation types considered. This result emphasizes the importance of simultaneously strengthening every area of defense rather than just air, land, or sea transport individually. Since there are different mitigation options affecting each of these sectors, optimizing across sectors would not be possible without considering multiple mitigation options, as we have done. With this in mind, our model could also be used as an iterative tool to identify weak portions of the network and continue to improve the system as the adversary's capabilities change over time. Although we only consider a single attack here, the model could be solved multiple times with updated probabilities based on how long the adversary has observed the system and the current mitigation options in place.

2.7 Conclusion

In this work we study the problem of selecting an optimal set of defense options to strengthen a network against a potential malicious attack, under uncertainty. We develop a robust optimization model and solution algorithm for selecting mitigation options to defend this network, where the adversary's objective is to cause as much damage as possible across a set of potential targets and the defender's objective is to minimize this damage.

This problem lends itself to a bi-level programming framework and falls under the category of network interdiction problems. However, there are some key distinctions between our problem of interest and approach and other network interdiction problems that have been studied. In particular, unlike studies that have simply considered which arcs to defend with a single defense option, we are interested in selecting a set of mitigation options that will work in conjunction to minimize the overall threat to the system. We consider three attributes of defense: situational awareness, detection, and interdiction, and study the combined impact of mitigation options that vary in strength in each of these areas. This approach allows us to consider joint strengths of complementary mitigation options in a

way that we haven't seen done before. Through this same approach we could combine any number of attributes describing the mitigation options. Although our approach was motivated by the Global Nuclear Detection Architecture it could be used in any situation for which a defender has multiple options for protecting a network.

Since we cannot know the adversary's probability of success with certainty, we consider a robust variation where a certain number of arcs are allowed to deviate from the nominal value. The additional constraints required to consider multiple mitigation options make our problem such that it cannot be reformulated as a single level program, which is the standard approach to solving bi-level programs. We develop a constraint generation based algorithm to solve the problem, which we plan to test on other problems as well in the future.

We test our method on a large example of the U.S. supply chain network, including international and domestic ports, and air, train, and maritime transport. We find that increasing the mitigation budget has the greatest impact on the resulting expected damage in the first few percent of the total cost to implement all mitigation options considered. We also find that decreasing the uncertainty budget has a much greater impact on expected damage than increasing the mitigation budget does. This observation suggests that gaining a better understanding of the adversary's capabilities and probability of successfully evading defense options would be an additional worthwhile investment along with funding the implementation of mitigation options.

CHAPTER 3
THE IMPACT OF DEVELOPMENT PRIORITIES ON POWER GENERATION EXPANSION PLANNING IN SUB-SAHARAN AFRICA

3.1 Literature Review

Many researchers have considered decentralized options as a way to reach rural villages more quickly and cost-effectively than expansion of the centralized power grid. Alfaro and Miller [41] compare the costs of four different decentralized electricity technologies in Liberia to rural Liberians' stated and demonstrated (through current kerosene expenditures) willingness to pay and find that the costs of small hydropower and biomass resources are less than the demonstrated willingness to pay. Brent and Rogers [42] perform a sustainability assessment on a proposed wind-solar off-grid system with storage in South Africa. They determine that the off-grid system studied is not sustainable, but suggest requirements to make such a system effective. Camblonga *et al.* [43] conducted surveys in three regions of Senegal to analyze potential electricity demand and study factors related to electricity development through village-centered micro-grids. Zeyringer *et al.* [44] take a two step approach to analyze distributed photovoltaic (PV) electrification options in Kenya, using regression to estimate electricity demand and then optimizing to select between grid extension and solar PV options. Ohiare [45] compares off-grid, mini-grid, and grid electrification options in Nigeria and determines that the grid option is the cheapest for most areas. However, the grid electricity cost used in this study only includes the cost of the grid connection and not the cost of centralized generation. Sanoh *et al.* [46] compare costs and grid expansion plans with centralized grid, mini-grid diesel, and off-grid PV-diesel options for electrification with a case study of Senegal and find that their results depend highly on the electricity demand and cost of transmission lines. Ilskoga *et al.* [47] propose electric-

ity co-operatives as a solution for rural electrification, citing an electricity co-operative in Tanzania as a successful example.

Levin and Thomas [48] present an algorithm to select which demand nodes would best be served by grid power in developing countries, assuming the remaining demand would be met by decentralized options. In a follow up study they develop a mixed integer program to analyze trade-offs between centralized and decentralized infrastructure for various levels of future demand using a case study of Rwanda [49]. In another study, Levin and Thomas [50] compare three distributed generation financing mechanisms to the cost of centralized grid subsidies and find that distributed generation subsidies are often a lower cost option for providing electricity in rural areas.

In evaluating electrification options for developing countries it is important to consider related policies and the electrification budget. Ahlborg and Hammar [51] find government policies and priorities to be the key driver for electrification, while limited funds and technical capabilities are a barrier.

More generally, there have been numerous technical reports and energy reviews for Africa, whether from government organizations, non-profit organizations, or independent consultants, analyzing the current situation as well as projecting electricity development pathways and setting electrification goals. The International Energy Agency [4] presents a broad overview of the energy situation in Africa in its Africa Energy Outlook report. McKinsey & Company's Brighter Africa report [52] gives predictions for electricity demand growth in Africa to 2040 based on desired growth in gross domestic product (GDP) and experience with more developed emerging markets about the percent increase necessary to achieve such growth. This report also discusses development path alternatives such as inter-country generation and renewable generation and considers the Grand Inga hydroelectric plant and potential natural gas discoveries, two situations that could potentially have a significant impact on electricity development in Africa. The International Renewable Energy Agency developed a power planning tool for electricity development in Southern Africa

and used this tool to analyze a development scenario with an emphasis on renewables [53]. Bazilian *et al.* [54] develop five demand scenarios for sub-Saharan Africa, excluding South Africa, to 2030 and determine that a much greater level of capacity will be required to meet 100% of demand by 2030 than has been projected by previous studies.

There have also been reports and reviews specifically addressing Rwanda. The African Development Bank Group [55] gives an overview of the energy situation in Rwanda and lays out plans and requirements for future development. They do not take an optimization approach, however. The Technical Assistance Facility for the SE4All Initiative [5, 56, 57, 58] has also written a series of draft reports outlining electricity development and financing strategies for Rwanda. Safari [59] gives an overview of the state of energy demand and production in Rwanda as of 2010.

Most closely related to our present work are a number of papers that use optimization to evaluate large scale electrification decisions without specifically focusing on centralized versus decentralized systems. Sanoh *et al.* [60] develop a simple linear program to determine energy types to be built across Africa to meet increasing demand, only considering inter-country transmission and assuming costs are shared between countries. Heinrich *et al.* [61] modify the MARKAL power system planning model to include emissions taxes and demand uncertainty, solving for a case study of South Africa. Panos *et al.* [62] also use MARKAL, combined with an econometric model, to analyze two electricity development scenarios, one prioritizing economic development and the other prioritizing environmental impact, for Latin America, Asia, and sub-Saharan Africa. Ekholm *et al.* [63] use a similar model, adding constraints on the cost of capital, to analyze the effect on generation mix, electricity cost, and CO_2 emissions. Arndt *et al.* [64] combine two previously developed tools (an optimization model and a general equilibrium model) to analyze the impact of a carbon tax and import regulations on electricity demand, price, and greenhouse gas emissions, as well as GDP and employment in South Africa. Although these studies consider certain policy modifications, such as emissions taxes or cost of capital constraints, to stan-

dard power system planning models they all assume that the demand specified will be fully met. Even Heinrich *et al.* [61], who consider demand uncertainty through a scenario tree of a few demand cases, still assume that the realized demand will be met, possibly in a more costly way than if there were no uncertainty. In contrast, we specify, as a parameter, the fraction of demand to be met in each year of the time horizon and separate this parameter from the potential demand in order to compare the costs of electrification under four different metrics that allow for gradually increasing electrification rates over time and explicitly consider urban and rural electrification in each region. Furthermore, the generation decisions made in the above studies are all at a low resolution, for the whole country or even multi-country region. In contrast, we consider a higher resolution of regional information within the country and account for both rural and urban demand in each region.

Balachandra and Chandru [65] consider unmet demand by specifying a cost for unmet demand in their objective function. However, they are concerned with the tactical planning problem, not the long term capacity expansion problem that we study. Additionally, they also consider the region (a state in India) as a whole, rather than considering specific locations of generators and demand within the region. Their main focus is on determining at what point it becomes economical to build new capacity rather than letting demand go unmet. Our objective is determine a least cost power generation and transmission portfolio in order to meet a certain fraction of demand.

Furthermore, unlike other studies we have seen for developing countries, we account for both long term capacity expansion decisions and short term power output and transmission decisions by using a representative day for each year in the time horizon, similar to what was done for the U.S. in Mai *et al.* [66]. We choose to use an average representative day rather than, for example, the peak day because electricity is still underdeveloped in sub-Saharan Africa, so we are more interested in meeting average demand for a large fraction of the population than meeting 100% of demand for a smaller fraction of the population. We also directly consider both urban and rural populations as well as centralized

and decentralized generator types to explicitly account for the specific factors that impact electricity development in Africa.

3.2 Model

We develop a geospatial-temporal power generation expansion planning model for sub-Saharan Africa. We model two levels of timesteps to capture both strategic and operational planning decisions. We optimize over T years, considering a sample hourly profile for each year in order to capture hourly variations in load, wind potential, and solar potential. We scale the costs based on this hourly profile to represent the costs for the full year. Currently we assume that the sample hourly profile consists of consecutive hours. This is a reasonable assumption because the countries we are most interested in lie on or near the equator, so any seasonal variations are small. However, the model could easily be modified to consider a few disjoint sets of consecutive hours to represent different seasons.

Decisions about generators, storage units, and transmission lines to build or retire are made on an annual basis, whereas decisions related to the energy output are made on an hourly basis. The allowed emissions are also on an annual basis. We add constraints on the fraction of demand that must be met at each time period, and consider variations on this requirement to address the case in which 100% of demand cannot be met. For the power storage decisions, we assume that the state of the storage system within a year is cyclic. For example, if we use a 24-hour representative day for the year, the starting state (hour 0) will be the same as the end state (hour 24) within each year.

3.2.1 Nomenclature

Variables and parameters that will be used throughout the various models are defined below. Values in parentheses at the end of the variable description indicate the units. We use C and D to denote centralized and decentralized resources, respectively. Within each region, we consider an urban and rural part, which we call the "region type."

Index Sets:

- $g \in \mathcal{G}$: generator types. Let $\mathcal{G}^C$ denote centralized generation types and $\mathcal{G}^D$ distributed generation types, so $\mathcal{G} = \mathcal{G}^C \cup \mathcal{G}^D$. Let $\mathcal{G}^{\text{fixed}}$ be the generator types that are dispatchable (i.e. for which generation can be controlled), and $\mathcal{G}^{\text{var}}$ be those that are non-dispatchable (i.e. for which availability depends on the weather and thus varies by time).

- $i \in \mathcal{L}$: transmission line types, which vary by voltage

- $j \in \mathcal{RT}$: resource types. Let $\mathcal{G}^j$ be the set of generators that use resource type j. Let $\mathcal{RT}^{\text{renewable}}$ be the set of renewable resources (i.e. those for which consumption now does not deplete future reserves) and $\mathcal{RT}^{\text{depletable}}$ be the set of non-renewable resources.

- $t \in \mathcal{T} := \{1, \ldots, T\}$: years in the time horizon. The optimization horizon is from 1 to the final year T. The system is in its initial state when $t = 0$. However, we also allow for negative indices on parameters related to construction in order to consider units that have begun, but not completed, construction before the start of the optimization horizon.

- $h \in \mathcal{H} := \{1, \ldots, H\}$: set of consecutive hours used for hourly decisions within each year

- $v \in \mathcal{V}$: regions in the country, before accounting for urban and rural components

- $r \in \mathcal{R}$: region types (0 for rural, 1 for urban). Thus, $(v, 0)$ denotes the rural part of region v, and $(v, 1)$ denotes the urban part of region v.

Decision Variables[1]:

[1]For all variables that are indexed over the region type (r) and the generation type (g), the variable is fixed to 0 for centralized generation systems in rural regions because we assume that these systems are only constructed in urban areas. This assumption is without loss of generality because the rural and urban areas within each district are not geographically separated in our model, so the transmission cost between them is 0.

- $p^{\text{gen}}_{vrgth} \in \mathbf{R}_+$: energy output from generator type g at location v, region type r, in year t and hour h (MWh)

- $p^{\text{store}}_{vrth} \in \mathbf{R}_+$: energy in storage at location v, region type r, in year t at the end of hour h (MWh)

- $p^{\text{store+}}_{vrth} \in \mathbf{R}_+$: energy increase in storage at location v, region type r, in year t and hour h, before losses (MWh)

- $p^{\text{store}-}_{vrth} \in \mathbf{R}_+$: energy extracted from storage at location v, region type r, in year t and hour h, before losses (MWh)

- $p^{\text{trans}}_{v_1 v_2 ith} \in \mathbf{R}_+$: energy transmitted from supply node v_1 to sink node v_2 across transmission line type i in year t and hour h, before losses (MWh)

- $p^{\text{use-}C}_{vrth} \in \mathbf{R}_+$: energy consumed from centralized resources at node v, region type r, in year t and hour h, after losses (MWh)

- $p^{\text{use-}D}_{vrth} \in \mathbf{R}_+$: energy consumed from decentralized resources at node v, region type r, in year t and hour h (MWh)

- $z^{\text{gen}}_{vrgt} \in \mathbf{R}_+$: installed generation capacity of type g at location v, region type r, and year t. When $t = 0$ this is an input parameter. (MW)

- $z^{\text{gen}+}_{vrgt} \in \mathbf{R}_+$: generation capacity of type g, for which construction begins at location v, region type r, at the beginning of year t. For $t \in \{-CT^{\text{gen}}_g + 1, \ldots, 0\}$ this is an input parameter. (MW)

- $z^{\text{gen}-}_{vrgt} \in \mathbf{R}_+$: generation capacity of type g retired at location v, region type r, at the beginning of year t (MW)

- $z^{\text{store}}_{vrt} \in \mathbf{R}_+$: installed storage capacity at location v, region type r, and year t (MWh)

- $z^{\text{trans}}_{v_1 v_2 i t} \in \mathbf{R}_+$: available transmission capacity of type i between nodes v_1 and v_2 in year t. When $t = 0$ this is an input parameter. Note that $z^{\text{trans}}_{v_1 v_2 t} = z^{\text{trans}}_{v_2 v_1 t}$, so we only define $z^{\text{trans}}_{v_1 v_2 t}$ for $v_2 > v_1$. (MW)

- $z^{\text{trans+}}_{v_1 v_2 i t} \in \mathbf{R}_+$: new transmission capacity of type i between nodes v_1 and v_2, for which construction is started at the beginning of year t. For $t \in \{-CT^{\text{trans}_i} + 1, \ldots, 0\}$ this is an input parameter. As for $z^{\text{trans}}_{v_1 v_2 i t}$, we only define $z^{\text{trans+}}_{v_1 v_2 i t}$ for $v_2 > v_1$. (MW)

Parameters[2]:

- α: factor governing the relationship between solar home system capacity and associated battery capacity (h)

- H^{annual}: number of times that the hourly interval occurs in a year. For example, if H is 24, H^{annual} will be 365.

- $c^{\text{Const-gen}}_{gt}$: capital cost for generator type g in year t ($/MW)

- $c^{\text{Const-trans}}_{it}$: capital cost for a new transmission line of type i in year t ($/(MW·km))

- c^{dist}: cost to distribute centralized resources before losses ($/MWh)

- c^{gen}_{gt}: fuel cost after losses for generator type g in year t. For resources that are not fuel based this cost is 0. ($/MWh)

- $c^{\text{OM-gen-fixed}}_{g}$: annual (fixed) operations and maintenance cost for generation type g. Assume the same across all locations. ($/MW)

- $c^{\text{OM-gen-var}}_{g}$: variable operations and maintenance cost for generation type g. Assume the same across all locations. ($/MWh)

- $c^{\text{OM-trans}}_{i}$: annual operations and maintenance costs for transmission lines of type i. Assume the same across all locations. ($/(MW·km))

[2] All costs are before discounting, and transmission and distribution parameters only apply to centralized resources.

- $\text{Cap}_{vj}^{\text{resource}}$: resource potential at each period for renewable resource type j at location v, before losses (MW)

- CO_{2eq_g}: CO_2-equivalent emissions per unit energy output from generation type g (tons/MWh)

- $\text{CO}_{2\text{eq}_t}^{\text{max}}$: maximum allowed CO_2-equivalent emissions from all plant types in period t (tons)

- CT_g^{gen}: construction time to build generator type g (years)

- CT_i^{trans}: construction time to build transmission lines of type i (years)

- d_{vrth}: energy demand at node v, region type r, in year t and hour h (MWh)

- $\delta_{v_1 v_2}$: distance between nodes v_1 and v_2. Note that $\delta_{v_1 v_2} = \delta_{v_2 v_1}$. (km)

- E_{vj}^{resource}: total energy available across the time horizon from depletable resource type j in region v (MWh)

- $f_g^{\text{gen-fixed}}$: capacity factor of generator $g \in \mathcal{G}^{\text{fixed}}$, i.e., the maximum fraction of total capacity fixed generator g can generate in any hour (decimal between 0 and 1)

- $f_{vgh}^{\text{gen-var}}$: fraction of peak capacity of generator $g \in \mathcal{G}^{\text{var}}$ at node v that is available at hour h (decimal between 0 and 1)

- $f_t^{\text{elec-tot}}$: minimum total fraction of demand to be met in year t (decimal between 0 and 1)

- $f_{vt}^{\text{elec-reg}}$: minimum fraction of demand to be met for node (region) v in year t. When $t = 0$ this is the initial fraction of demand that is met at node v. (decimal between 0 and 1)

- f_{vg}^{peak}: fraction of overall peak potential capacity from generator type $g \in \mathcal{G}^{\text{var}}$ available in region v at peak output (applies specifically to wind and solar power, for which overall potential varies by region). (decimal between 0 and 1)
- $f_g^{\text{ramp}+}$: max ramp up rate for dispatchable generators as a fraction of the end energy output (decimal between 0 and 1)
- $f_g^{\text{ramp}-}$: max ramp down rate for dispatchable generators as a fraction of the end energy output (decimal between 0 and 1)
- ℓ_i^{trans}: transmission losses per distance for line type i ((decimal between 0 and 1)/km)
- γ: discount rate for a year (decimal between 0 and 1)
- η^{dist}: distribution efficiency (decimal between 0 and 1)
- η_g^{gen}: efficiency of generator type g (decimal between 0 and 1)
- $\eta^{\text{store}+}$: efficiency when charging storage (decimal between 0 and 1)
- $\eta^{\text{store}-}$: efficiency when discharging storage (decimal between 0 and 1)
- LT_g^{gen}: lifetime of generator type g, starting when construction is completed (years)
- $\tau^{\text{store+}}$: time to fully charge storage unit (h)
- $\tau^{\text{store-}}$: time to fully discharge storage unit (h)

3.2.2 Objective

We seek to minimize the discounted cost of electrifying a given percent of the population over the time horizon,

$$\min \sum_{t=1}^{T} \frac{1}{(1+\gamma)^t} \Bigg(\sum_{v \in \mathcal{V}} \sum_{r \in \mathcal{R}} \sum_{g \in \mathcal{G}} (c_{gt}^{\text{Const-gen}} z_{vrgt}^{\text{gen}+} + c_g^{\text{OM-gen-fixed}} z_{vrgt}^{\text{gen}} + H^{\text{annual}} \sum_{h=1}^{H} (c_g^{\text{OM-gen-var}} + c_{gt}^{\text{gen}}) p_{vrgth}^{\text{gen}}) + \sum_{\substack{v_1, v_2 \in \mathcal{V}: \\ v_1 < v_2}} \sum_{i \in \mathcal{L}} \delta_{v_1 v_2} (c_t^{\text{Const-trans}_i} z_{v_1 v_2 it}^{\text{trans}+} + c_i^{\text{OM-trans}} z_{v_1 v_2 it}^{\text{trans}}) + H^{\text{annual}} \sum_{v \in \mathcal{V}} \sum_{r \in \mathcal{R}} \sum_{h=1}^{H} c^{\text{dist}} \frac{p_{vrth}^{\text{use-}C}}{\eta^{\text{dist}}} \Bigg). \tag{3.1}$$

The first set of terms in the sum represents the generation cost, both the cost to construct and maintain generators and the cost to generate power. The second set of terms represents the cost of building and maintaining transmission lines and transmitting power. The third set of terms is the cost of distributing electricity. $\frac{p_{v_2rth}^{\text{use-}C}}{\eta^{\text{dist}}}$ gives the energy distributed from centralized resources before losses. A distribution cost is not incurred for decentralized resources. Furthermore, we do not include storage costs because we only consider storage units (batteries) that are paired with solar home systems, and the cost to install these batteries will be included in the cost of the solar home systems.

3.2.3 Constraints

Power Balance and Availability Constraints

The following constraints regulate the expansion of the system and feasible generation output. Although we only consider power generation system expansion decisions and the associated costs on an annual scale, we model hourly power output to ensure the generation and transmission capacities are sufficient to meet the demand requirements.

First, we must have power balance throughout the system. We have different power balance constraints for centralized and decentralized resources because decentralized resources are disconnected from the transmission and distribution system. We assume that

centralized resources can only be built in urban regions, but energy from these resources may be distributed in urban or rural regions. Distributed resources may be built in urban or rural regions, but energy from these resources must be consumed in the same region that it is produced.

The constraints governing power balance of centralized resources are,

$$\sum_{g \in \mathcal{G}^C} p^{\text{gen}}_{v_2 1 g t h} + \sum_{v_1 \in \mathcal{V}} \sum_{i \in \mathcal{L}} \max(0, 1 - \ell^{\text{trans}}_i \delta_{v_1 v_2}) p^{\text{trans}}_{v_1 v_2 i t h} = \sum_{v_1 \in \mathcal{V}} \sum_{i \in \mathcal{L}} p^{\text{trans}}_{v_2 v_1 i t h} + \sum_{r \in \mathcal{R}} \frac{p^{\text{use-}C}_{v_2 r t h}}{\eta^{\text{dist}}}$$
$$\forall\, v_2 \in \mathcal{V}, t \in \mathcal{T}, h \in \mathcal{H}. \quad (3.2)$$

In the above constraints, the left hand side is the energy available from centralized resources to node v_2 in hour h of year t, either from generation at node v_2 or transmission from other nodes. Recall that for the index r, 0 corresponds to rural and 1 corresponds to urban regions, so the generation term on the left hand side indicates that centralized generation is only allowed in urban regions. The right hand side is centralized energy that is used at node v_2, both in urban and rural regions, either by sending it to other nodes or consuming it to meet demand. We divide $p^{\text{use-}C}_{v_2 r t h}$ by η^{dist} to get the energy used prior to distribution losses.

The constraints for distributed resources are similar except we do not allow for transmission between regions, and we consider storage for solar home systems,

$$\sum_{g \in \mathcal{G}^D} p^{\text{gen}}_{v r g t h} + \eta^{\text{store}-} p^{\text{store}-}_{v r t h} = p^{\text{use-}D}_{v r t h} + p^{\text{store}+}_{v r t h} \;\forall\, v \in \mathcal{V}, r \in \mathcal{R}, t \in \mathcal{T}, h \in \mathcal{H}. \quad (3.3)$$

We do not divide $p^{\text{use-}D}_{v r t h}$ by η^{dist} because the distribution efficiency only applies to centralized resources that are distributed within a region. We assume that decentralized resources are close enough to the demand that distribution costs and losses are negligible.

The power sent along each edge cannot exceed the available transmission capacity. Thus, we require the following constraints,

$$p^{\text{trans}}_{v_1 v_2 i t h} + p^{\text{trans}}_{v_2 v_1 i t h} \leq z^{\text{trans}}_{v_1 v_2 i t} \cdot (1 \text{ hr}) \quad \forall \{v_1, v_2 \in \mathcal{V} : v_2 > v_1\}, i \in \mathcal{L}, t \in \mathcal{T}, h \in \mathcal{H}, \tag{3.4}$$

$$p^{\text{trans}}_{v_1 v_2 i t h} = 0 \quad \forall \{v_1, v_2 \in \mathcal{V} : v_2 = v_1\}, i \in \mathcal{L}, t \in \mathcal{T}, h \in \mathcal{H}. \tag{3.5}$$

We multiply by 1 hour to convert the transmission line capacity to MWh for the hour. In the first set of constraints, we add $p^{\text{trans}}_{v_1 v_2 i t h}$ and $p^{\text{trans}}_{v_2 v_1 i t h}$ because the energy transmitted is directional, but the transmission line capacity is not. At optimality, one of the two values in the sum will be 0.

We cannot generate more than the available capacity for each generation type at each location. These constraints are slightly different for generation types for which availability varies within the hour than for those for which it is constant. For generation types that are dispatchable we have,

$$p^{\text{gen}}_{v r g t h} \leq f^{\text{gen-fixed}}_{g} z^{\text{gen}}_{v r g t} \cdot (1 \text{ hr}) \; \forall \, v \in \mathcal{V}, r \in \mathcal{R}, g \in \mathcal{G}^{\text{fixed}}, t \in \mathcal{T}, h \in \mathcal{H}. \tag{3.6}$$

We also have max ramp-up and ramp-down constraints for dispatchable generators,

$$p^{\text{gen}}_{v r g t 1} - p^{\text{gen}}_{v r g t H} \leq f^{\text{ramp+}}_{g} z^{\text{gen}}_{v r g t} \; \forall \, v \in \mathcal{V}, r \in \mathcal{R}, g \in \mathcal{G}^{\text{fixed}}, t \in \mathcal{T}, \tag{3.7a}$$

$$p^{\text{gen}}_{v r g t h} - p^{\text{gen}}_{v r g t (h-1)} \leq f^{\text{ramp+}}_{g} z^{\text{gen}}_{v r g t} \; \forall \, v \in \mathcal{V}, r \in \mathcal{R}, g \in \mathcal{G}^{\text{fixed}}, t \in \mathcal{T}, h \in \{2, \ldots, H\}. \tag{3.7b}$$

$$p^{\text{gen}}_{vrgtH} - p^{\text{gen}}_{vrgt1} \leq f^{\text{ramp}-}_{g} z^{\text{gen}}_{vrgt} \; \forall \, v \in \mathcal{V}, r \in \mathcal{R}, g \in \mathcal{G}^{\text{fixed}}, t \in \mathcal{T}, \tag{3.8a}$$

$$p^{\text{gen}}_{vrgt(h-1)} - p^{\text{gen}}_{vrgth} \leq f^{\text{ramp}-}_{g} z^{\text{gen}}_{vrgt} \; \forall \, v \in \mathcal{V}, r \in \mathcal{R}, g \in \mathcal{G}^{\text{fixed}}, t \in \mathcal{T}, h \in \{2, \ldots, H\}. \tag{3.8b}$$

We assume that the hourly horizon within each year is cyclic in Constraints (3.7a) and (3.8a).

For generation types that are non-dispatchable (specifically wind and solar power) we multiply both by the fraction of maximum potential that would be available at peak times and the fraction of this value that is available at the given time,

$$p^{\text{gen}}_{vrgth} \leq f^{\text{peak}}_{vg} f^{\text{gen-var}}_{vgh} z^{\text{gen}}_{vrgt} \cdot (1 \text{ hr}) \; \forall \, v \in \mathcal{V}, r \in \mathcal{R}, g \in \mathcal{G}^{\text{var}}, t \in \mathcal{T}, h \in \mathcal{H}. \tag{3.9}$$

In this case both of the fractions f^{peak}_{vg} and $f^{\text{gen-var}}_{vgh}$ depend on the region because the effectiveness of the installed generators depends on how strong the (wind or solar) resource is in that region. As for transmission, we multiply by 1 hour to convert the generation capacity to MWh for the hour in both (3.6) and (3.9).

Similarly, we cannot store more than the current storage capacity,

$$p^{\text{store}}_{vrth} \leq z^{\text{store}}_{vrt} \; \forall \, v \in \mathcal{V}, r \in \mathcal{R}, t \in \mathcal{T}, h \in \mathcal{H}. \tag{3.10}$$

The only type of storage we consider is batteries paired with solar home systems, so we have an additional requirement that we can only increase storage up to the amount that is generated from solar home systems in each period,

$$p_{vrth}^{\text{store}+} \leq p_{vrgth}^{\text{gen}} \; \forall \, v \in \mathcal{V}, r \in \mathcal{R}, g = SHS, t \in \mathcal{T}, h \in \mathcal{H}. \tag{3.11}$$

where SHS indicates the generation type is solar home systems.

We also cannot extract more from storage than is available at the current period,

$$p_{vrth}^{\text{store}-} \leq p_{vrth}^{\text{store}} \; \forall \, v \in \mathcal{V}, r \in \mathcal{R}, t \in \mathcal{T}, h \in \mathcal{H}. \tag{3.12}$$

Energy balance constraints ensure that the energy in storage the energy in storage must equal the energy in storage in the previous period plus the change in energy,

$$p_{vrt1}^{\text{store}} = p_{vrtH}^{\text{store}} + \eta^{\text{store}+} p_{vrt1}^{\text{store}+} - p_{vrt1}^{\text{store}-} \; \forall \, v \in \mathcal{V}, r \in \mathcal{R}, t \in \mathcal{T}, \tag{3.13a}$$

$$p_{vrth}^{\text{store}} = p_{vrt(h-1)}^{\text{store}} + \eta^{\text{store}+} p_{vrth}^{\text{store}+} - p_{vrth}^{\text{store}-} \; \forall \, v \in \mathcal{V}, r \in \mathcal{R}, t \in \mathcal{T}, h \in \mathcal{H}. \tag{3.13b}$$

We assume that the hourly horizon within each year is cyclic in Constraints (3.13a).

Additionally, the change of energy in storage in each hour is restricted by the maximum charge/discharge rate,

$$\frac{p_{vrth}^{\text{store+}}}{1 \text{ hr}} \leq \frac{z_{vrt}^{\text{store}}}{\tau^{\text{store+}}} \; \forall \, v \in \mathcal{V}, r \in \mathcal{R}, t \in \mathcal{T}, h \in \mathcal{H}, \tag{3.14}$$

$$\frac{p_{vrth}^{\text{store-}}}{1 \text{ hr}} \leq \frac{z_{vrt}^{\text{store}}}{\tau^{\text{store-}}} \; \forall \, v \in \mathcal{V}, r \in \mathcal{R}, t \in \mathcal{T}, h \in \mathcal{H}. \tag{3.15}$$

Construction, Retirement, and Capacity Constraints

Assume that the lifetime of the plant starts when construction is completed, and plants are retired the year after their lifetime is reached. Generator extensions are not considered. To ensure that generators have been retired by their lifetime, we require that at least as many generators have been retired by period t as have started construction by period $t - LT_g^{\text{gen}} - CT_g^{\text{gen}}$,

$$z_{vrg0}^{\text{gen}} + \sum_{t=-CT_g^{\text{gen}}+1}^{\tau-LT_g^{\text{gen}}-CT_g^{\text{gen}}} z_{vrgt}^{\text{gen}+} \leq \sum_{t=1}^{\tau} z_{vrgt}^{\text{gen}-} \; \forall \, v \in \mathcal{V}, r \in \mathcal{R}, g \in \mathcal{G}, \tau \in \{LT_g^{\text{gen}}+1, \ldots, T\}. \tag{3.16}$$

In Constraints (3.16), we assume that existing generation capacity in the initial state (z_{vrg0}^{gen}) will be retired LT_g^{gen} periods after the start of the time horizon. If we know the construction dates of the initial plants and want to force them to retire earlier, we can require that $\sum_{t=1}^{\tau} z_{vrgt}^{\text{gen}-} \geq Z_{vrg\tau} \; \forall \; \tau \in \{1, \ldots LT_g\}$, where $Z_{vrg\tau}$ is the number of plants in the initial configuration that must be retired by period τ, which is a constant value based on the years that the initial plants were constructed.

Generation capacity balance constraints ensure that the generation capacity at the end of year t equals the generation capacity at the end of the previous year adjusted by the capacity constructed and retired,

$$z_{vrgt}^{\text{gen}} = z_{vrg(t-1)}^{\text{gen}} + z_{vrg(t-CT_g^{\text{gen}})}^{\text{gen}+} - z_{vrgt}^{\text{gen}-} \; \forall \, v \in \mathcal{V}, r \in \mathcal{R}, g \in \mathcal{G}, t \in \mathcal{T}. \tag{3.17}$$

Since we only consider storage that is associated with solar home systems, the storage capacity is directly proportional to the capacity of solar home systems,

$$z^{\text{store}}_{vrt} = \alpha \cdot z^{\text{gen}}_{vrgt} \; \forall \; v \in \mathcal{V}, r \in \mathcal{R}, g = SHS, t \in \mathcal{T}, \tag{3.18}$$

where, again, SHS indicates the generator type is solar home systems.

We do not allow transmission lines to retire, so the transmission capacity only changes as transmission is constructed,

$$z^{\text{trans}}_{v_1 v_2 i t} = z^{\text{trans}}_{v_1 v_2 i (t-1)} + z^{\text{trans+}}_{v_1 v_2 i (t - CT^{\text{trans}}_i)} \; \forall \; \{v_1, v_2 \in \mathcal{V} : v_2 > v_1\}, i \in \mathcal{L}, t \in \mathcal{T}, \tag{3.19}$$

where $z^{\text{trans}}_{v_1 v_2 i 0}$ is the transmission capacity of type i between v_1 and v_2 at the start of the planning period.

For renewable resource types, the maximum installed capacity is constrained by the maximum resource capacity in at each location,

$$\sum_{r \in \mathcal{R}} \sum_{g \in \mathcal{G}^j} \frac{z^{\text{gen}}_{vrgt}}{\eta^{\text{gen}}_g} \leq \text{Cap}^{\text{resource}}_{vj} \; \forall \; j \in \mathcal{RT}^{\text{renewable}}, v \in \mathcal{V}, t \in \mathcal{T}. \tag{3.20}$$

The max capacity, $\text{Cap}^{\text{resource}}_{vj}$, may be infinite for some resource types. For centralized resources, capacity may only be constructed in the urban region, so we set the capacity in rural regions to 0,

$$z^{\text{gen}}_{v0gt} = 0 \; \forall \; v \in \mathcal{V}, g \in \mathcal{G}^C, t \in \mathcal{T}. \tag{3.21}$$

For depletable resources, the availability is limited by the fuel reserve, so rather than directly constraining the capacity we constrain the total power output across the time horizon

by the energy available from the corresponding fuel type in each region,

$$H^{\text{annual}} \sum_{r \in \mathcal{R}} \sum_{g \in \mathcal{G}^j} \sum_{t=1}^{T} \sum_{h=1}^{H} \frac{p_{vrgth}^{\text{gen}}}{\eta_g^{\text{gen}}} \leq E_{vj}^{\text{resource}} \; \forall \; j \in \mathcal{RT}^{\text{depletable}}, v \in \mathcal{V}. \tag{3.22}$$

Emissions Constraints

We constrain the CO_{2eq} emissions from energy generation for the year,

$$H^{\text{annual}} \sum_{g \in \mathcal{G}} \text{CO}_{2\text{eq}_g} \sum_{v \in \mathcal{V}} \sum_{r \in \mathcal{R}} \sum_{h=1}^{H} p_{vrgth}^{\text{gen}} \leq \text{CO}_{2\text{eq}_t}^{\text{max}} \; \forall \; t \in \mathcal{T}. \tag{3.23}$$

Electricity Consumption Constraints

We do not allow the energy consumed to exceed demand at any node,

$$p_{vrth}^{\text{use-}C} + p_{vrth}^{\text{use-}D} \leq d_{vrth} \; \forall \; v \in \mathcal{V}, r \in \mathcal{R}, t \in \mathcal{T}, h \in \mathcal{H}. \tag{3.24}$$

Furthermore, because demand is increasing at the rate of population growth, which is non-negative, and we never want to unelectrify previously electrified populations, we require that the energy used in each region is non-decreasing across years,

$$p_{vrth}^{\text{use-}C} + p_{vrth}^{\text{use-}D} \geq p_{vr(t-1)h}^{\text{use-}C} + p_{vr(t-1)h}^{\text{use-}D} \; \forall \; v \in \mathcal{V}, r \in \mathcal{R}, t = \{2, \ldots, T\}, h \in \mathcal{H}. \tag{3.25}$$

In the first year, the average electricity usage in each region must at least meet current electrification levels,

$$\frac{\sum_{r\in\mathcal{R}}(p^{\text{use-}C}_{vr1h}+p^{\text{use-}D}_{vr1h})}{\sum_{r\in\mathcal{R}} d_{vr1h}} \geq f^{\text{elec-reg}}_{v0} \; \forall \; v \in \mathcal{V}, h \in \mathcal{H}. \tag{3.26}$$

We do not have initial electrification rates as urban and rural values, so we only require that the total fraction of demand met across the urban and rural areas is at least the current electrification rate for each region. We assume that this holds for every hour because a population is not truly electrified if its electricity demand can only be met part of the time.

Electrification Goals

We require that a minimum percent of demand is met in each time period. We consider four variations on these constraints. These constraints distinguish our model from typical power system planning models by allowing us to consider scenarios in which demand is not fully met.

In the first variant, we require that the total demand met across all regions is at least the minimum fraction of demand,

$$\frac{\sum_{v\in\mathcal{V}}\sum_{r\in\mathcal{R}}(p^{\text{use-}C}_{vrth}+p^{\text{use-}D}_{vrth})}{\sum_{v\in\mathcal{V}}\sum_{r\in\mathcal{R}} d_{vrth}} \geq f^{\text{elec-tot}}_{t} \; \forall \; t \in \mathcal{T}, h \in \mathcal{H}. \tag{3.27}$$

In the second, we require that the total fraction demand met is at least the minimum fraction of demand for both the urban and the rural regions,

$$\frac{\sum_{v\in\mathcal{V}}(p^{\text{use-}C}_{vrth}+p^{\text{use-}D}_{vrth})}{\sum_{v\in\mathcal{V}} d_{vrth}} \geq f^{\text{elec-tot}}_{t} \; \forall \; r \in \mathcal{R}, t \in \mathcal{T}, h \in \mathcal{H}. \tag{3.28}$$

In the third, we require that the fraction of demand met in each region is at least the minimum fraction of demand for that region,

$$\frac{\sum_{r\in\mathcal{R}}(p_{vrth}^{\text{use-}C}+p_{vrth}^{\text{use-}D})}{\sum_{r\in\mathcal{R}}d_{vrth}} \geq f_{vt}^{\text{elec-reg}} \; \forall \; v\in\mathcal{V}, t\in\mathcal{T}, h\in\mathcal{H}. \tag{3.29}$$

Finally, in the fourth constraint variant we require that the minimum fraction of demand is met for both the urban and rural areas of each region,

$$\frac{p_{vrth}^{\text{use-}C}+p_{vrth}^{\text{use-}D}}{d_{vrth}} \geq f_{vt}^{\text{elec-reg}} \; \forall \; v\in\mathcal{V}, r\in\mathcal{R}, t\in\mathcal{T}, h\in\mathcal{H}. \tag{3.30}$$

We only include one of these four constraint variations at a time in our computational experiments. The first constraint variant gives the model the flexibility to select which demand is met in the most economically efficient way. The other constraint variants sacrifice some amount of economic efficiency in order to promote various measures of fairness. The second and third constraint variants are tighter than the first (assuming $f_{vt}^{\text{elec-reg}}$ is consistent with $f_{t}^{\text{elec-tot}}$), but neither one of these constraint variants is necessarily tighter than the other. The fourth constraint variant is the most restrictive, but ensures that both rural and urban regions across the country are being electrified.

Variable Bounds and Type Constraints

Finally, we restrict all variables to be non-negative,

$$p_{vrgth}^{\text{gen}} \geq 0 \; \forall \; v\in\mathcal{V}, r\in\mathcal{R}, g\in\mathcal{G}, t\in\mathcal{T}, h\in\mathcal{H}, \tag{3.31}$$

$$p_{vrth}^{\text{store}},\; p_{vrth}^{\text{store+}},\; p_{vrth}^{\text{store-}} \geq 0 \; \forall \; v\in\mathcal{V}, r\in\mathcal{R}, t\in\mathcal{T}, h\in\mathcal{H}, \tag{3.32}$$

$$p_{v_1v_2ith}^{\text{trans}} \geq 0 \; \forall \; v_1, v_2\in\mathcal{V}, t\in\mathcal{T}, h\in\mathcal{H}, \tag{3.33}$$

$$p_{vrth}^{\text{use-}C},\; p_{vrth}^{\text{use-}D} \geq 0 \; \forall \; v\in\mathcal{V}, r\in\mathcal{R}, t\in\mathcal{T}, h\in\mathcal{H}, \tag{3.34}$$

$$z^{\text{gen}}_{vrgt},\ z^{\text{gen}+}_{vgt},\ z^{\text{gen}-}_{vgt} \geq 0 \ \forall\ v \in \mathcal{V}, r \in \mathcal{R}, g \in \mathcal{G}, t \in \mathcal{T}, \tag{3.35}$$

$$z^{\text{trans}}_{v_1 v_2 it},\ z^{\text{trans}+}_{v_1 v_2 it} \geq 0 \ \forall\ \{v_1, v_2 \in \mathcal{V} : v_2 > v_1\}, t \in \mathcal{T}. \tag{3.36}$$

We don't need to explicitly enforce non-negativity for z^{store}_{vrt} since it is a fixed proportion of z^{gen}_{vrSHSt}.

3.3 Rwanda Case Study

We test our model on a case study of Rwanda. According to a report from 2015, at the end of 2014, 22% of households in Rwanda had electricity access and the government in Rwanda has set a goal of reaching 100% household electrification by 2025 [5]. Rwanda is also working to develop the natural gas reserve at Lake Kivu, which it shares with the Democratic Republic of the Congo. We analyze how the country can eventually, if not by 2025, reach this goal of complete electrification.

3.3.1 Data Sources and Assumptions

A lack of electricity implies a lack of internet, so data resources are less available for many countries in Africa than they would be in the U.S. In this section we discuss the data used, which was compiled from a variety of reports, websites, and research papers. We also discuss our methods for calculating data values that are not directly available and give our assumptions for parameters set.

All costs are in 2015 USD. For sources that do not specify a dollar year we assume that all costs are valued at the year before publication for published sources or the year the website was last updated if the source is online only and adjust to 2015 USD. Inflation rates from the United States Department of Labor, Bureau of Labor Statistics [67] are used.

Model Resolution

We use the 30 districts of Rwanda, shown in Figure 3.1, as our regions in consideration (nodes in the model), further distinguishing between urban and rural demand within each of these districts.

Figure 3.1: Map of the districts in Rwanda. Created in ArcMap using shapefile from Map Library [68].

Although the main purpose of the model is to inform long-term capacity planning decisions, it is important to capture fluctuations in demand, wind, and solar patterns that may affect these decisions. For this reason, we model two different time intervals: a year and an hour. Capacity planning decisions are made on an annual basis, and power generation decisions are made on an hourly basis. We use a 30-year time horizon with one 24-hour

representative day each year (so $H^{\text{annual}} = 365$) for hourly data. Rwanda is very close to the equator, so there is no need to capture seasonal variations. The 30-year time horizon starts in 2015. That is, year 0, the starting state, corresponds to year 2015, and we optimize from years 2016 to 2045. We use an annual discount rate of 10% [69], which is commonly used for developing countries. Hourly data and results are shown in Coordinated Universal Time (UTC).

Regional Demand and Distances

To estimate urban and rural demand we start with data on the urban and rural population in each of the 30 districts in Rwanda, as given by the 2012 Rwanda Census [70], adjusted to 2015 values using the 2010-2015 urban and rural population growth rates (6.43% and 1.42%, respectively) for Rwanda given in [71]. These value are then multiplied by the electricity demand per electrified person to get the average annual residential demand in each region. To get the total (residential, industrial, public sector, etc.) demand in each region, we divide the residential demand by the fraction of total demand that is residential, assuming the fraction that is residential does not vary by region type. The total demand is then adjusted by urban and rural growth rates to get the demand for each year in the time horizon.

The demand per electrified person, $d^{\text{elec-person}}$, is calculated according to Equation 3.37 below,

$$d^{\text{elec-person}} = \frac{p^{\text{gen-tot}} \cdot \eta^{\text{trans}} \cdot f^{\text{household}}}{\text{Pop}^{\text{tot}} \cdot f^{\text{elec}}}. \tag{3.37}$$

$p^{\text{gen-tot}}$ is the total electricity generation for the country (512 GWh in 2015 according to Rwanda Utilities Regulatory Authority, Economic Regulation Unit [72]). η^{trans} is the transmission efficiency, which was 0.8 on average from December 2015 to March 2016 accord-

ing to Rwanda Utilities Regulatory Authority, Economic Regulation Unit [72]. $f^{\text{household}}$ is the fraction of demand that is residential, i.e. household demand, (0.51 according to Republic of Rwanda Ministry of Infrastructure [73]). Pop^{tot} is the total population, as calculated previously. f^{elec} is the total fraction of the population with electricity access, which was about 23% in 2015 according to Republic of Rwanda Ministry of Infrastructure [74]. Thus, the numerator gives the total residential fulfilled demand and the denominator gives the total population with electricity access. Using the 2015 values, Equation 3.37 gives a demand per electrified person of 80.58 kWh/person/year.

The fraction of demand that is residential is given for some regions in Lahmeyer International and Electrogaz [75]. Across all other regions, we assume the fraction of demand that is residential is equal and calculate this value such that the overall fraction for the country is 0.51.

To obtain hourly values for the 24-hour representative day we divide the demand for the year by $365 \cdot 24$ to get the average hourly demand and adjust these values so the shape of the 24-hour period matches the load curve given in Miketa and Merven [53], while keeping the overall average over the 24 hours the same.

To determine the distance between each pair of nodes we used the latitude and longitude for each region given in [76] and calculate the distances between each pair using the Haversine formula.

Power Generation Resources

The generator types considered along with their corresponding resource types, dispatchability, and scale (centralized or distributed) are shown in Table 3.1. These generator types are a subset of those used in the International Renewable Energy Agency (IRENA) Southern Africa Power Pool Report [53] for which the data can be found at [77].

Table 3.1: Generator types considered and corresponding resource types, dispatchability, and scale.

Generator Type	**Resource**	**Dispatchability**	**Scale**
Diesel	Diesel	Dispatchable	Centralized
Diesel 100 kW	Diesel	Dispatchable	Distributed
Heavy Fuel Oil (HFO)	Diesel	Dispatchable	Centralized
Open Cycle Gas Turbine (OCGT)	Natural Gas	Dispatchable	Centralized
Combined Cycle Gas Turbine (CCGT)	Natural Gas	Dispatchable	Centralized
Supercritical Coal	Coal	Dispatchable	Centralized
Hydroelectric	Hydro	Dispatchable	Centralized
Small Hydroelectric	Hydro	Dispatchable	Distributed
Biomass	Biomass	Dispatchable	Centralized
Geothermal	Geothermal	Dispatchable	Centralized
Bulk Wind (20% Capacity Factor)	Wind	Variable	Centralized
Utility Solar Photovoltaic (PV)	Solar	Variable	Centralized
Rooftop PV with 2h Battery	Solar	Variable	Distributed

Generator costs for 2016 are shown in Table 3.2. All costs are adjusted to 2015 USD. Generator construction and fuel costs are based on International Renewable Energy Agency [77]. These costs vary by year due to technology advances. We linearly interpolate for years not given in International Renewable Energy Agency [77] and further adjust the capital costs to account for end of time horizon behavior. The capital costs shown in Table 3.2 are before this adjustment is made. Operations and maintenance (O&M) costs are based on Eastern Africa Power Pool (EAPP) *et al.* [78] and do not vary by year.

Table 3.2: Generator costs for 2016.

Generator Type	**Capital** (10^6 \$/MW)	**Fuel** (\$/MWh)	**Fixed O&M** (10^3 \$/MW)	**Variable O&M** (\$/MWh)
Diesel	1.16	275.48	22.50	1.88
Diesel 100 kW	0.72	275.48	22.50	1.88
HFO	1.47	161.53	22.50	1.88
OCGT	0.66	118.70	46.33	3.86
CCGT	1.16	74.18	26.32	2.20
Coal	2.61	27.50	46.33	3.86
Hydro	2.17	0.00	47.00	3.36
Small Hydro	4.22	0.00	47.00	3.36
Biomass	2.56	15.45	46.33	3.86
Geothermal	4.09	0.00	44.65	3.19
Wind	2.43	0.00	23.22	3.87
Utility PV	1.95	0.00	30.33	0.25
Rooftop PV	6.08	0.00	30.33	0.25

Table 3.3 shows the generator construction times, lifetimes, CO_{2eq} emissions, efficiencies, and maximum ramp rates. These parameters do not vary by year. Generator construction times and lifetimes are also from the International Renewable Energy Agency [77]. Thermal efficiencies are from Eastern Africa Power Pool (EAPP) *et al.* [78]. Other efficiencies are assumed to be one. The maximum ramp rates for coal, natural gas, and hydro are based on Kerl *et al.* [79], other values were assumed. We assume the maximum ramp-up and ramp-down rates are the same.

Table 3.3: Other generator data.

Generator Type	**Construction Time** (years)	**Lifetime** (years)	**CO_{2eq} Emissions** (tonnes/MWh)	**Efficiency**	**Ramp Rate**
Diesel	1	25	0.812	0.27	1
Diesel 100 kW	0	20	0.812	0.27	1
HFO	2	25	0.812	0.27	1
OCGT	2	25	0.717	0.44	1
CCGT	3	30	0.448	0.57	1
Coal	4	35	0.996	0.28	0.25
Hydro	5	50	0.010	1.00	1
Small Hydro	2	30	0.010	1.00	1
Biomass	4	30	0.054	0.17	0.25
Geothermal	4	25	0.245	1.00	1
Wind	2	25	0.025	1.00	NA
Utility PV	1	25	0.044	1.00	NA
Rooftop PV	0	20	0.044	1.00	NA

CO_{2eq} emissions are calculated from the fuel carbon content, efficiency, and upstream supply chain emissions. Fuel carbon content for coal, diesel, and natural gas is based on U.S. Energy Information Administration [80], where the average of anthracite, bituminous, lignite, and subbituminous is used for coal. For biomass, calculations are based on Food and Agriculture Organization of the United Nations [81]. Hydro, geothermal, wind, and solar resources are assumed to have 0 fuel carbon content. The efficiencies used are the same as the generator efficiencies. The upstream supply chain emissions for diesel are a rough average of several values from the Environmental Assessment & Optimization

Group [82]. Natural gas and coal were assumed to be the same as diesel. Hydro upstream emissions are based on National Renewable Energy Laboratory [83] and solar on National Renewable Energy Laboratory [84]. Biomass was calculated using data from Dwivedi *et al.* [85] and Guest *et al.* [86] assuming 11 year cycle trees. Geothermal and wind are based on National Energy Technology Laboratory [87].

The maximum potential generation capacity for renewable resources varies by region. According to Drigo *et al.* [88], there is a shortage of biomass, which is mainly used for cooking in Rwanda, so we assume the biomass capacity available for electricity generation is 0 in every region. The only two districts with known non-zero geothermal potential are Musanze and Nyabihu, which have a combined potential of 300 MW [89]. We split the geothermal potential evenly across these two districts. There are many districts with hydroelectric potential. Data for undeveloped hydro is extracted from the Rwanda Hydropower Atlas [90] and added to the capacity from current hydroelectric plants in each district. We assume that the maximum capacity for solar is infinite but adjust for the effectiveness of solar panels in each region using the solar irradiance, which is captured in f_{vg}^{peak} and $f_{vgh}^{\text{gen-var}}$. We assume wind generation requires class 3-7 wind resources; regions with lower wind resources are modeled as having zero wind generation capability. According to the National Renewable Energy Laboratory [91], there is no wind potential meeting this criteria in Rwanda, so we assume wind is 0 everywhere.

Depletable resources - coal, diesel, and natural gas - are constrained by the total energy available based on fuel resources in the model. This value also varies by region. All regions are assumed to have the capability to import diesel fuel for power generation, as is a common approach to both utility and distributed generation, so we assume the maximum potential capacity for diesel is infinite. Rwanda does not have any actual coal resources. However, it does have peat resources, which we use in place of coal in the maximum potential capacity since the generation technology used for these two resources would be similar. The peat capacity is adapted from Energy Private Developers [92]. The only

region with non-zero natural gas resources is Karongi, which partially contains Lake Kivu. According to Rosen [93] there is 60 billion m^3 of methane available from Lake Kivu, which gives 633 TWh supply of natural gas in Karongi.

Capacity factors for dispatchable generation resources are shown in Table 3.4. The values for coal, natural gas, and geothermal are the values for load factor given in Castellano *et al.* [52]. The value for hydro is calculated by dividing the actual production from hydroelectric plants given by the Rwanda Utilities Regulatory Authority, Economic Regulation Unit [94] by the max potential production based on the capacities given by the Rwanda Energy Group [95]. Diesel and biomass are assumed to have the same value as coal.

Table 3.4: Capacity factors for dispatchable generation resources.

Diesel	Diesel 100 kW	HFO	OCGT	CCGT	Coal	Hydro	Small Hydro	Biomass	Geothermal
0.8	0.8	0.8	0.85	0.85	0.8	0.4	0.4	0.8	0.8

For variable resources, there are two values that affect the fraction of capacity that is available, f_{vg}^{peak} and $f_{vgh}^{\text{gen-var}}$. f_{vg}^{peak} represents the generation capability of the region at peak hours, and $f_{vgh}^{\text{gen-var}}$ represents the hourly fluctuations relative to this peak capability. For wind we use 1 and 0.2, respectively, in all regions because the wind type from IRENA used has a 20% capacity factor, and we assume this captures the data encoded in both parameters. For a country with non-zero wind potential it would be important to capture the wind variability across regions and times through these two variables, such that the average was 20%, but since we assume the wind potential is 0 across Rwanda this data is not relevant.

We consider hourly variations in the solar availability but assume solar PV and solar home systems have the same fraction of capacity available at each time. To calculate this fraction we use the solar irradiance values from HelioClim-3 Database of Solar Irradiance

version 5 [96]. We average the hourly solar irradiance over the year 2005 for each region to obtain the solar irradiance for our representative day and normalize these values by the maximum of the hourly averages in that region to get the fraction of peak output available at each hour. To calculate f_{vg}^{peak} for both solar generator types we divide average solar irradiance in each region by 1000, which is the maximum it could be.

Storage Resources

Recall that a battery paired with a solar home system is the only type of storage included in the model. Since the rooftop solar system from Miketa and Merven [53] used includes a 2 hour battery, $\alpha = 2$. We assume it takes the storage unit 24 hours to fully charge or discharge. Based on the advanced lead acid battery detailed in Aburub and Jewell [97] we use a round trip efficiency of 80%, which gives charge and discharge efficiencies of 89.4%, assuming both directions are the same.

Transmission and Distribution Resources

We consider two types of transmission lines, a 30 kV, 25 MW line and a 110 kV, 100 MW line. The data used for each of these lines and data sources are shown in Table 3.5.

Table 3.5: Data used for transmission lines.

Parameter	**30 kV**	**110 kV**
Capital cost ($/(MW· km))	2064.66	1548.50
Annual O&M cost ($/(MW· km))	20.65	15.48
Construction time (years)	1	1
Transmission loss (km^{-1})	0.0048	0.0011

Transmission costs in $/(MW· km) are calculated by dividing the transmission costs by capacities in Levin and Thomas [49] and converting to 2015 USD. For the transmission

losses, we use a resistance of 0.192, as was used for the smallest capacity line in Phillips and Middleton [98], and calculate the transmission losses based on Equation (16) from this paper, also assuming a 90% capacity rating. The transmission construction time is assumed.

We assume distribution costs are 0 and distribution efficiency is 0.9.

CO_{2eq} Emissions Limits

According to the U.S. Energy Information Administration [99], the CO_2 emissions from energy consumption in Rwanda were 0.9 million tonnes in 2014. The electrification rate in 2014 was about 21% based on Figure 1 of Republic of Rwanda Ministry of Infrastructure [74]. Thus, the CO_2 emissions if the entire population were electrified in the same way would be 4.29 million tonnes in 2014. We use this value, increased each year by the total population growth rate (2.74% according to United Nations, Department of Economic and Social Affairs, Population Division [71]) for our baseline CO_2 emissions constraints.

Initial System

Existing generators are based on Rwanda Energy Group [95]. Recall, in the model centralized resources may only be constructed in urban regions, so we assume all existing centralized resources are also in urban regions. Small hydro is the only resource for which we have non-zero initial capacity in the rural areas. The total initial capacities for generator types that are non-zero are shown in Table 3.6.

Table 3.6: Total initial capacity by region type. Types that are zero in both the urban and rural regions are excluded.

Generator Type	**Rural Capacity (MW)**	**Urban Capacity (MW)**
Diesel	0	34
HFO	0	27
OCGT	0	28.6
Hydro	0	92.15
Small Hydro	3.82	0
Utility PV	0	8.75

The existing transmission system data is based on the map shown in Safari [59]. We include both the 110 kV and 70 kV lines shown in this map as 110 kV lines in our model. By doing this we only assume that the capacity and losses of the initial 70 kV lines are the same as the the 110 kV lines since the cost and construction time data only applies to new lines, and we do not allow for new 70 kV lines to be built. We do not consider 70 kV lines as another line type because the characteristics are similar to the 110 kV lines and adding another line type would greatly increase the size of the problem instance. The 30 kV lines shown on the map are used for the 30 kV lines in our model. The initial transmission system considered is shown in Figure 3.2.

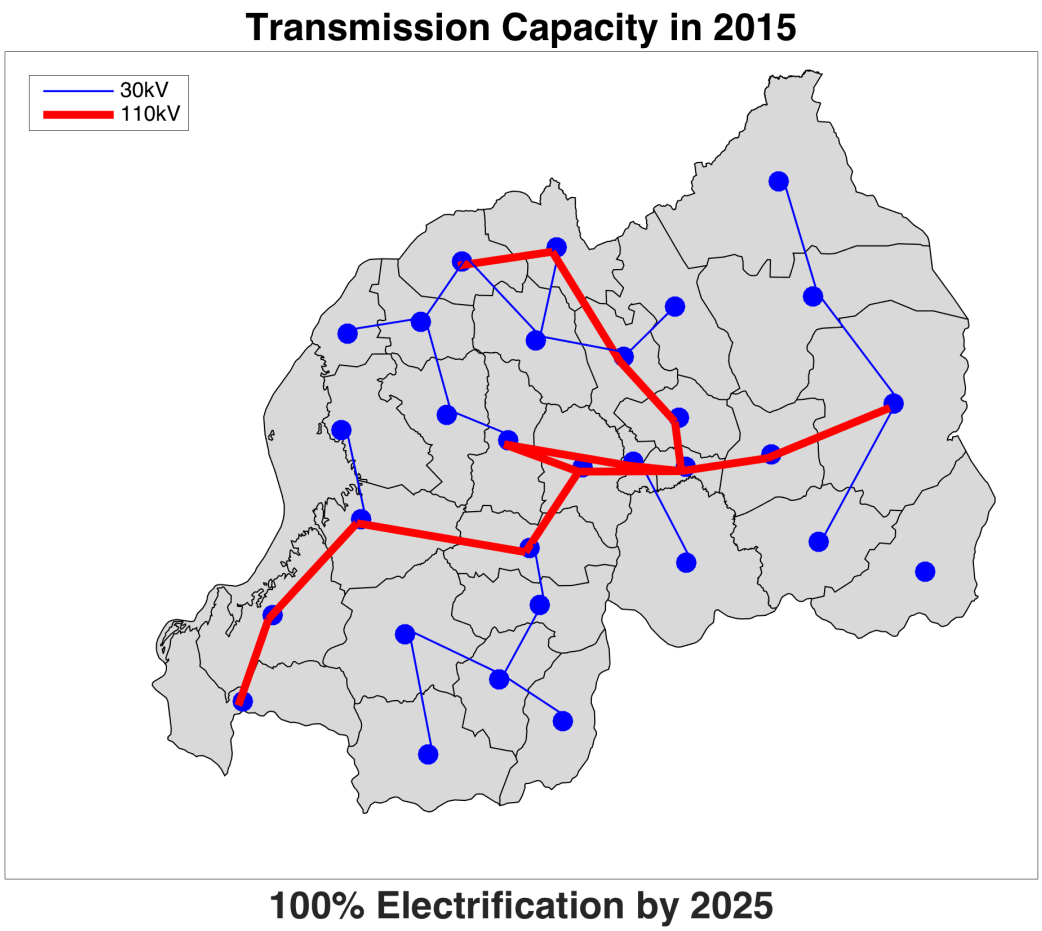

Figure 3.2: Map of the input transmission system for the start of the time horizon. Created in Matlab using shapefile from Map Library [68] with data from on Safari [59].

We assume that there are neither generators nor transmission lines that have started but not completed construction at the beginning of the time horizon.

3.3.2 Fraction of Demand Met Cases

We consider cases where 100% of demand is met by years 2020, 2025, 2030, 2035, 2040, and 2045 for each of the four electrification constraint variants, giving a total of 24 cases. For the regional electrification goals we assume the fraction of demand will increase linearly from the 2015 regional electrification rates in every region to 100% by the year specified. Similarly, for the total electrification goals we assume demand will increase linearly from the 2015 total electrification rate to 100% total electrification in the year specified.

The total and regional initial electrification rates are extracted from Figures 1 and 2, respectively, in Republic of Rwanda Ministry of Infrastructure [74]. Note that these figures actually give the percent of the population with grid access, which we use as a substitute for the fraction of demand met since we do not have actual data for these values.

We present aggregate results for these 24 cases and more detailed results for the case when 100% of demand is met by 2025 since 2025 is the year by which Rwanda would like to reach full electrification [5].

3.4 Results

We programmed the model in Python and solved with Gurobi 6.5.1 on a Linux 64 Xeon E5645 machine with 48 GB RAM. Although the problem is a linear program, it is very large. Before pre-solving, the Rwanda case study has around 2.5 million constraints and 2.2 million variables. With some variation depending on the instance, Gurobi reduces these values to around 1.4 million constraints and 1.6 million variables in the pre-solve phase. Each test took between 1 hour and 2.5 hours to solve. The problem can be solved much more quickly with less memory by skipping by five, or even two, years. However, we present the higher resolution, full time horizon results results here.

In all figures for which we show results for the four variants of the fraction of demand met constraints (electrification goal) "Total" indicates Constraints (3.27) are used, "UR Total" indicates Constraints (3.28) are used, "Regional" indicates Constraints (3.29) are used, and "UR Regional" indicates Constraints (3.30) are used.

3.4.1 Electrification Years 2020 to 2045

We first study the effect of varying the year at which 100% electrification is reached. Figure 3.3 shows the objective value (discounted cost) in each case normalized by the discounted cost to reach full electrification by 2025. The cost to reach full electrification by 2020 is about 121% of the cost to reach full electrification by 2025. This cost monotonically

decreases as the year at which 100% electrification is reached increases, such that the cost to reach full electrification by 2045 is about 60% of the cost to reach full electrification by 2025. The costs for the "Total" and "UR Total" demand constraint variants are slightly different but indistinguishable on this graph, as are the costs for the "Regional" and "UR Regional" demand constraint variants.

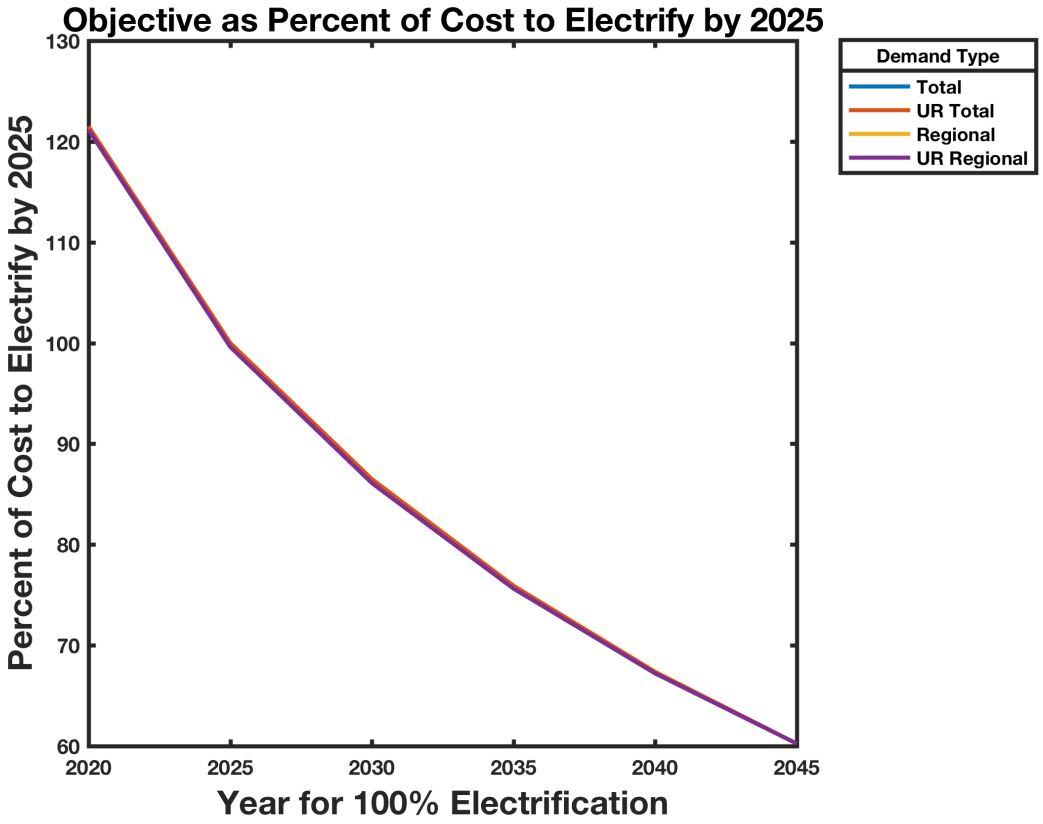

Figure 3.3: Discounted cost to reach full electrification by the given year as a percent of the discounted cost to reach full electrification by 2025.

Figure 3.4 shows the percent of the objective value that is capital cost and operational cost in each of the 24 cases. We see that the cost is close to evenly split between capital and operational costs and that the percents only vary a small amount across the cases.

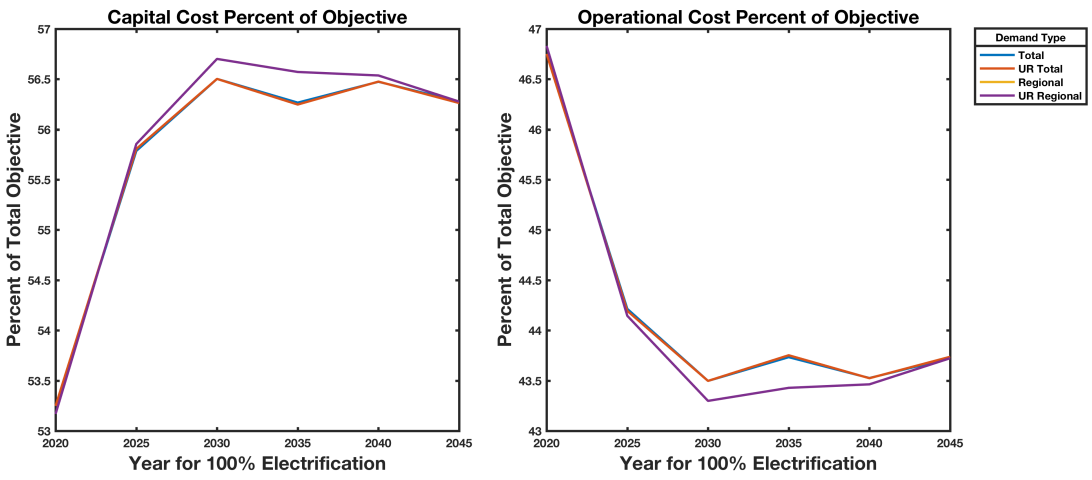

(a) (b)

Figure 3.4: Percent of objective that is (a) capital cost and (b) operational cost.

Part of the decrease in cost shown in Figure 3.3 is due to discounting. Figure 3.5 shows the country-wide cost in each year, before discounting, for the six cases and each of the demand constraint options. These figures demonstrate the budget that will be needed by each year to meet the corresponding electrification goal. Across the cases the trend is that the cost is greatest in the first and last years.

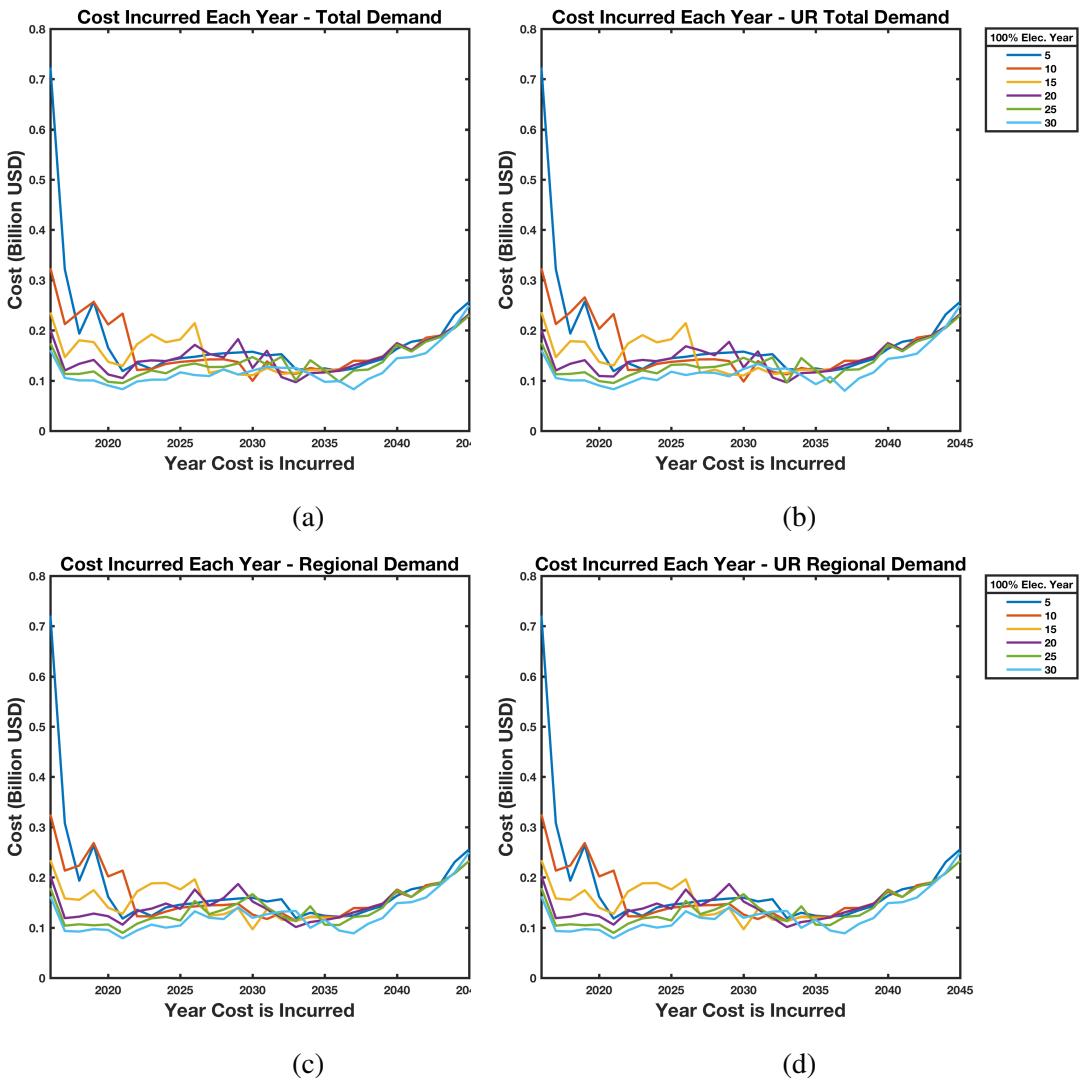

Figure 3.5: Undiscounted cost incurred in each year with (a) total, (b) total urban and rural, (c) regional, and (d) regional urban and rural demand constraints.

Figure 3.6 shows the total capacity for the country from each generation type in years 2015, 2025, 2035, and 2045 across the 24 cases. In Figure 3.6(a), the generation mix is the same across all cases, as expected since this year corresponds to the initial state of the power generation system, which is input to the model. For the other years, the total capacity generally decreases as the year to reach 100% electrification is increased. One exception is in Figure 3.6(d), which corresponds to the final year of the time horizon. In this figure, all cases have similar total capacities since 100% electrification is reached by the end of the

time horizon in all cases tested. For any given year, the generation mix is similar across all cases, even though the total capacity varies.

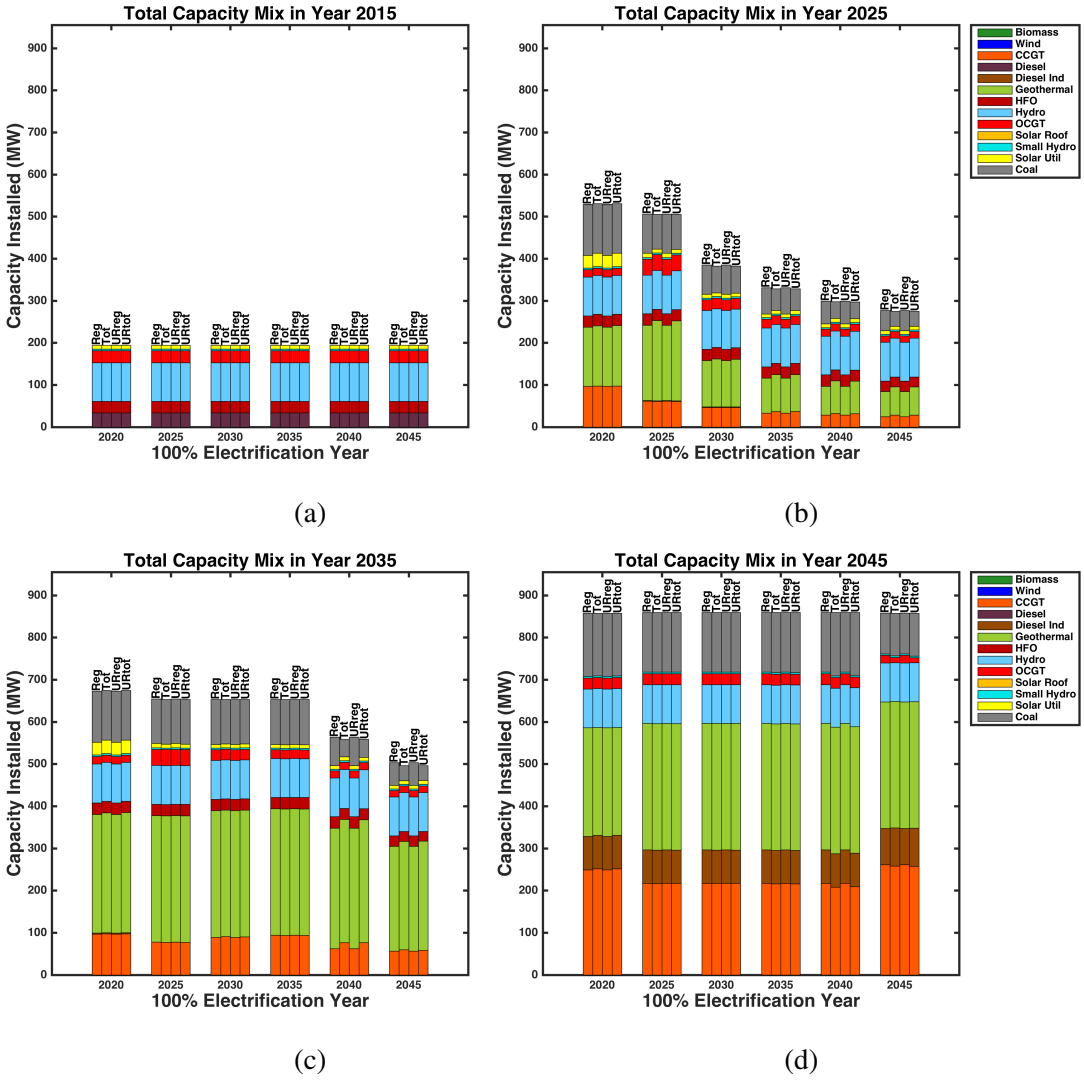

Figure 3.6: Total capacity mix across the 24 cases in years (a) 2015, (b) 2025, (c) 2035, and (d) 2045.

Figures 3.7 shows the total transmission capacity for the 110kV line in years 2020, 2025, 2035, and 2045. The 30 kV transmission is constant at 450 MW throughout time horizon.

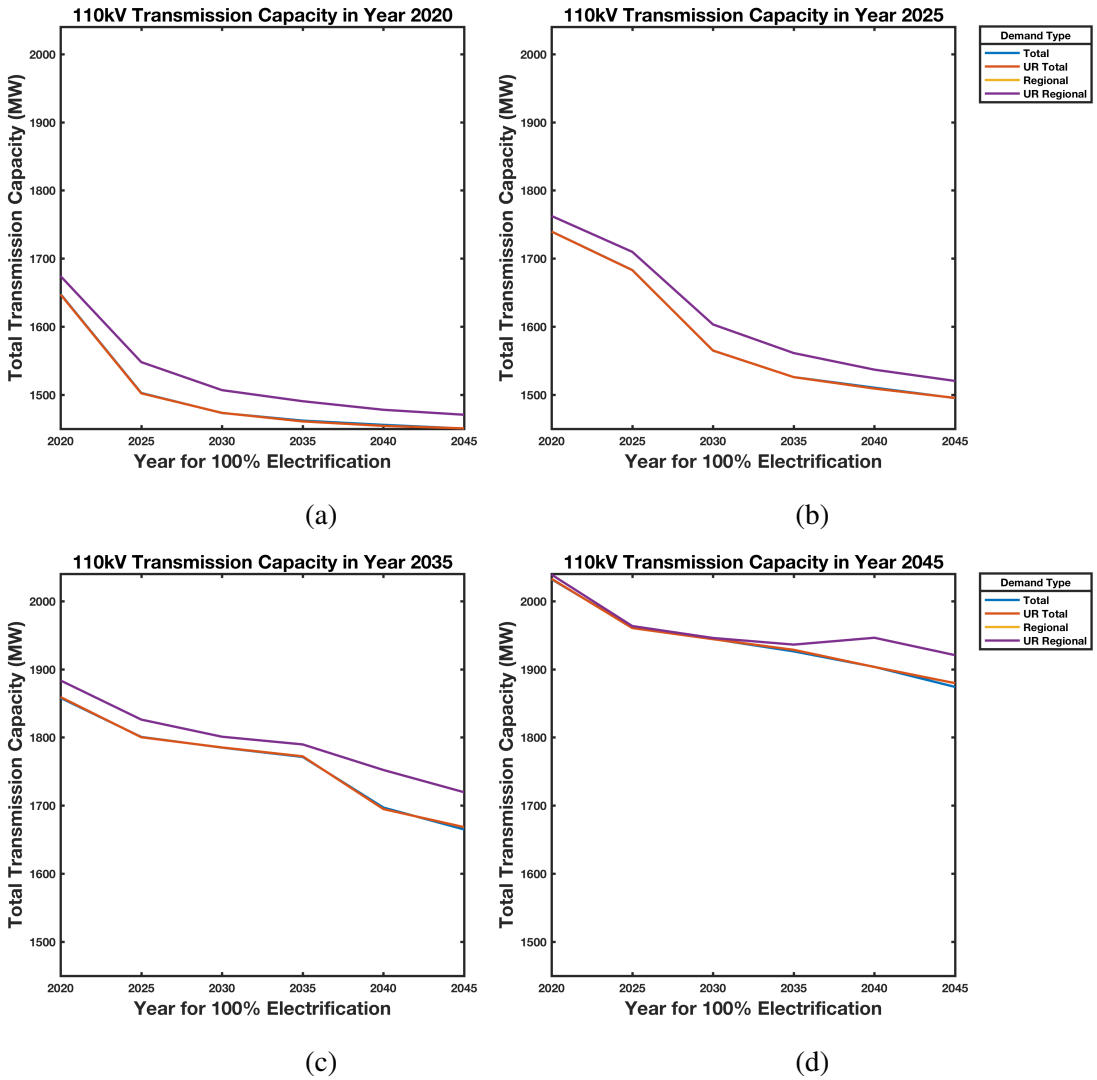

Figure 3.7: Total transmission line capacity for the 110 kV line in (a) 2020, (b) 2025, (c) 2035, and (d) 2045.

3.4.2 100% Demand Met by 2025

We analyze in more detail the case in which 100% of demand is met by 2025. Figure 3.8 shows the total installed power generation capacity in Rwanda across the time horizon for the four demand constraint options in this case.

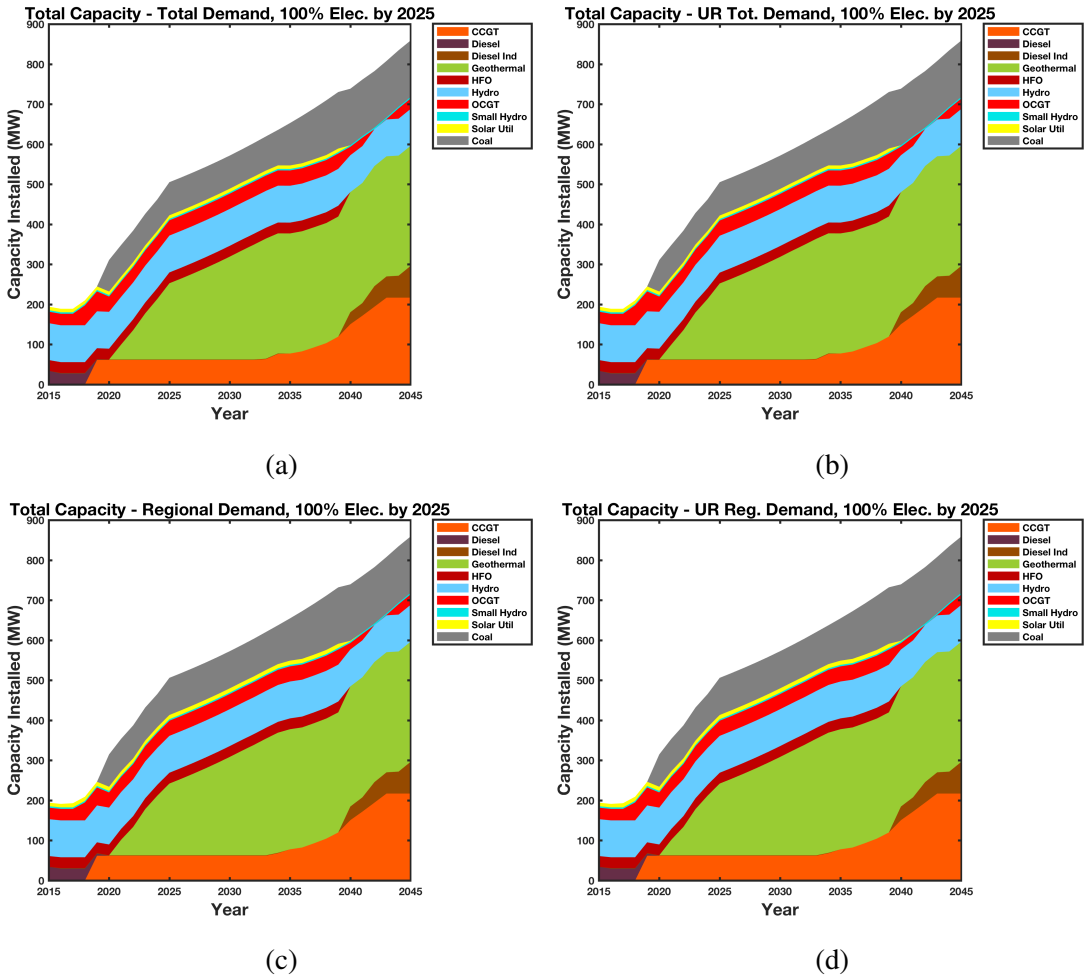

Figure 3.8: Total capacity mix for Rwanda across time when 100% electrification is reached by 2025 for (a) total, (b) urban and rural total, (c) regional, and (d) urban and rural regional fraction of demand met constraints.

Figure 3.9 shows the total total energy output in Rwanda across the time horizon when 100% of demand is met by 2025. These plots show the hourly energy output for the representative day every fifth year to more clearly show the hourly fluctuations. There is a cyclic pattern in the energy output due to the 24-hour load curve used.

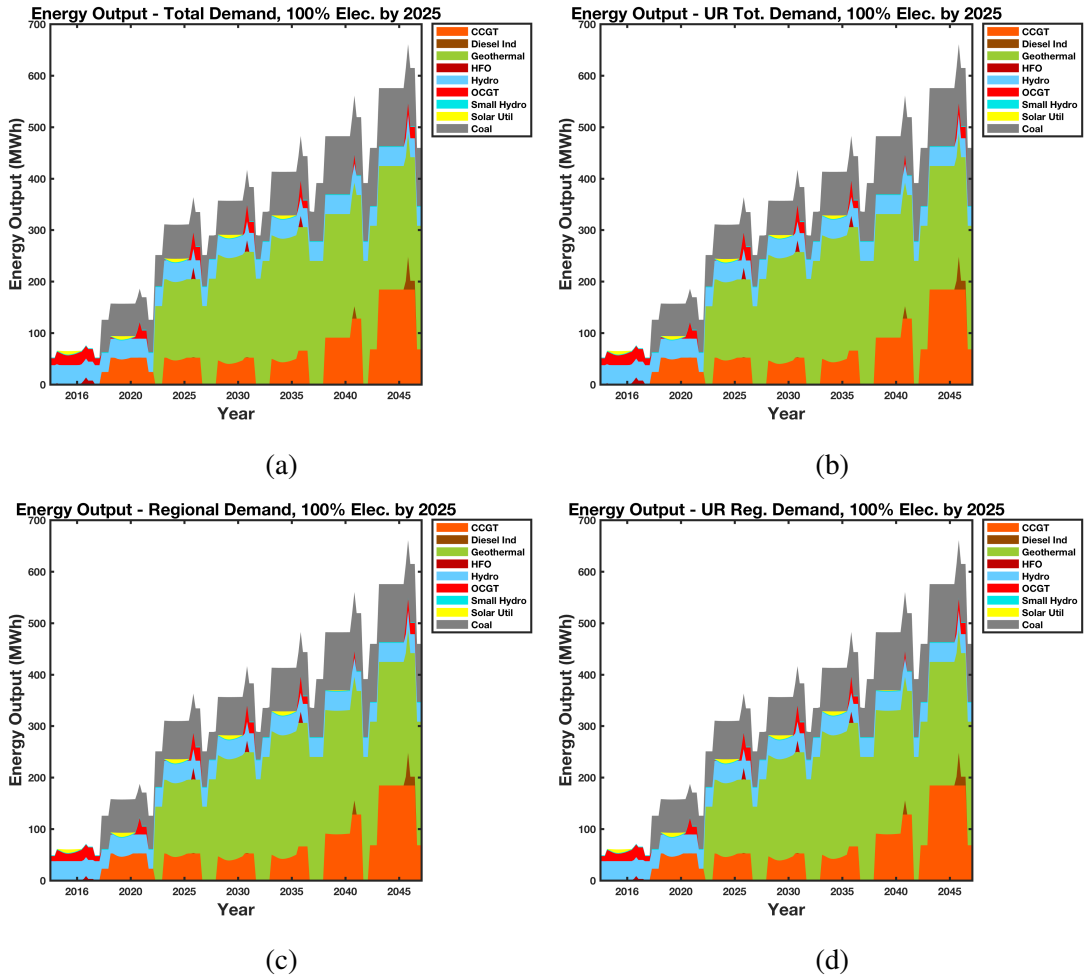

Figure 3.9: Total energy mix for Rwanda across time when 100% electrification is reached by 2025 for (a) total, (b) urban and rural total, (c) regional, and (d) urban and rural regional fraction of demand met constraints.

Both the capacity and energy patterns are very similar across the four electrification constraint variants. However, we do see some regional differences. Figure 3.10 shows the capacity over time in Nyanza and Kirehe, two districts where we see regional differences, for the total and regional electrification constraint variants.

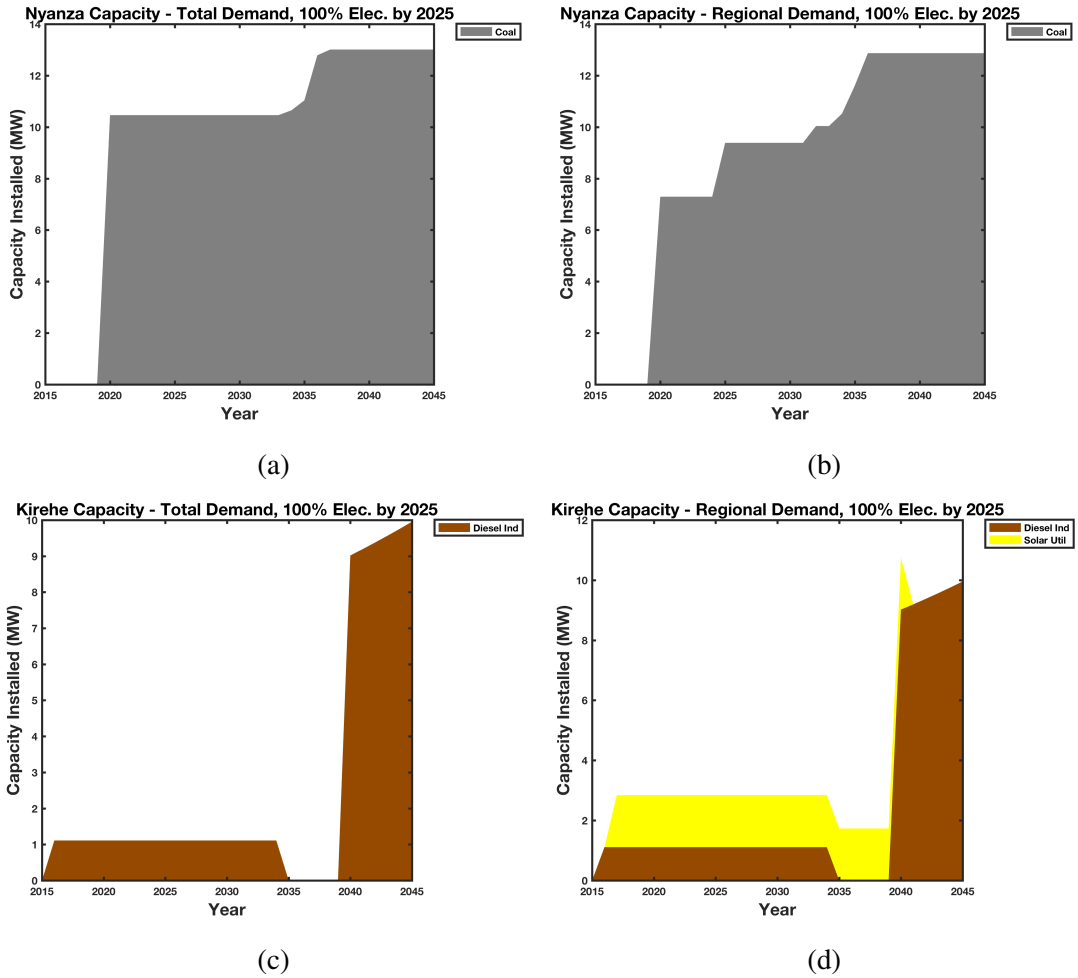

Figure 3.10: The capacity mix in (a), (b) Nyanza and (c), (d) Kirehe across time when 100% electrification is reached by 2025. (a) and (c) are subject to the total fraction of demand met constraints and (b) and (d) are subject to the regional fraction of demand met constraints.

Figure 3.11 shows the transmission system at the end of the time horizon for the four fraction of demand met constraint variants when 100% of demand is met by 2025. The transmission system for the Total and UR Total demand constraints is the same, as is the transmission system for the Regional and UR Regional demand constraints. However, there are differences between the transmission system built for the Total and Regional demand constraints.

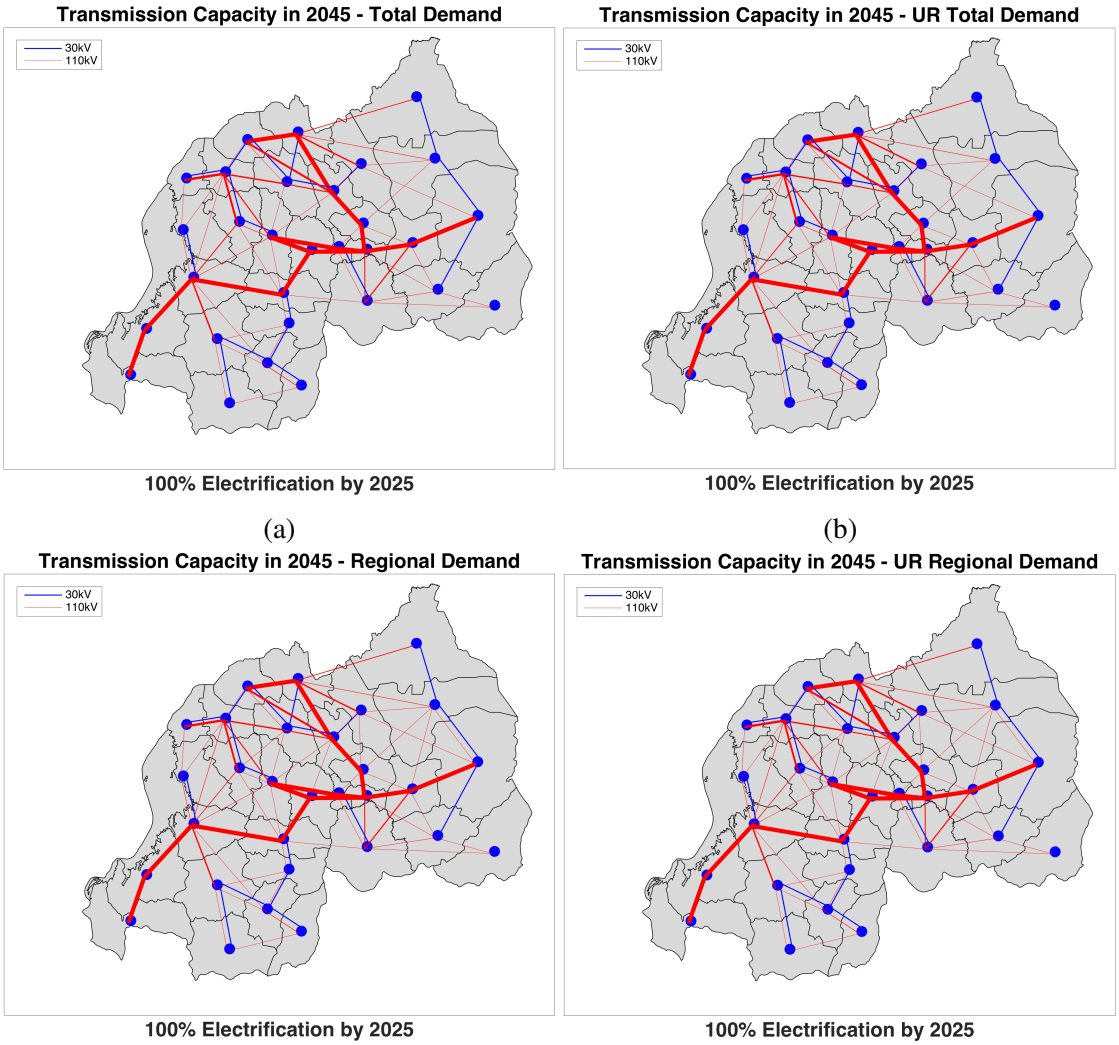

Figure 3.11: Map of the transmission system at the end of the time horizon for the (a) Total, (b) UR Total, (c) Regional, and (d) UR Regional demand met constraints when 100% electrification is reached by 2025. Blue lines are 30 kV, Red lines are 110 kV. The line thickness indicates the installed capacity. Map created with Matlab using shapefile from Map Library [68].

3.4.3 Sensitivity Analysis

To explore drivers for renewable and distributed generation we perform a sensitivity analysis on the CO_2-equivalent emissions restrictions, solar home system costs, and transmission costs, varying these parameters for the case in which 100% of demand is met by 2025.

We first compare the case in which the maximum allowed CO_2-equivalent emissions is held constant at the 2014 value of 0.9 million tonnes [99] for the entire time horizon.

Figure 3.12 shows the total installed power generation capacity in Rwanda across the time horizon in the constant CO_2-equivalent emissions case for the four demand constraint options. Comparing this figure to Figure 3.8 we see that coal is largely replaced with utility scale solar PV, there is no small scale diesel constructed at the end of the time horizon, and the total capacity installed at the end of the time horizon is almost twice as much as in the default case.

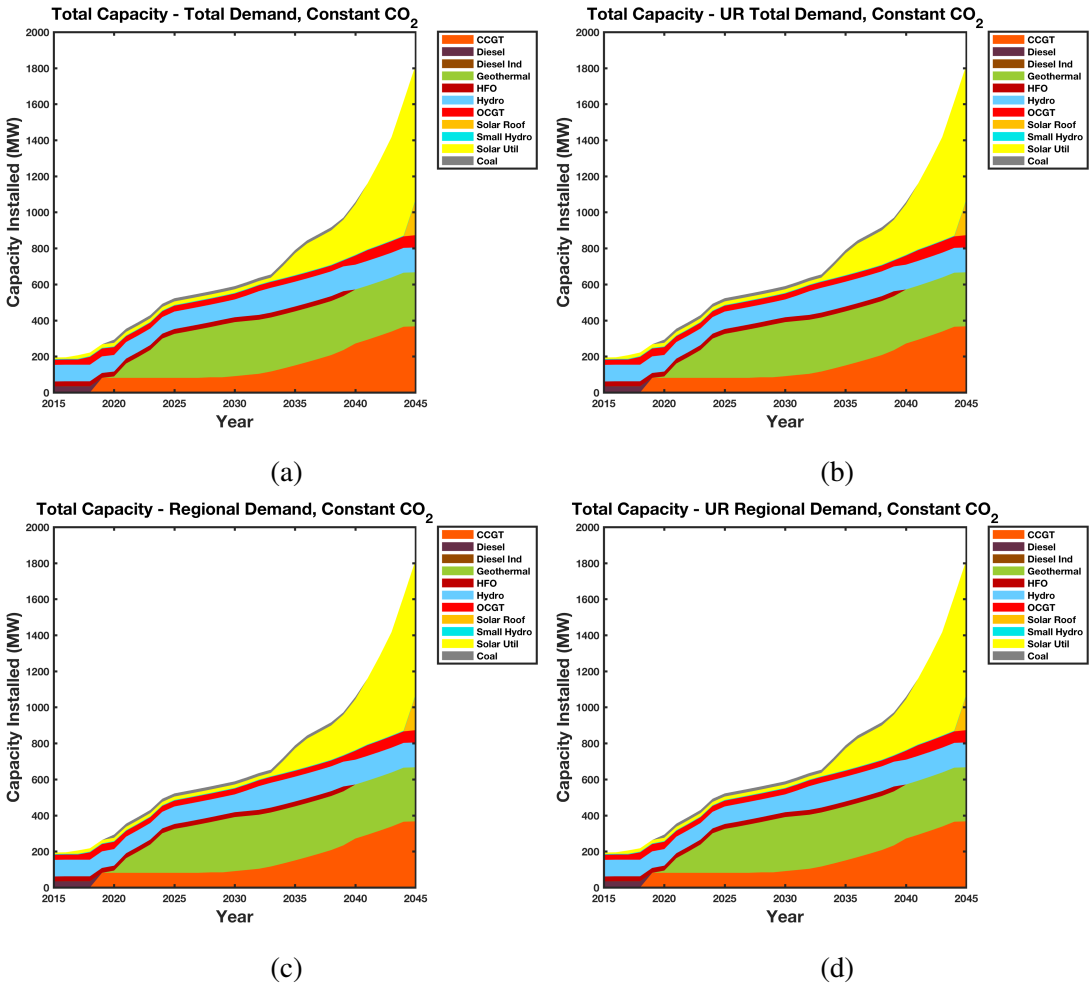

Figure 3.12: Total capacity mix for Rwanda across time when 100% electrification is reached by 2025 for (a) total, (b) urban and rural total, (c) regional, and (d) urban and rural regional fraction of demand met constraints when maximum allowed CO_2 emissions are held constant throughout the time horizon.

Next we halve the capital costs for solar home system and compare to the original case. Figure 3.13 shows the total installed power generation capacity in Rwanda across the time horizon when solar home system costs are halved. The results displayed are almost identical to Figure 3.8 except we see a small amount of solar home systems (solar roof) built at the end of the time horizon where there was none before.

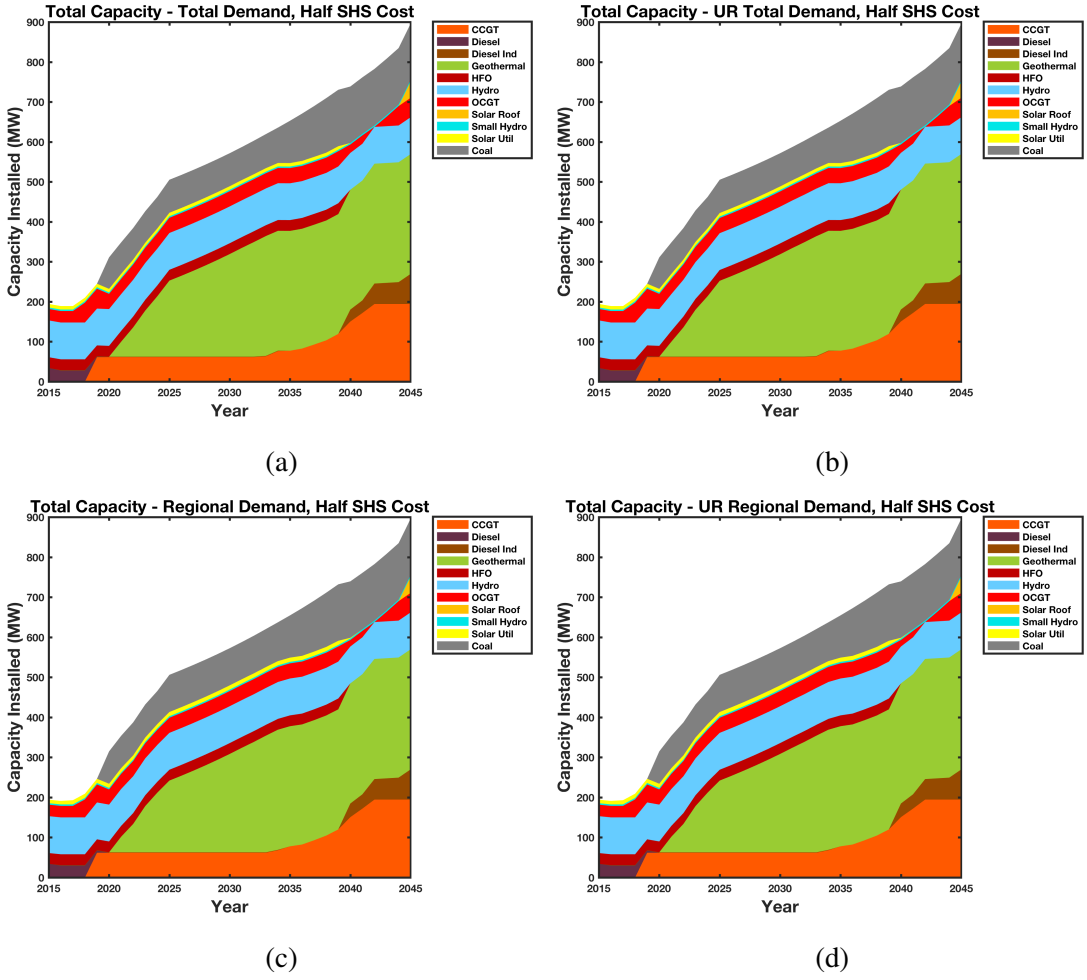

Figure 3.13: Total capacity mix for Rwanda across time when 100% electrification is reached by 2025 for (a) total, (b) urban and rural total, (c) regional, and (d) urban and rural regional fraction of demand met constraints when SHS costs are halved.

Next we double the transmission costs. Figure 3.14 shows the total installed power generation capacity in Rwanda across the time horizon when transmission costs are doubled. These plots look almost identical to those in Figure 3.8.

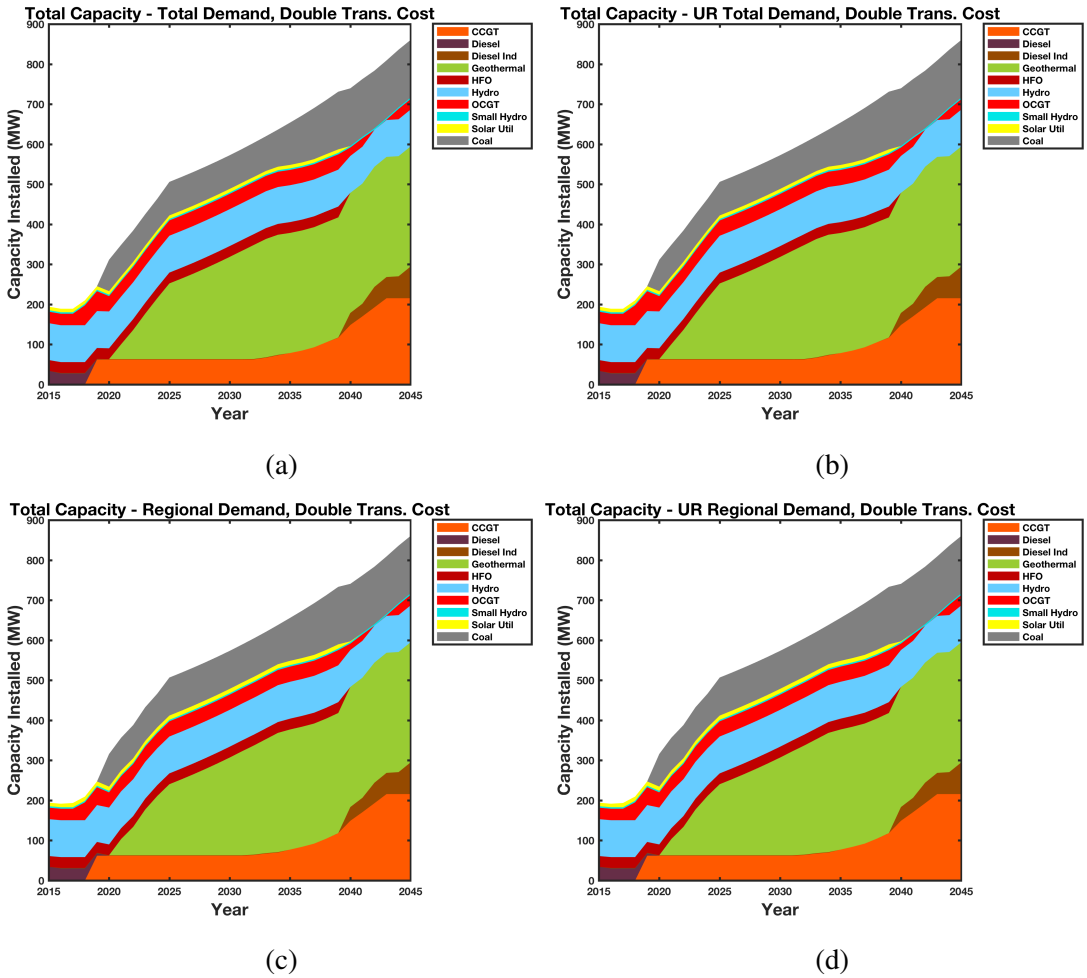

Figure 3.14: Total capacity mix for Rwanda across time when 100% electrification is reached by 2025 for (a) total, (b) urban and rural total, (c) regional, and (d) urban and rural regional fraction of demand met constraints when transmission costs are doubled.

Finally, we halve the solar home system costs while simultaneously doubling the transmission losses. We consider this case specifically to explore a situation in which we would expect distributed generation to be favored. Figure 3.15 shows the total installed power generation capacity in Rwanda across the time horizon in this case. The plots appear almost identical to those in Figure 3.13, so it appears that doubling the transmission costs does not have an added impact on the capacity mix when the solar home system costs are also halved.

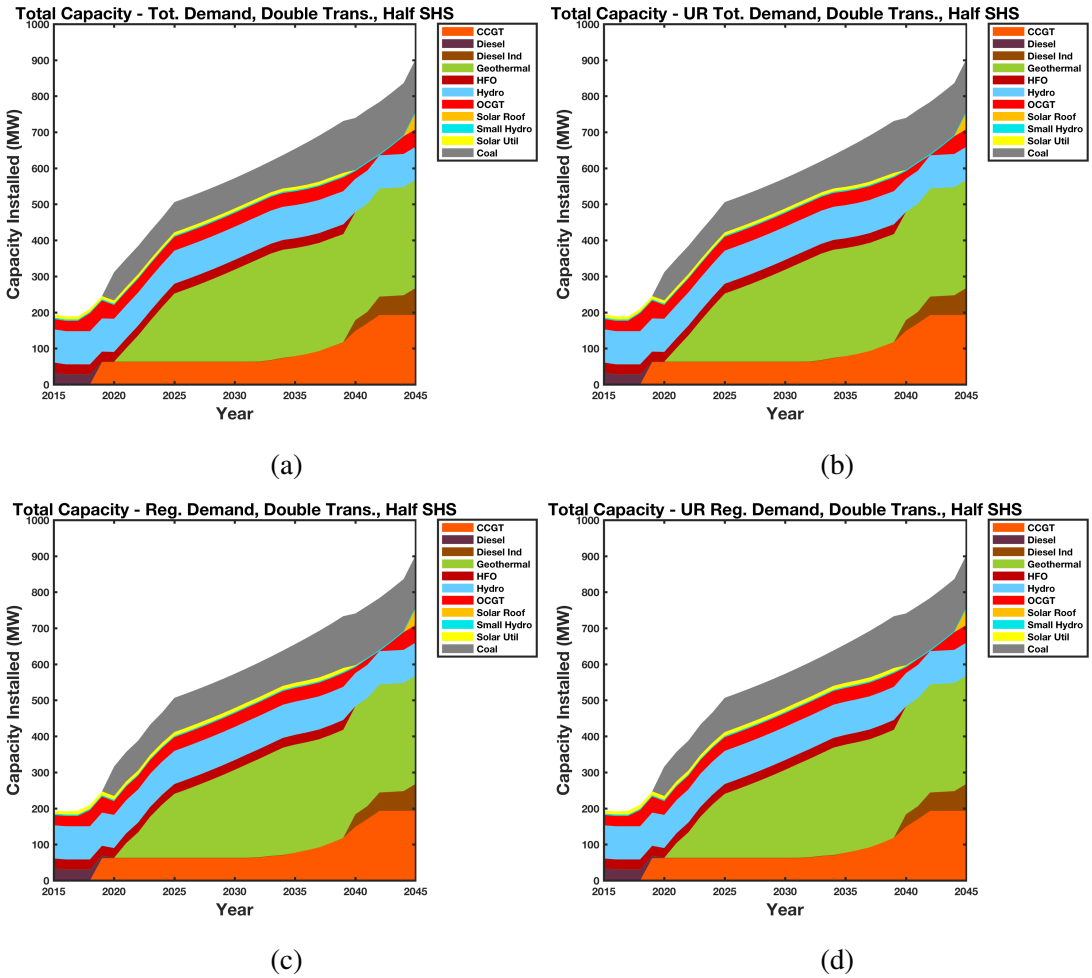

Figure 3.15: Total capacity mix for Rwanda across time when 100% electrification is reached by 2025 for (a) total, (b) urban and rural total, (c) regional, and (d) urban and rural regional fraction of demand met constraints when SHS costs are halved and transmission costs are doubled.

We compare the objective values across these four cases and the original case when 100% electrification is reached by 2025. The results are shown in Table 3.7. Halving the solar home system costs does decrease the overall cost, but only very slightly (about 0.003%). The rest of the variants increase the cost. Doubling the transmission costs increases the cost only about 0.5%. Keeping the $CO_{2\text{-eq}}$ emissions limit constant increases the costs about 3.4%.

Table 3.7: Optimal objective values across the four electrification goal options for original data and cases tested in the sensitivity analysis.

Electrification Objective	Original	Constant CO_{2eq}	SHS Costs Halved	Double Trans. Cost	Half SHS Cost Double Trans. Cost
	Cost (Billion $)				
Total	1.769	1.829	1.769	1.778	1.777
UR Total	1.769	1.829	1.769	1.778	1.777
Regional	1.762	1.822	1.762	1.772	1.772
UR Regional	1.762	1.822	1.762	1.772	1.772

Table 3.8 shows the total 110 kV transmission line capacity for Rwanda at the end of the time horizon across the five cases. The 30 kV line is constant at the initial total capacity of 450 MW for all cases.

Table 3.8: Installed capacity across the four electrification goal options for original data and cases tested in the sensitivity analysis.

Electrification Objective	Original	Constant CO_{2eq}	SHS Costs Halved	Double Trans. Cost	Half SHS Cost Double Trans. Cost
	Capacity (GW)				
Total	1.961	2.181	1.949	1.810	1.802
UR Total	1.961	2.181	1.948	1.810	1.801
Regional	1.963	2.188	1.954	1.818	1.809
UR Regional	1.963	2.188	1.954	1.818	1.809

3.5 Discussion

For the case study of Rwanda, the year in which 100% electrification is reached affects both the cost and the installed capacity across the time horizon. However, the total installed

capacity by the end of the time horizon is similar across all cases, as is the generation mix. That is, although varying the year in which 100% of demand must be met affects when generators are built, the results converge over time once 100% electrification is met. There is approximately a 50% decrease in cost between the cases when 100% of electrification is met by 2020 and 2045. The cost to electrify earlier should be higher since the effective demand is larger. However, as demonstrated by the Figure 3.4, the operational costs to meet this demand are not the only factor since the percent of total cost that these account for only changes a small amount. The change in the total cost is also affected by the capital cost, which is heavily discounted when paid in later years.

The costs incurred in each year differ the most in the first half of the time horizon and converge towards the end of the time horizon as the year in which 100% electrification is reached varies. In most cases, these costs are highest in the first few years. This observation makes sense because the capital costs will be paid in the beginning for generators that are used throughout the time horizon. Similarly, the increase in cost at the end of the time horizon in all cases is likely due to the fact that many of the generator types considered have a 25-year lifetime, so new generators must be constructed at the end of the 30-year time horizon.

The changes in demand met (both the metric used and the year in which full electrification is reached) are mainly accounted for through changes in the transmission system. The total transmission capacity decreases around 10% between the cases when 100% of electrification is met by 2020 and 2045. Figure 3.11 demonstrates the difference in the final transmission system for the four electrification contraint variants when full electrification is reached by 2025. Although the final transmission system is very similar in all cases, there are noticeable differences between the transmission system for the total demand and the regional demand constraints.

The differences between the total and regional demand constraints and the UR variants for each of these are almost unnoticeable for both the transmission system and generation

capacity and output. This result is likely due to the structure of the data. We use the same location for the urban and rural areas within each region in the model because we only have general location data for the regions (districts) rather than detailed data on where the urban and rural populations are located. Although there may be a single location within each district where the urban population is centered, the rural population is likely scattered across the region. In order to model this dispersion, we would have to include multiple rural areas within each region. Doing so would increase the size of the model, which is already very large. Since requiring demand to be met in the urban and rural regions only very slightly affects the solution with our current model, it may be worth removing the urban and rural specification and instead determining how power should be distributed within a region in a second, separate, model.

Both the capacity mix and total cost were robust to the changes in the demand met constraints, transmission costs, and solar home system costs. Although we expected increasing transmission costs and decreasing solar home system costs to increase reliance on distributed systems, this change was not observed other than a very small increase in solar home systems at the end of the time horizon. We do, however, see significant changes in the generation mix and cost when the constraints on CO_{2eq} emissions are tightened. In this case, much of the coal capacity is replaced with utility scale solar, which starts increasing greatly around 2033. By the end of the time horizon, the total capacity constructed in this case is about twice that of the baseline, likely due to the high variability in solar power.

Enforcing tighter emissions constraints does have a significant impact on the capacity mix. A much higher capacity of solar home systems was installed to replace coal and a small amount of diesel generation. The total capacity at the end of the time horizon was also much higher, likely due to the fluctuations in solar power. However, in this case as well we still only see a low level of distributed generation.

The transmission system is also affected by tightening the emissions constraints. In this case, about 11% more transmission capacity is built. The effect on transmission capacity

of halving solar home system costs is small (about 0.6% decrease). However, there is about an 8% decrease in transmission capacity when the transmission cost is doubled (both with and without halving the solar home system cost).

In all cases, the recommended generation mix consists almost entirely of centralized resources. This finding, although unexpected, is not unreasonable. Doubling the transmission costs only increases the total costs about 5%, which indicates that transmission accounts for a small fraction of the overall cost. Thus, it is cheaper to build up the transmission system than to rely on more costly decentralized resources. This observation also explains why the generation mix is very similar across the four demand constraint options. Rwanda is a geographically small country, so it's possible the transmission costs may have a greater impact on a much larger country such as the Democratic Republic of the Congo.

3.6 Conclusion

In this work we developed a model for electricity development planning in sub-Saharan Africa. Unlike much other work for developing countries, our model includes both strategic and operational planning decisions. Our model includes decisions on how to build and operate the power system including generators, storage units, and transmission lines. We distinguish between centralized and decentralized resource options as well as rural and urban regions.

We test our model on a case study of Rwanda, varying both the minimum fraction of demand met and how this fraction is quantified. We compare the costs and generation mixes across 24 different demand cases and perform a sensitivity analysis on parameters that we expect could affect renewable and distributed generation decisions in the case in which 100% of the country is electrified by 2025. Counter to our expectations, we find that, in all data variants tested, the generation mix consists almost entirely of centralized resources. The small increase in the objective when transmission costs are doubled suggests that the transmission costs represent only a small fraction of the system costs. Thus, in a larger

country, the distributed resources might be more favored.

In addition to the model results, the data collection process is another valuable aspect of this project. Through compiling data from a variety of resources and making approximations where necessary we have gained a detailed understanding of the current electricity system in sub-Saharan Africa, which we hope will be useful for others as well.

3.7 Future Work

3.7.1 Efficiency Improvements

A long runtime is acceptable for strategic planning problems such as this one since the problem would not need to be solved repeatedly. However, we did have some issues solving the problem because it required a large amount of memory: between 4 and 4.5 GB of RAM. In the future, there are some external pre-processing steps that may be implemented before solving the program with Gurobi.

For the case study tested, both the costs and the losses were higher for the 30 kV line than for the 110 kV line. Since there are no limits on the transmission capacity of a certain type that can be installed, it is not economical to build 30 kV lines. Indeed, we see that the total 30 kV line capacity stays constant at the initial value of 450 MW throughout the time horizon. If this is the case for other countries as well, we could still include the initial 30 kV lines, but remove the option of constructing new ones to reduce the number of z^{trans} and $z^{\text{trans}+}$ variables by half. The p^{trans} variables are still required as long as the initial 30 kV lines are included, however. It also should be noted that this is only possible because we consider a linear programming relaxation of the problem. In the integer case, the 30 kV transmission lines would still have a higher cost per MW·km, but the unit capacity would be smaller, potentially giving a lower cost per unit.

When testing the program we skipped by five years in the model and data. These tests only took around 2-4 minutes to run on an Intel Xeon computer with 2.40 GHz CPU and 6GB RAM. For the cases compared, the results when we skipped by five years were very

similar to the results for the the full time horizon but at a lower resolution. If the main purpose of the analysis is to determine how to allocate a development budget that includes energy, this resolution may be sufficient. If more detail is required, the runtime and memory issues could still be improved by solving the problem in two stages: first skipping by 5 years to get the low resolution results for the full time horizon, then solving for the annual decisions for each 5-year sub-problem, constrained by the full time horizon decisions.

3.7.2 Multi-Country Model

We would also like to extend our analysis to other countries, in particular Rwanda's four neighboring countries: Uganda, Tanzania, Burundi, and Democratic Republic of the Congo. One benefit of performing a multi-country analysis is that one country may have a significant natural resource, Lake Kivu for example, that is too large and not worth developing to meet its own needs but may be more worthwhile if neighboring countries could share the cost. There could also be benefits from resource diversification if neighboring countries were rich in different resources.

The current version of the model can account for multiple countries in a basic sense. On one extreme, we can solve the model for multiple countries considering each country individually and not accounting for trade between countries. On the other extreme, we can solve the model across all countries simultaneously with a single budget and unrestricted trade between countries. The scenarios in between the two extremes, where countries are considered in relation to each other but with separate budgets and certain restrictions on trade, are more realistic but require a more complex game theoretic approach. Another approach may be to model the countries with one unified objective but include constraints regulating trade and electrification requirements in each country.

CHAPTER 4
OPTIMIZING WIND FARM SITING DECISIONS TO REDUCE THE NEGATIVE IMPACTS OF WIND VARIABILITY

As concerns about environmental impacts of fossil fuels and energy security grow, it is important to consider alternate energy options such as wind and solar power. However, increased reliance on wind and solar resources makes meeting electricity demand more difficult because these resource types are uncontrollable and variable. A high level of wind power variability can burden the rest of the system because other generation types must be ramped up and down to account for the fluctuations in wind power. Sometimes a generator may even be left on when it is not in use if the ramp up cost is high, negating the benefit of wind power. In this research we aim to select a reliable wind portfolio to reduce this burden on the rest of the system. We develop a capacity planning model for wind power that selects a set of wind sites based on two criteria:

- Maximizing the demand met by power generated from wind and
- Minimizing the change in demand deficit over time.

4.1 Background

In their detailed review of 12 wind integration studies, one key conclusion by Dowds *et al.* [100] is that, "integrating large amounts of wind power into the power system is technologically feasible and that integration costs may be reduced by larger balancing authority areas." In fact, many researchers have found that geographically dispersing wind farms can reduce the aggregate wind variability. Archer and Jacobson [101] determine that by interconnecting wind sites in the U.S. Midwest, there is potential for up to 33% of wind power to be used for average (ignoring demand peaks) baseload power with the same reliability

as a coal plant. Using a portfolio investment approach to allocate wind resources across four simulated off-shore wind sites around the U.K., Drake and Hubacek [102] find that they can reduce the aggregate variance by 36% while only reducing average power output by 9.2% when compared to a single wind farm of the same total capacity. Katzenstein *et al.* [103] study the benefit of interconnecting wind farms within the Electric Reliability Council of Texas (ERCOT) and Bonneville Power Authority areas and find the greatest variability reductions come from interconnecting the first few plants. They confirm this result for ERCOT in later work in which they compare the marginal cost of wind variability as an increasing number of wind sites are interconnected [104]. Santos-Alamillos *et al.* [105] use principal component analysis to determine if the current wind farms in Spain are distributed in a way that minimizes variability and if future wind sites could be located more effectively for this purpose. They identify three regions with complementary wind patterns and determine that evenly spreading wind farms across these three regions would lead to a more reliable aggregate wind resource. Holttinen *et al.* [106] even include geographic dispersion of wind farms as one of the important factors to consider in wind integration studies. Our question of concern is then, how can the advantages of geographic dispersion be used to strategically select wind farm locations in order to minimize wind power variability while maintaining a high level of power output?

A widely applied method for wind site selection is to overlay a variety of features describing site suitability using geographic information systems (GIS) and then rank sites using multi-criteria decision analysis based on analytic hierarchy processes or analytic network processes [107, 108, 109, 110]. Azadeh *et al.* [111] consider multiple site attributes for wind site selection in a more quantitative way, using hierarchical data envelopment analysis to rank potential sites. The advantage of these methods is that they incorporate multiple features in their analysis of potential wind sites. However, the site selection tools used do not allow for site interactions to be considered. Furthermore, these studies only consider average wind speed and are not concerned with reducing wind variability.

A variety of other methods for evaluating potential wind sites have also been considered. Lewis [112] develops a metric for assessing wind sites based on wind speed and locational marginal price but does not consider interactions between sites. Hoppock and Patiño-Echeverri [113] compare costs of potential higher capacity factor distant wind farms to lower capacity factor local wind farms. Mokryani and Siano [114] use a genetic algorithm to select the location and turbine size from a small number of candidate wind sites, and then solve the optimal power flow problem to determine how many wind turbines of the selected size to build at each selected site. Jain *et al.* [115] use particle swarm optimization in combination with Monte Carlo Simulation to select locations and sizes for distributed wind generators and capacitors but only consider a small area across which they assume wind potential is uniform. Phillips and Middleton [98] develop a mixed integer program to simultaneously select wind sites, transmission lines, and load centers for Texas but only consider a single time period and therefore cannot capture variability.

Oftentimes wind sites with a high power output also have high variability. A number of authors have considered wind power output mean-variability tradeoffs through portfolio optimization techniques to optimally allocate capacity resources across potential wind sites [102, 116, 117, 118]. In addition to mean and variability metrics similar to those considered in other studies, Reichenberg *et al.* [119] seek to minimize the conditional value at risk but find that adding this objective makes the variability objective redundant. Grothe and Schnieders [120] also consider value at risk without considering the mean and variability objectives. While portfolio optimization is useful for determining capacities for a predetermined set of wind farms or how wind power capacity should be distributed across a region, it is limited in its applicability to wind site selection because it does not allow a discrete number of sites to be selected. Reichenberg *et al.* [121] sought to address this shortcoming by developing a heuristic to select a given number of wind sites from a set of candidate sites in attempt to minimize the coefficient of variation. We develop a similar heuristic in the first part of this work. Distinctions between [121] and this work will be

discussed in Section 4.2.

Other options for compensating for not only wind variability but also uncertainty that have been considered are: demand response [122, 123], co-locating wind and solar power [124, 125, 118], and energy storage [124, 123]. Jacobson *et al.* [123] consider other resources types as well and determine that, in the contiguous U.S., a 100% renewable portfolio by 2050 is possible with sufficient energy storage and demand response. Gupta [126] reviews a broad range of wind power research including studies related to accounting for variability at the grid level and through the wind turbines themselves. Behera *et al.* [127] review the use of optimization heuristics for a variety of wind energy related problems including: locating turbines within a wind farm, locating distributed wind power sites, generation scheduling with wind power, and making mechanical improvements to wind turbines. Researchers have also considered optimizing wind turbine location within a wind farm to reduce wake effects [128, 129]. These options are not in conflict with effective wind site selection and could be used jointly to mitigate the impact of wind variability. Additionally, although the case study we present in this paper is for wind site selection, our model could also be used for simultaneously locating solar power.

4.2 Approach Overview

One shortcoming of many (though not all) previous related studies is that they consider wind without considering load. However, since wind and load are correlated [100] and it is the fluctuations in net load that the rest of the power system must account for, we believe it is important to simultaneously consider load and wind power. For this purpose we develop a metric, which we call demand deficit, defined as,

$$\tilde{d}_t = (d_t - \sum_{s \in \mathcal{S}_0} w_{s,t})^+, \tag{4.1}$$

where d_t is the demand at time t, $w_{s,t}$ is the available wind power from site s at time t, and $\mathcal{S}_0$ is the set of wind sites that will be used to meet demand. x^+ indicates the maximum of 0 and x. Demand deficit is simply the positive part of net load. We use demand deficit rather than net load because we assume excess wind power will be curtailed. We only consider the power available from wind resources because it will benefit the system to select strong wind sites according to the two criteria, regardless of which resource types will be used to meet the remainder of demand. Adding controllable resources to meet the remainder of demand should not affect the wind sites selected. Simultaneously selecting wind and solar power locations may affect the wind sites selected. However, as we will see, our model could be used to select solar sites as well simply by modifying the data input.

Our goal is to select a set of wind sites that both minimizes demand deficit and minimizes the variability in demand deficit. A key question is how to define variability. Drake and Hubacek [102], Roques *et al.* [117], and Thomaidis *et al.* [118] use the total standard deviation for the wind portfolio selected. (It appears that Thomaidis *et al.* [118] actually use the variance, though they say they use the standard deviation. The results would be equivalent if they were only minimizing variance, but since they minimize a weighted sum with the mean, the results are not equivalent). Cassola *et al.* [116] and Reichenberg *et al.* [119] use different variants of a metric measuring the total stepwise change of energy output over time. In the first part of this work we use a similar metric, specifically the sum of the absolute differences in demand deficit between each consecutive pair of time periods. However, none of these metrics give proper weight to extreme changes in wind power, which, as Dowds *et al.* [100] point out, is the primary risk to system reliability when incorporating wind power. Reichenberg *et al.* [119] and Grothe and Schnieders [120] recognize the importance of considering extremities and therefore seek to optimize the conditional value at risk and value at risk, respectively. However, these metrics only measure the probability of low wind power output rather than capturing sudden extreme fluctuations in wind. In the second part of this work, in order to capture these extreme changes in our model, we

use the maximum increase in demand deficit across a certain number of consecutive time periods as our variability metric.

We model our problem as a bi-objective non-linear integer program, where our two objectives are to minimize demand deficit and minimize the change in demand deficit over time. The latter is measured either as the average absolute change across consecutive periods or the maximum change across a fixed number of periods. The model constrains the number of wind sites selected to a given integer value. We are unable to efficiently solve the exact optimization for the full time horizon, which is why we first approach the problem using two heuristics. However, part of the challenge of solving our specific problem instance is the large amount of wind data used. With the heuristics, we find an approximate solution using 10-minute wind data at 281 sites for a year. We then perform an exploratory data analysis to select a subset of the data that still captures the key wind characteristics to use for the optimization. Details of this data analysis are described in Section 4.5.2. By linearizing the model and reducing the size of the data set we are able to solve the problem exactly in a reasonable amount of time. We solve for a weighted sum of the two objectives, varying the weights to compare demand deficit and variability trade-offs. Reichenberg *et al.* [121] used a site selection heuristic similar to the forward algorithm we present here. However, they combined the mean and standard deviation into a single metric, the coefficient of variation. It is necessary to keep the two objectives separate in order to directly compare trade-offs between the two objectives. We believe our problem instance is of realistic size, so this method could be applied to wind farm siting in other areas as well.

Finally, we compare our results to the results if sites are selected based on the mean wind output, as is often done. We also present the results for the extreme case, where the weight for the mean demand deficit is 1 and the variability weight is 0 as this case represents a variant on selecting sites based on the mean alone when load is also considered.

4.3 Case study

We perform a case study on the Southwest Power Pool (SPP), a regional transmission organization (RTO) within the Eastern Interconnection [130]. Wind data is taken from the Eastern Wind Data Set from the National Renewable Energy Laboratory [131]. This data set contains 10-minute simulated wind power data for 1,326 potential wind sites across the Eastern Interconnection [132]. Data is given from 2004-2006. Potential wind sites in the Eastern Wind Dataset are shown in Figure 4.1 with a rough outline of the SPP shown in black.

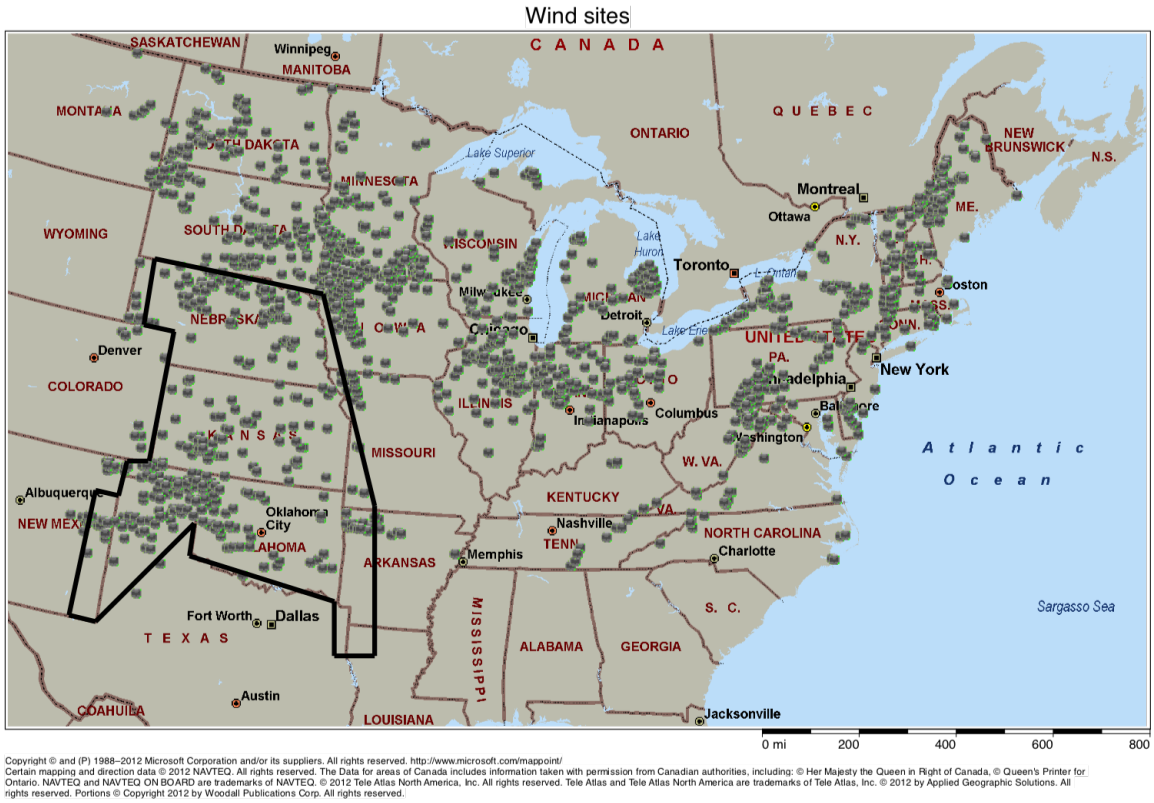

Figure 4.1: Potential wind sites considered in the Eastern Wind Dataset

For demand data, we use the Federal Energy Regulatory Commission Form 714 Database [133]. This database contains hourly demand data for 207 balancing authorities and planning areas from 2006-2013. We use demand data for the SPP, as given in this database.

Using ArcGIS, we determine the subset of wind sites that is within the SPP based on the latitude and longitude given for each site in the Eastern Wind Data Set. The Eastern Wind Data Set includes 281 potential wind plants in the SPP region. We only consider wind sites within the SPP because wind sites outside of this region would be owned by other RTOs and managed through contracts. We use 2006 data for these wind sites and SPP demand since this is the only year for which the two databases overlap. When 10-minute data is required, we use the 10-minute wind data as is and linearly interpolate between hours to get 10-minute demand data. When hourly data is required we average the 10-minute wind data across each hour and use the hourly demand data as is.

Wind data is given in Coordinated Universal Time (UTC) and demand data in Central Standard Time (CST), so we shift the wind data by 6 hours to make wind times CST. We are able to do this because the first day of 2007 was included in the wind data.

4.4 Heuristic Solution

We first develop two heuristics to solve the problem using 10-minute data for all of 2006.

4.4.1 Model

In our initial model formulation the first objective is to minimize the average demand deficit, given by,

$$\text{minimize} \sum_{t=1}^{T} \frac{(d_t - \sum_{s \in \mathcal{S}} w_{s,t} x_s)^+}{T}, \tag{4.2}$$

where d_t is the demand at time t, $w_{s,t}$ is the available wind from site s at time t, and x_s is a decision variable indicating whether or not wind s site is selected. T is the number of periods in the time horizon. In our case study, $T = 52,560$ since we have 52,560 10-minute increments in a year. $\mathcal{S}$ is the set of indices of wind sites, of which there are 281 in the SPP.

The second objective is to minimize the average variability, measured as the absolute change in demand deficit between any two consecutive periods,

$$\text{minimize} \sum_{t=2}^{T} \frac{|(d_t - \sum_{s\in\mathcal{S}} w_{s,t}x_s)^+ - (d_{t-1} - \sum_{s\in\mathcal{S}} w_{s,t-1}x_s)^+|}{T-1}, \tag{4.3}$$

where we take the sum from $t = 2$ since we are interested in the change over time and the first period is our starting point. We consider the change in demand deficit rather than the change in wind power output in order to minimize the burden to the rest of the system.

Our goal is to minimize both of these objectives when a total of N sites are selected. Thus, we have the following constraints,

$$\text{subject to} \sum_{s\in\mathcal{S}} x_s = N, \tag{4.4}$$

$$x_s \in \{0, 1\}. \tag{4.5}$$

4.4.2 Solution Approach

The original problem (before linearizing) is a cardinality constrained subset selection problem with two non-linear objectives. Although we can convert the problem to a bi-objective mixed integer program, we are unable to solve this problem exactly using the full dataset. Furthermore, since we cannot necessarily minimize the two objectives simultaneously we must determine how to balance the two objectives in order to get an efficient solution.

There are several approaches we could take to solving this problem. We first present two greedy algorithms, which select sites iteratively until N sites have been selected. Our heuristics consider the non-linear objectives directly and also account for the multi-objective aspect of the problem.

Forward Greedy Algorithm

For the forward greedy algorithm we add sites one at a time based first on minimizing the demand deficit then minimizing variability.

Let $\mathcal{S}_n$ be the set of sites selected when n sites are included. I_α is another set of sites, which we use to keep track of the top $\lceil \alpha |\mathcal{S} \backslash \mathcal{S}_{n-1}| \rceil$ site options at step n that are selected according to the demand deficit criteria, where α is the fraction of remaining sites we would like to rank according to the variability criteria ($\alpha \in (0, 1]$). $\mathcal{S}$ is the complete set of sites.

The forward greedy algorithm is outlined below. At each step of the algorithm we save $\mathcal{S}_n$, so that at the completion of the algorithm we have a solution for any number of sites that may be included up to N.

Initialization: Start with 0 wind sites. That is, $n = 0$ and $\mathcal{S}_0 = \emptyset$. Let $I_\alpha = \emptyset$.

For $n = 1$ to N:

1. Rank sites $i \in \mathcal{S} \backslash \mathcal{S}_{n-1}$ from lowest to highest according to the criteria,

$$\sum_{t=1}^{T} \frac{((d_t - \sum_{s \in \mathcal{S}_{n-1}} w_{s,t}) - w_{i,t})^+}{T}.$$

2. Let I_α be the top (lowest demand deficit) $\lceil \alpha |\mathcal{S} \backslash \mathcal{S}_{n-1}| \rceil$ of these sites. Note $|\mathcal{S} \backslash \mathcal{S}_{n-1}| = |\mathcal{S}| - n + 1$.

3. Let $k = \arg\min_{i \in I_\alpha} \sum_{t=2}^{T} \frac{|((d_t - \sum_{s \in \mathcal{S}_{n-1}} w_{s,t}) - w_{i,t})^+ - ((d_{t-1} - \sum_{s \in \mathcal{S}_{n-1}} w_{s,t-1}) - w_{i,t-1})^+|}{T-1}$.

4. $\mathcal{S}_n = \mathcal{S}_{n-1} \cup k$.

At each iteration of the algorithm we evaluate the sites $\mathcal{S} \backslash \mathcal{S}_{n-1}$ that are not already included, rank these first by the demand deficit criteria (step 1), select the top $\lceil \alpha |\mathcal{S} \backslash \mathcal{S}_{n-1}| \rceil$ (α times the number of remaining sites, rounded up) of these to evaluate according to the variability criteria (step 2), then of this subset we add the site that minimizes the average variability when considered in conjunction with the current set of sites (steps 3 and 4).

Backward Greedy Algorithm

The backward greedy algorithm is very similar except that we start with all sites and eliminate sites one at a time until we have N sites remaining. An outline of the algorithm is shown below.

Initialization: Start with all wind sites. That is, $n = |\mathcal{S}|$ and $\mathcal{S}_{|\mathcal{S}|} = \mathcal{S}$. Let $I_\alpha = \emptyset$.

For $n = |\mathcal{S}| - 1$ to N (counting down):

1. Rank sites $i \in \mathcal{S}_{n+1}$ from lowest to highest according to the criteria,

$$\sum_{t=1}^{T} \frac{((d_t - \sum_{s \in \mathcal{S}_{n+1}} w_{s,t}) + w_{i,t})^+}{T}.$$

2. Let I_α be the top (lowest demand deficit) $\lceil \alpha |\mathcal{S}_{n+1}| \rceil$ of these sites. Note $|\mathcal{S}_{n+1}| = n + 1$.

3. Let $k = \arg\min_{i \in I_\alpha} \sum_{t=2}^{T} \frac{|((d_t - \sum_{s \in \mathcal{S}_{n+1}} w_{s,t}) + w_{i,t})^+ - ((d_{t-1} - \sum_{s \in \mathcal{S}_{n+1}} w_{s,t-1}) + w_{i,t-1})^+|}{T-1}$.

4. $\mathcal{S}_n = \mathcal{S}_{n+1} \backslash k$.

At each iteration of the algorithm we evaluate the remaining sites $\mathcal{S}_{n+1}$, rank these first by evaluating which will leave the lowest demand deficit if removed (step 1), select the top $\lceil \alpha |\mathcal{S}_{n+1}| \rceil$ of these to evaluate according to the variability criteria (step 2), then of this subset remove the site that minimizes total variability of remaining sites (steps 3 and 4).

We program these two algorithms in C. The algorithms took between 27 seconds and 1 minute 36 seconds, depending on α, to calculate the sites selected for all potential N values. $\alpha = 1$ corresponds to selecting sites based on the variability criteria only. In order to consider both end cases we let $|I_\alpha| = 1$ in all iterations of the algorithm when $\alpha = 0$. That is, $\alpha = 0$ represents the case when sites are selected based on the demand deficit criteria only.

4.4.3 Results

We run the forward algorithm for $N = 281$ and the backward algorithm for $N = 1$, saving the order in which sites were added or removed so that at the completion of each algorithm we can see which sites to include for any number of sites between 1 and 281. Solutions for $\alpha \in \{0, 0.1, 0.25, 0.5, 0.75, 1\}$ are compared.

Figures 4.2 and 4.3 show how the average demand deficit changes as the number of sites selected is increased for the forward and backward algorithms, respectively. It appears that the backward algorithm is more effective in reducing demand deficit than the forward algorithm.

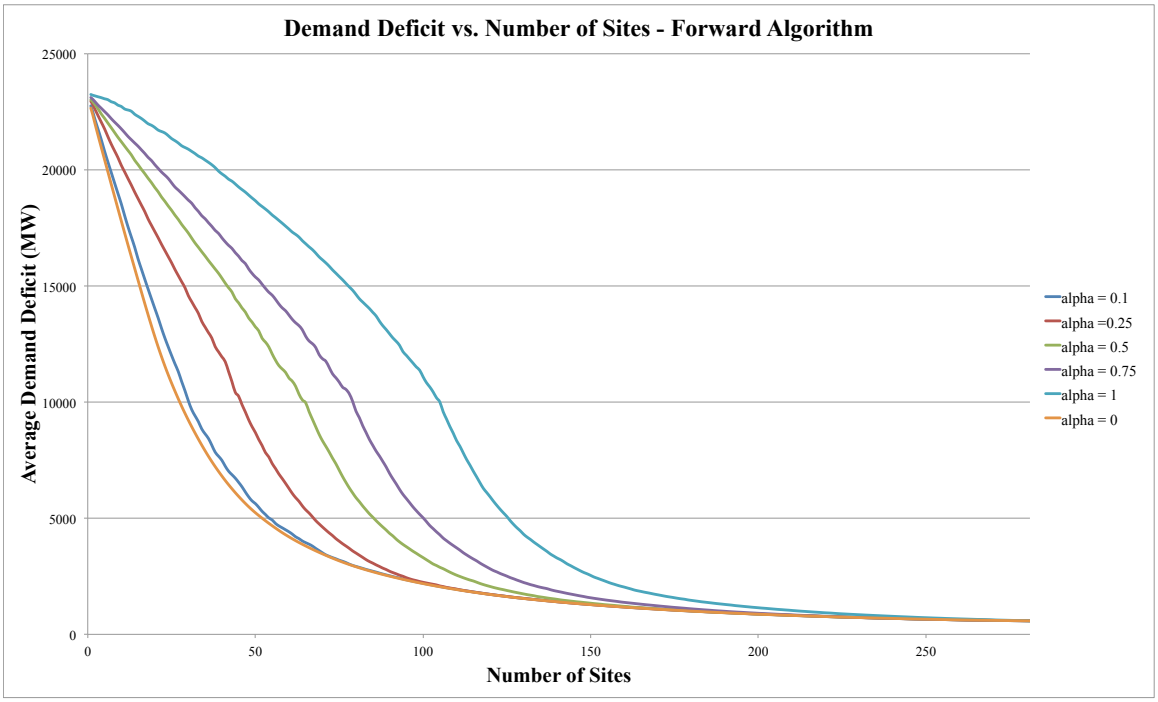

Figure 4.2: Average demand deficit when 1 to 281 wind sites are selected using the forward algorithm. The different contours correspond to different values of α.

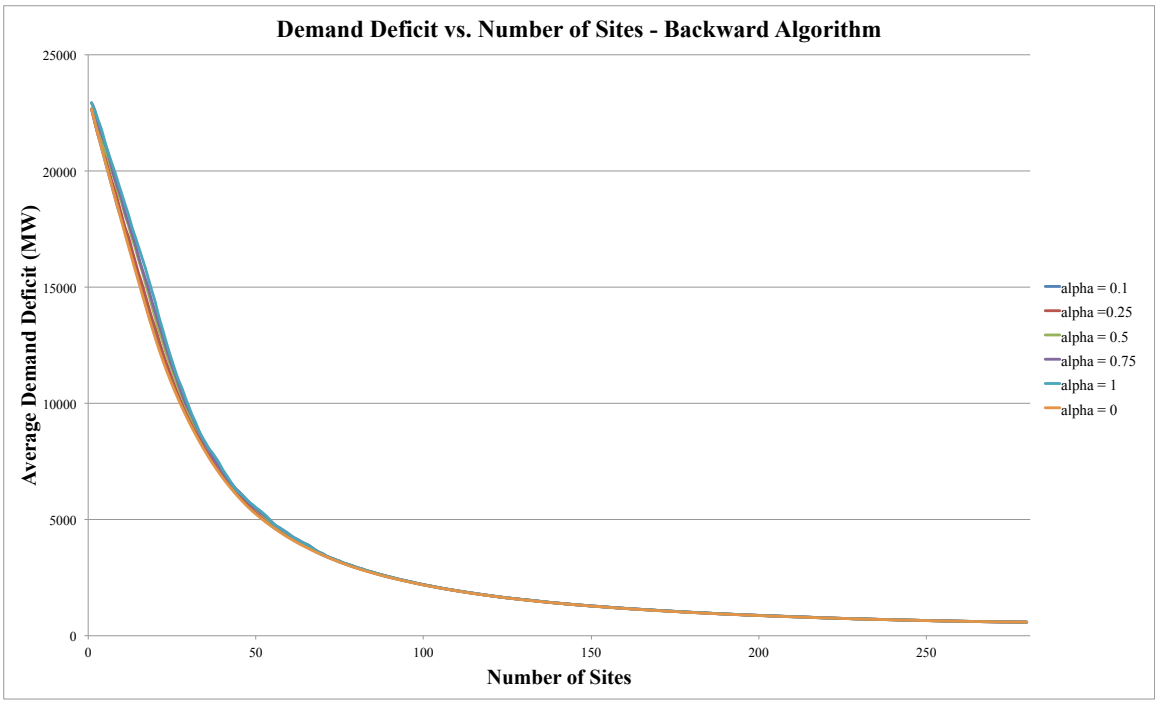

Figure 4.3: Average demand deficit when 1 to 281 wind sites are selected using the backward algorithm. The different contours correspond to different values of α.

Figures 4.4 and 4.5 show how the average variability in demand deficit changes as the number of sites selected is increased for the forward and backward algorithms, respectively. For the backward algorithm, the reduction in variability occurs with fewer sites, but the maximum variability is higher in most cases.

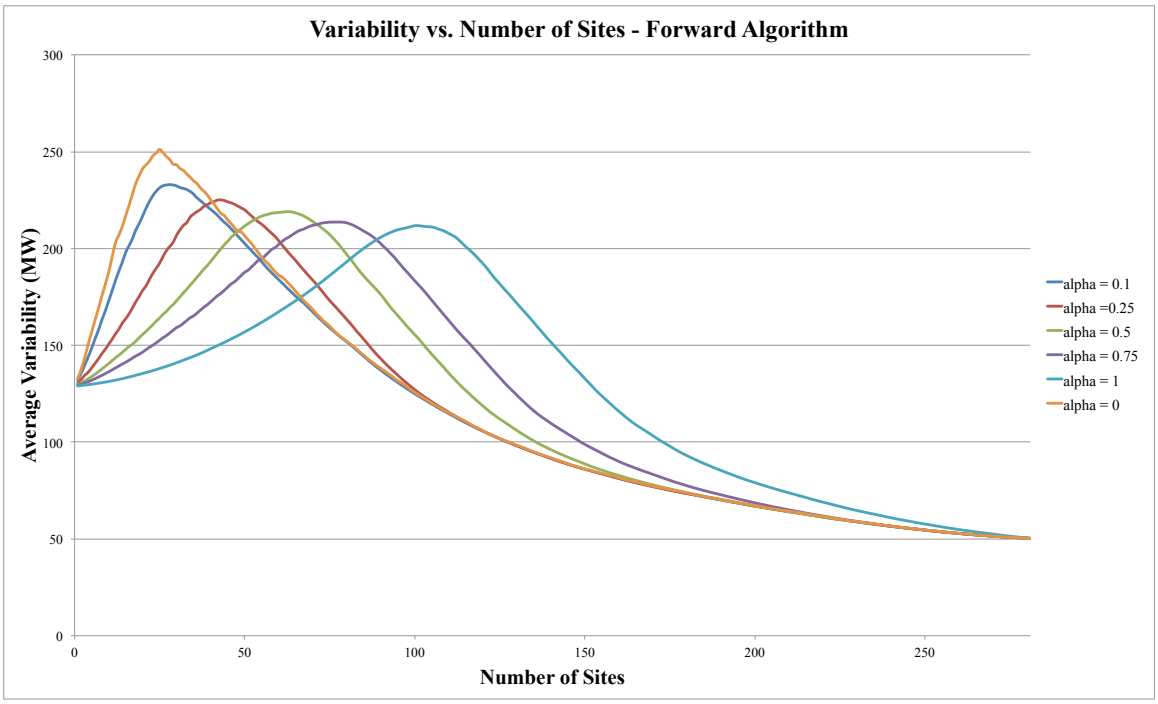

Figure 4.4: Average variability in the demand deficit for different numbers of wind sites using the forward algorithm. The different contours correspond to different values of α.

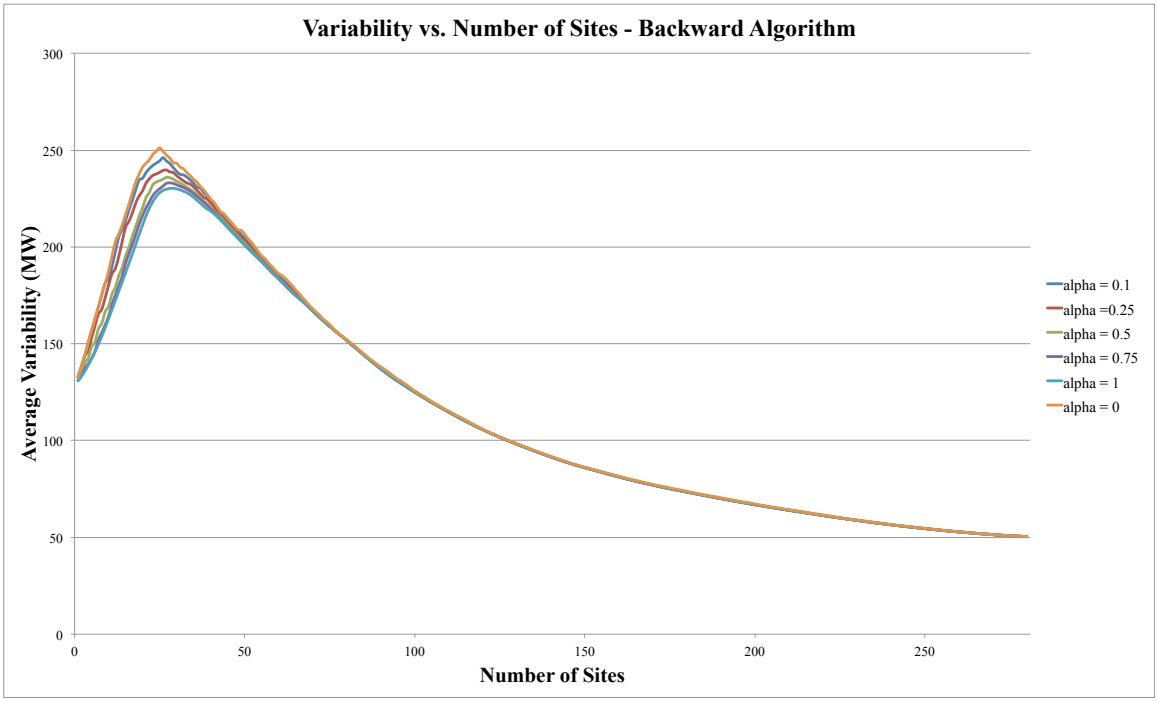

Figure 4.5: Average variability in the demand deficit for different numbers of wind sites using the backward algorithm. The different contours correspond to different values of α.

Figures 4.6 and 4.7 show how the average variability changes as the average demand deficit increases. From these plots we see that the two objectives are not directly competing as the number of sites is increased, although they are competing as α is increased.

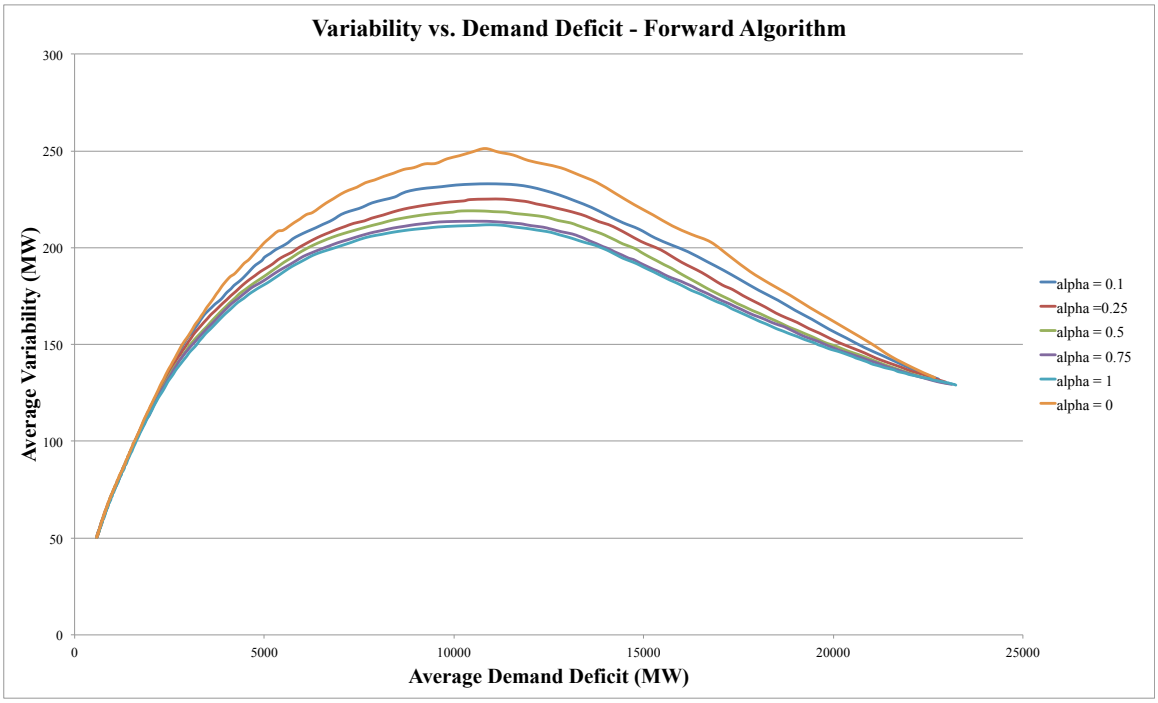

Figure 4.6: Shows how the variability in demand deficit changes as demand deficit changes using the forward algorithm. The different contours correspond to different values of α.

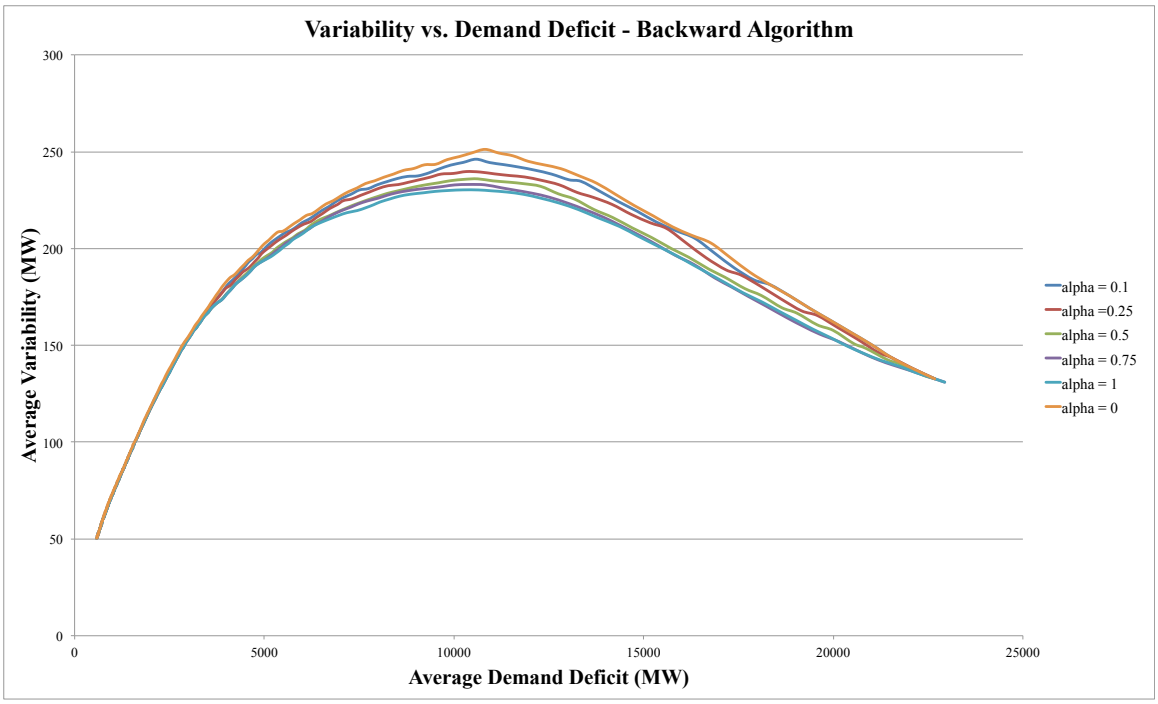

Figure 4.7: Shows how the variability in demand deficit changes as demand deficit changes using the backward algorithm. The different contours correspond to different values of α.

4.4.4 Discussion

As expected, the average demand deficit monotonically decreases in all cases as more sites are added. In contrast, the variability first increases then decreases. It is clear that the demand deficit could never increase by adding another site. We would expect the variability to initially increase, however, because we are considering more random variables. For example, suppose demand were constant. In this case the variability in demand deficit would be zero when we have zero wind sites. With one wind site, however, the variability would be greater than zero as long as the wind from that site was not also constant.

If wind sites were independent then the variance of the total power output from wind sites would be the sum of the variances from each site. Of course the wind sites are not in fact independent, but to a certain extent we still expect that adding more wind sites should increase the variance in the total available power from wind. We are interested in the average change in demand deficit, which is bounded by the maximum demand deficit

in any single period. Initially, when the demand deficit far exceeds the power output from wind, adding additional wind sites will increase the variability in the average. As more wind sites are added, however, the max demand deficit, and thus the max possible change in demand deficit, decreases. Eventually, adding more wind sites will decrease the demand deficit in every period enough that the variability must also decrease. Furthermore, if the wind power in a given period exceeds demand, the demand deficit for that period is zero, and adding another wind site will not change that but may decrease non-zero demand deficit in adjacent periods.

For the forward algorithm, the decrease in demand deficit occurs much more quickly with lower α values, but once about 230 out of the 281 sites have been added the average demand deficit is close to the same across all cases. For the backward algorithm, however, there is very little difference in demand deficit across the different α values. We observe a similar situation for the variability plots: the variability depends much more highly on α in the forward algorithm than in the backward algorithm. Although, for the backward algorithm, the peak variability is higher for the cases other than $\alpha = 0$, both the demand deficit and the variability decrease quicker (with fewer sights) than for the forward algorithm across non-zero α cases. Overall, it seems the backward algorithm outperforms the forward algorithm. Since the variability and demand deficit are very similar across all cases when a high number of sites is selected, at this point in the algorithm it doesn't matter much which sites are selected. It may be that the backward algorithm performs better because it starts with a high number of sites and removes sites, so by the time a small number of sites is reached, more iterations of the algorithm have been performed than in the forward algorithm, allowing more opportunities for sites to be compared.

Figures 4.6 and 4.7 show that, with respect to the number of sites, demand deficit and variability are not directly competing. Indeed, once enough sites have been added to get past the peak of variability, adding more sites will improve both objectives. However, for a given number of sites, the demand deficit increases and variability decreases as α is

increased, so the two objectives are in competition with respect to α.

Both demand deficit and variability are minimized when we include all 281 sites. However, this may not be possible due to budget constraints. With limited funds, the decision maker may choose to build fewer sites than the budget would allow to reduce variability. On the other hand, if there are enough funds to get past the peak of variability then the decision maker may want to build as many sites as possible to minimize both variability and demand deficit.

4.5 Exact Optimization

Next we solve a modification of the exact optimization model on a the subset of the data chosen via preliminary data analysis.

4.5.1 Model

Upon further literature review we determined that a more appropriate variability metric would be to minimize the maximum increase in demand deficit over some number of consecutive time periods. This metric better accounts for sudden decreases in wind power, which are more likely to cause power system failures.

In order to consider a disjoint subset of the full time horizon, let $\mathcal{J} = \{1, \ldots, J\}$ be the set of disjoint time intervals considered and $\mathcal{T}_j = \{T_j^{\text{start}}, \ldots, T_j^{\text{end}}\}$ be the set of time periods in the interval j. $\mathcal{T} = \cup_{j \in \mathcal{J}} \mathcal{T}_j$ is the complete set of time periods considered and $|\mathcal{T}| = T$. We allow for disjoint time intervals in order to model distinct parts of the year, for example multiple seasons, without considering the full time horizon.

The first objective is to minimize the average demand deficit at each time,

$$\text{minimize} \sum_{t \in \mathcal{T}} \frac{(d_t - \sum_{s \in \mathcal{S}} w_{s,t} x_s)_+}{T}, \tag{4.6}$$

where, again, d_t is the demand at time t, $w_{s,t}$ is the available wind from site s at time t, and x_s is a decision variable indicating whether or not that wind site is selected. $\mathcal{S}$ is the complete set of sites.

The variability objective is to minimize the maximum increase in demand deficit over any sequence of up to τ consecutive time periods within any time interval,

$$\text{minimize} \max_{j \in \mathcal{J}, i \in \{1,\ldots,\tau\}, t \in \{T_j^{\text{start}}+i,\ldots,T_j^{\text{end}}\}} (d_t - \sum_{s \in \mathcal{S}} w_{s,t} x_s)_+ - (d_{t-i} - \sum_{s \in \mathcal{S}} w_{s,t-i} x_s)_+, \quad (4.7)$$

where τ is the number of periods over which we consider the increase in demand deficit starting from each period within the season. Notice that for each $t' \in \{T_j^{\text{start}}, \ldots, T_j^{\text{end}}\}$, we consider the increase in demand deficit from t' to $t \in \{t'+1, \ldots, \min(t'+\tau, T_j^{\text{end}})\}$.

We again seek to minimize these two objectives by selecting N wind sites. Thus, we have the following constraints,

$$\sum_{s \in \mathcal{S}} x_s = N, \quad (4.8)$$

$$x_s \in \{0, 1\}. \quad (4.9)$$

If we minimize a weighted sum of the objectives this problem is equivalent to the following linear integer program,

$$\text{minimize } c_1 \sum_{t \in \mathcal{T}} \frac{\gamma_t}{T} + c_2 \delta, \tag{4.10}$$

$$\text{subject to} \sum_{s \in \mathcal{S}} x_s = N, \tag{4.11}$$

$$\gamma_t \geq d_t - \sum_{s \in \mathcal{S}} w_{s,t} x_s \; \forall \, t \in \mathcal{T}, \tag{4.12}$$

$$\delta \geq u_t - u_{t-i}, \; \forall \, j \in \mathcal{J}, i \in \{1, \ldots, \tau\}, t \in \{T_j^{\text{start}} + i, \ldots, T_j^{\text{end}}\}, \tag{4.13}$$

$$d_t - \sum_{s \in \mathcal{S}} w_{s,t} x_s \leq M z_t \; \forall \, t \in \mathcal{T}, \tag{4.14}$$

$$\sum_{s \in \mathcal{S}} w_{s,t} x_s - d_t \leq M(1 - z_t) \; \forall \, t \in \mathcal{T}, \tag{4.15}$$

$$u_t \leq d_t - \sum_{s \in \mathcal{S}} w_{s,t} x_s + M(1 - z_t) \; \forall \, t \in \mathcal{T}, \tag{4.16}$$

$$u_t \geq d_t - \sum_{s \in \mathcal{S}} w_{s,t} x_s \; \forall \, t \in \mathcal{T}, \tag{4.17}$$

$$u_t \leq M z_t \; \forall \, t \in \mathcal{T}, \tag{4.18}$$

$$u_t, \gamma_t \geq 0 \; \forall \, t \in \mathcal{T}, \tag{4.19}$$

$$x_s \in \{0, 1\} \; \forall \, s \in \mathcal{S}, \tag{4.20}$$

$$z_t \in \{0, 1\} \; \forall \, t \in \mathcal{T}, \tag{4.21}$$

where $M \in \mathbf{R}$ is a sufficiently large constant and $c_1, \; c_2$ are the selected weights for Objectives (4.6) and (4.7), respectively.

To see the equivalence, first notice that since $\gamma_t \geq d_t - \sum_{s \in \mathcal{S}} w_{s,t}$ in Constraints (4.12) and $\gamma_t \geq 0$ in Constraints (4.19), γ_t, when minimized, will be equal to whichever of the two right hand sides is larger. Thus, $\gamma_t = (d_t - \sum_{s \in \mathcal{S}} w_{s,t} x_s)_+$ at optimality.

Now consider the case when $d_t - \sum_{s \in \mathcal{S}} w_{s,t}$ is positive. In this case, Constraints (4.14) force z_t to be 1, which then forces $u_t = d_t - \sum_{s \in \mathcal{S}} w_{s,t} x_s$ due to Constraints (4.16) and (4.17). On the other hand, if $d_t - \sum_{s \in \mathcal{S}} w_{s,t}$ is negative, then Constraints (4.15) force z_t

to be 0, which then forces $u_t = 0$ due to Constraints (4.18) and (4.19). It follows that $u_t = (d_t - \sum_{s\in\mathcal{S}} w_{s,t}x_s)_+$, and when δ is minimized $\delta = u_t - u_{t-i}$ due to Constraints (4.13). Therefore, the two problems are equivalent.

Constraints (4.14) and (4.15) are redundant. To see this, observe that from Constraints (4.17) and (4.18) we get $d_t - \sum_{s\in\mathcal{S}} w_{s,t}x_s \leq u_t \leq Mz_t \; \forall \; t \in \mathcal{T}$, so Constraints (4.14) are redundant. Similarly, from Constraints (4.16) and (4.19) we have $0 \leq u_t \leq d_t - \sum_{s\in\mathcal{S}} w_{s,t}x_s + M(1-z_t) \; \forall \; t \in \mathcal{T}, \implies \sum_{s\in\mathcal{S}} w_{s,t}x_s - d_t \leq M(1-z_t)$, so Constraints (4.15) are redundant. Thus, the model can be reduced to,

$$\text{minimize} \;\; c_1 \sum_{t\in\mathcal{T}} \frac{\gamma_t}{T} + c_2\delta, \tag{4.22}$$

$$\text{subject to} \sum_{s\in\mathcal{S}} x_s = N, \tag{4.23}$$

$$\gamma_t \geq d_t - \sum_{s\in\mathcal{S}} w_{s,t}x_s \; \forall \; t \in \mathcal{T}, \tag{4.24}$$

$$\delta \geq u_t - u_{t-i}, \; \forall \; j \in \mathcal{J}, i \in \{1,\ldots,\tau\}, t \in \{T_j^{\text{start}} + i, \ldots, T_j^{\text{end}}\}, \tag{4.25}$$

$$u_t \leq d_t - \sum_{s\in\mathcal{S}} w_{s,t}x_s + M_t^1(1-z_t) \; \forall \; t \in \mathcal{T}, \tag{4.26}$$

$$u_t \geq d_t - \sum_{s\in\mathcal{S}} w_{s,t}x_s \; \forall \; t \in \mathcal{T}, \tag{4.27}$$

$$u_t \leq M_t^2 z_t \; \forall \; t \in \mathcal{T}, \tag{4.28}$$

$$u_t, \gamma_t \geq 0 \; \forall \; t \in \mathcal{T}, \tag{4.29}$$

$$x_s \in \{0,1\} \; \forall \; s \in \mathcal{S}, \tag{4.30}$$

$$z_t \in \{0,1\} \; \forall \; t \in \mathcal{T}. \tag{4.31}$$

In the above formulation, we change M to depend on the constraint because we want to choose M to be as small as possible for each constraint. We choose $M_t^1 = \sum_{s\in\mathcal{S}_{N,t}^{\max}} w_{s,t} - d_t$, where $\mathcal{S}_{N,t}^{\max}$ is the set of N sites that have the highest wind at time t. This M is suffi-

ciently large because when $z_t = 1$ this term doesn't matter, and when $z_t = 0$, $u_t = 0$ and $M_t^1 - d_t - \sum_{s \in \mathcal{S}} w_{s,t} x_s \geq 0$. We choose $M_t^2 = d_t$ because $\sum_{s \in \mathcal{S}} w_{s,t} x_s \geq 0$ for any x_s, so $u_t \leq d_t$ by Constraints (4.26).

4.5.2 Data Analysis

We perform an exploratory data analysis with the goal of selecting a subset of time periods to consider that capture the important characteristics of the full data set. We start by averaging the 10-minute wind data for each hour. Doing so will reduce the variability, which is undesirable, but we were unable to solve the model with enough 10-minute data to adequately represent the year according to our analysis. Although it would be preferable to use 10-minute data, using hourly data is still consistent with other studies that we have seen. As far as we are aware, we are the first to attempt to use 10-minute wind data in solving this problem.

We focus on the seasons with the highest and lowest wind in attempt to capture extreme fluctuations while maintaining an overall average that is approximately that of the full year. According to the wind patterns shown for the Upper Plains and Lower Plains, in which most of the SPP is contained, in Lott [134], the high wind season appears to peak somewhere around the end of March or beginning of April, and the low wind season appears to reach its lowest point around the end of August or beginning of September. A plot (Figure 4.8) of the daily wind averages for all sites in the SPP from our dataset shows a similar pattern, although there are large fluctuations between days and some outliers.

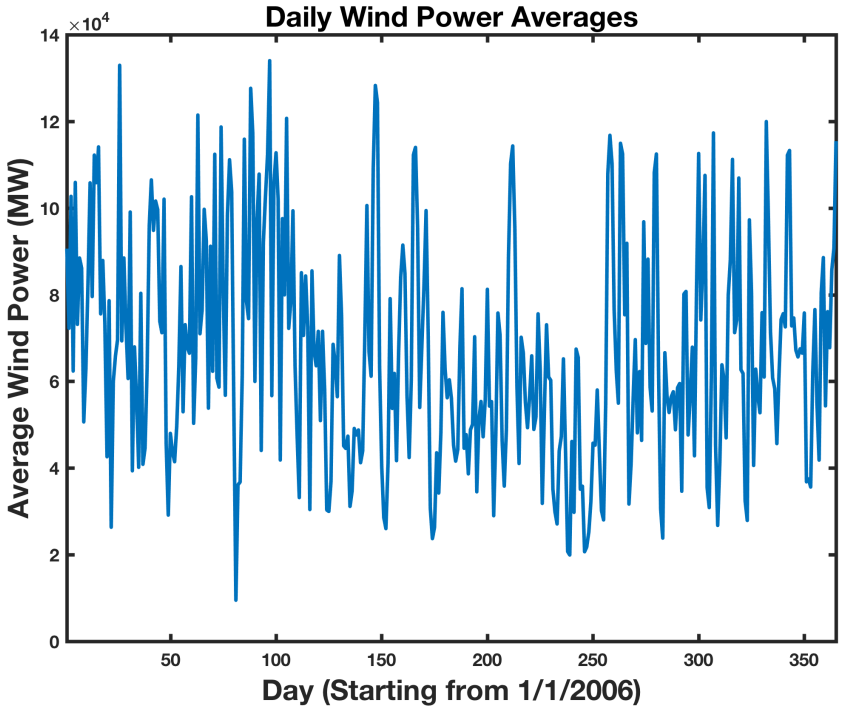

Figure 4.8: Shows the 2006 daily averages of total wind power from all sites in the SPP.

From these results we decide to use April 1 and September 1 as the peak of our high and low wind seasons, respectively. Starting from these days we plot the average demand deficit and maximum variability when 1 to 89 days in each season are considered. (We originally stopped at 89 days because we began our analysis by considering the four calendar seasons, of which the shortest in 2006 was 89 days. However, since the results sufficiently converge within that timeframe for the high and low seasons, we do not consider any further from the start two days for these seasons either).

The demand deficit and variability plots for 5 sets of 80 randomly chosen wind sites are shown in Figures 4.9 and 4.10, respectively. Although there is a slight increase in average demand deficit after this value, the average demand deficit mostly converges around 22 days/season for the high and low seasons. The maximum variability cannot decrease, and will likely continue to increase, as more days are considered, so these plots are not as useful as the demand deficit plots. However, we see that the first large plateau in the variability plot begins around 7 days/season. Since this is less than 22 days/season we

use 22 days/season for each of the two seasons (high and low, starting from April 1 and September 1, respectively) as our representative data subset.

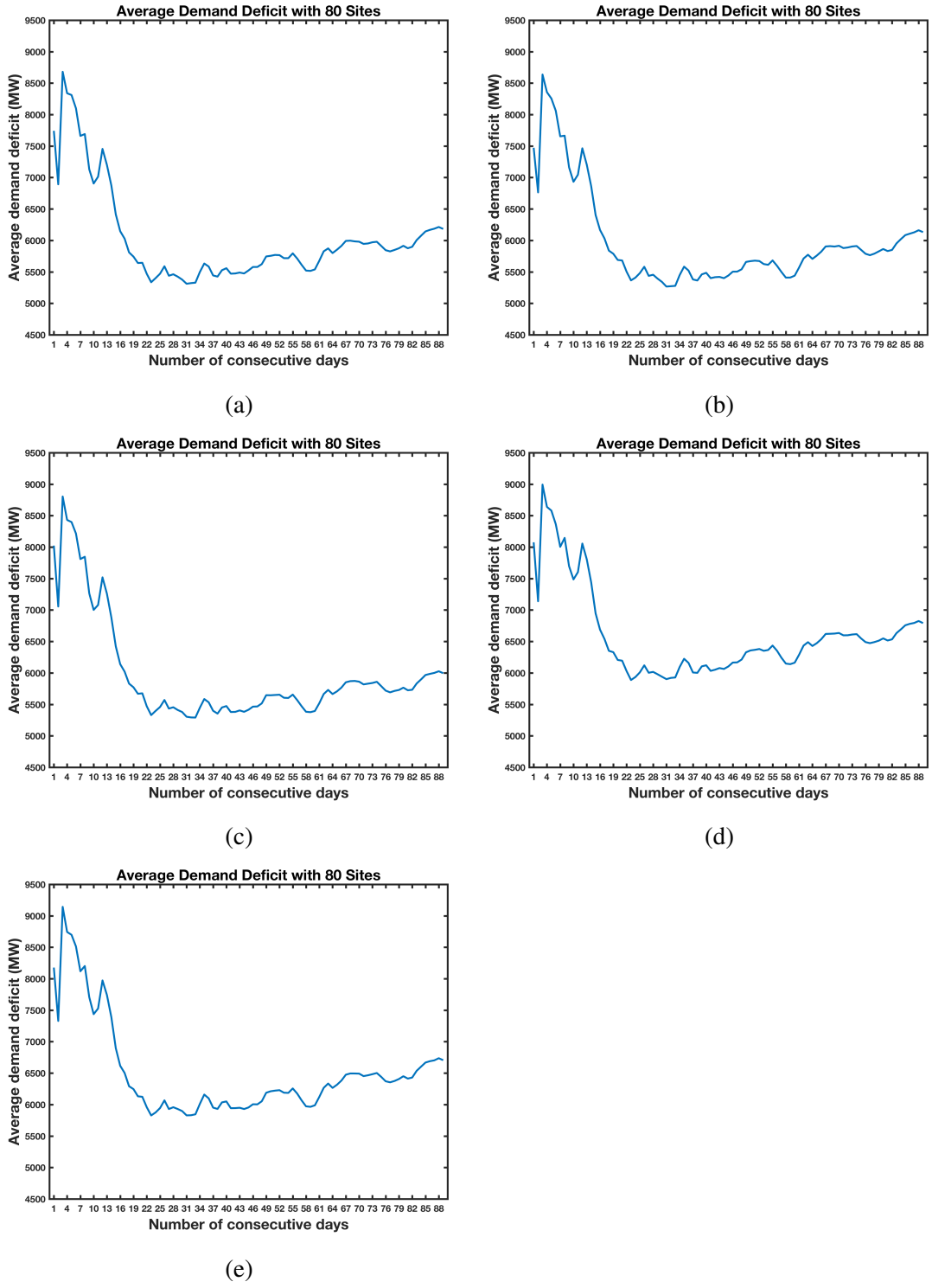

Figure 4.9: Demand deficit for 5 sets of 80 randomly chosen wind sites.

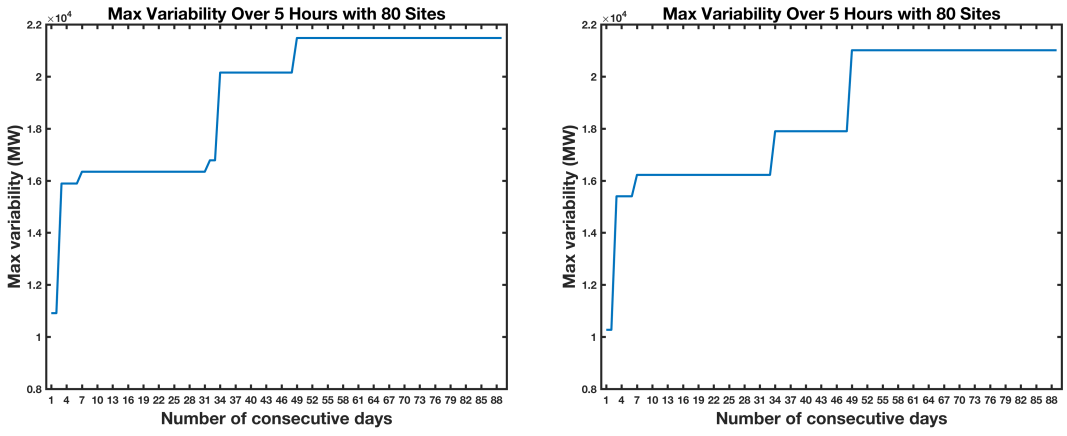

(a)

(b)

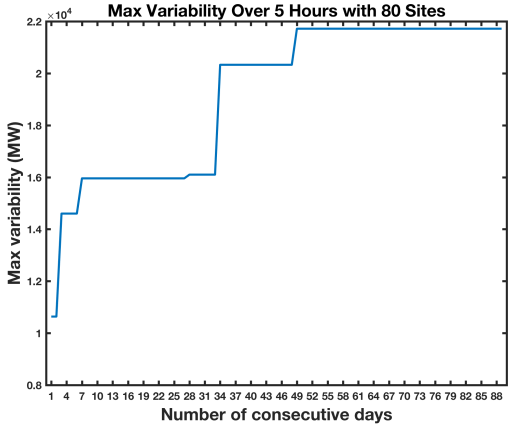

(c)

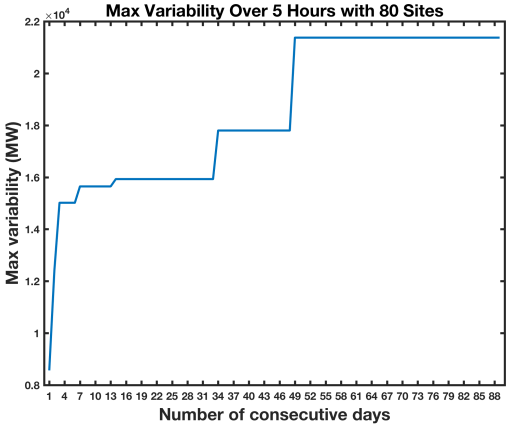

(d)

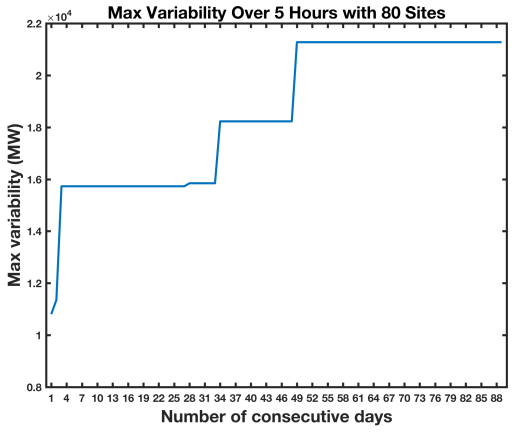

(e)

Figure 4.10: Variability for 5 sets of 80 randomly chosen wind sites.

We assume that the type of sudden wind fluctuations that would greatly impact the rest of the system would occur in 24 hours or less. Although only the 5 hour lookahead plots are

shown here we also create equivalent plots for when we look ahead 1 hour and 24 hours. The variability when we look ahead only one hour is between a fourth and a third of that when we look ahead 5 hours. When we look ahead 24 hours, however, the variability is only slightly higher than when we look ahead 5 hours. Thus, we determine it is sufficient to look ahead 5 hours in our model.

4.5.3 Results

We program the model using Python with Gurobi and solve using hourly data for 22 consecutive days in each of the two seasons, starting from April 1 and September 1, and selecting 80 sites. We select 80 sites because this value was past the variability peak shown in the results for the backward heuristic and also gave a low demand deficit using this heuristic.

We solve for a weighted sum of the two objectives and compare these results to the results if sites were selected based on the average wind only, since this approach is commonly used. We also compare to the heuristic results for both directions using the max variability objective with $\alpha = 0, 0.5,$ and 1. For the exact optimization, we consider the cases where $(c_1, c_2) = (1, 0.01), (0.01, 1), (1, 1),$ and $(1, 0.33)$. Recall that c_1 is the weight on the average demand deficit objective, and c_2 is the weight on the variability objective. The first case prioritizes the demand deficit objective. The second case prioritizes the variability objective. The third case weights the two objectives equally. In the fourth case, we give the variability objective a third of the weight of the demand deficit objective because, as seen in Figures 4.9 and 4.10, at 22/days per season the average demand deficit is about a third of the maximum variability, so this pair of weights makes the magnitude of the two parts more similar. Of these four tests, the test with weights (1, 0.33) took the longest and solved in about 38 minutes. The others solved much quicker.

We compare the results of these tests in two ways: first by evaluating the two objectives based on the hourly data for the two 22-day seasons alone, then by evaluating the two objectives based on the 10-minute data for the full year. Since the exact optimization model

is too large to solve for the full time horizon, the two 22-day season solutions are used to evaluate both metrics post-optimization. When solving the heuristics to compare, we use the hourly data for the two 22-day seasons in the first case and the 10-minute data for the full year in the second case. Results are also compared to the baseline, which is determined by selecting the 80 sites with the highest average wind across the time period considered (two 22-day seasons in the first case and the full year in the second case).

Table 4.1 shows the average demand deficit and maximum variability across the eleven cases when these metrics are evaluated only on the data used in the optimization model (hourly data for two seasons, 22 days/season). When the demand deficit objective is prioritized there is about a 2% decrease in demand deficit and about a 1% increase in variability from the baseline. In contrast, when the variability objective is prioritized there is a 353% increase in demand deficit for a decrease of 38% in variability. The percent changes from the baseline when the two objectives are balanced more equally are much closer to each other.

When $\alpha = 0$ the backward and forward algorithm give the same objective values. Although the demand deficit in these two cases is almost the same as the demand deficit for the exact optimization with weights $(c_1, c_2) = (1, 0.01)$, the variability objective is higher because there are multiple solutions with almost the same average demand deficit. For $\alpha = 0.5$ and $\alpha = 1$, the percent increase in demand deficit from the baseline is smaller for the backward algorithm than the forward algorithm, but the percent decrease in variability is as well.

Table 4.1: Average demand deficit and max variability in demand deficit calculated using hourly data for the two 22-day seasons. c_1 is the weight on the average demand deficit objective; c_2 is the weight on the variability objective. The baseline is the case when wind sites are selected based on average wind alone. Results for the forward and backward greedy algorithms with $\alpha = 0, 0.5$, and 1 are also presented.

Case	Average Demand Deficit (MW)	Dem. Def. Change from Baseline (%)	Max Variability (MW)	Max Var. Change from Baseline (%)
Average Wind (Baseline)	2,605	-	16,568	-
$c_1 = 1$, $c_2 = 0.01$	2,549	-2.12	16,788	1.33
$c_1 = 0.01$, $c_2 = 1$	11,795	352.87	10,310	-37.77
$c_1 = 1$, $c_2 = 1$	3,378	29.70	12,047	-27.29
$c_1 = 1$, $c_2 = 0.33$	3,031	16.38	12,701	-23.34
Forward, $\alpha = 0$	2,549	-2.13	17,008	2.66
Forward, $\alpha = 0.5$	5,233	100.93	14,316	-13.59
Forward, $\alpha = 1$	10,584	306.36	11,505	-30.56
Backward, $\alpha = 0$	2,549	-2.13	17,008	2.66
Backward, $\alpha = 0.5$	3,129	20.13	15,147	-8.58
Backward, $\alpha = 1$	4,251	63.21	14,491	-12.54

Table 4.2 shows the average demand deficit and maximum variability across the eleven cases when these metrics are evaluated based on the 10-minute data for all of 2006. In this case, the baseline sites are selected using data for the full year, as are sites selected by the heuristic. The sites selected by the optimization are selected using the partial data and evaluated after the optimization using the data for the full year. Interestingly, both the demand deficit and the variability decrease across the full time horizon when the demand deficit objective is prioritized. When the variability objective is prioritized, the percent changes in demand deficit and max variability are about the same as when only the two

season, 22 days/season data is considered. However, when the two objectives have more equal weights, we see a much smaller improvement in variability for what is about the same increase in demand deficit. The backward greedy algorithm with $\alpha = 0.5$ is able to achieve a larger decrease in variability for a smaller increase demand deficit than the cases with $(c_1, c_2) = (1, 1)$, and $(c_1, c_2) = (1, 0.33)$ in the exact optimization.

Table 4.2: Average demand deficit and max variability in demand deficit calculated using 10-minute data for the for the entire year (2006). c_1 is the weight on the average demand deficit objective; c_2 is the weight on the variability objective. The baseline is the case when wind sites are selected based on average wind alone. Results for the forward and backward greedy algorithms with $\alpha = 0, 0.5$, and 1 are also presented.

Case	Average Demand Deficit (MW)	Dem. Def. Change from Baseline (%)	Max Variability (MW)	Max Var. Change from Baseline (%)
Average Wind	2,978	-	27,106	-
$c_1 = 1$, $c_2 = 0.01$	2,953	-0.85	26,356	-2.77
$c_1 = 0.01$, $c_2 = 1$	13,648	358.25	17,048	-37.11
$c_1 = 1$, $c_2 = 1$	3,940	32.29	25,770	-4.93
$c_1 = 1$, $c_2 = 0.33$	3,482	16.91	26,533	-2.12
Forward, $\alpha = 0$	2,911	-2.25	26,615	-1.81
Forward, $\alpha = 0.5$	7,606	155.40	20,503	-24.36
Forward, $\alpha = 1$	12,664	325.24	15,089	-44.34
Backward, $\alpha = 0$	2,911	-2.25	26,615	-1.81
Backward, $\alpha = 0.5$	3,321	11.49	24,428	-9.88
Backward, $\alpha = 1$	3,837	28.84	23,785	-12.25

4.5.4 Discussion

Although when we compare the demand deficit and variability metrics across cases using the data subset used in the model the optimization gives good results, when we compare these same metrics calculated for the full-horizon 10-minute data, only a small decrease in variability is achieved for a proportionally much larger change in demand deficit compared to sites selected based on the average wind only. This finding is discouraging as it seems to indicate that our data subset did not in fact represent the full time horizon adequately. However, these results may be in part due to the characteristics of the data set used. Even when we consider the full time-horizon using the heuristics, the percent change in demand deficit is of greater magnitude than the corresponding percent change in variability in all cases (although with $\alpha = 0$ we slightly decrease both objectives from the baseline). From looking at the plots in Figure 4.9 as well as a few of the wind data plots we see that the wind is highly correlated between sites. Across the 5 combinations of 80 randomly selected wind sites, the shape of the demand deficit curve is almost identical and there are only small changes in the magnitude. This suggests that the potential improvements made by optimization may be limited for this region even if the full time horizon were considered. Perhaps the results found would be better for a larger region across which the correlation between wind farms was lower. In order to consider a larger region without increasing the number of potential sites (and thus, the size of the data), sites that are very close together could be grouped. If the total capacity for each of these groups is larger than the desired capacity per site then x_s could be changed to be integer between 0 to the maximum number of sites in each group. Alternatively, the optimization could be performed in two stages, first selecting larger areas in which to place wind farms and then optimizing wind site placement within each area that is selected.

We may be able to solve our problem for a larger number of days if fewer sites were selected. If, for example, we only chose 50 sites rather than 80, this would give on the order of 10^{55} rather than 10^{71} options for site combinations. We also could solve a few instances

of the problem for a larger number of days, though still not for the entire year. However, it should be noted that, while using a larger set of representative days may lead to better results for 2006, it might not necessarily improve the solution for other years. Dowds *et al.* [100] observe that wind patterns change every 4-5 years, so a longer time horizon would be ideal for capturing wind fluctuations. We use 2006 data only because it is the only year for which we have both demand and wind data. The heuristics could be run for a larger set of data, if it were available. In future work, we would like to further compare the performance of the heuristics to the exact optimization for different numbers of sites and both variability objective options, as well more completely explore the trade-offs between the two objectives by finding an approximate Pareto frontier.

4.6 Conclusion

In this research we consider three methods to select wind farm locations with the goal of minimizing demand deficit and variability of demand deficit. We first develop two heuristics to select wind sites via a forward or backward greedy algorithm using 10-minute wind data for a year. We then solve the exact optimization problem on a subset of the data. This data subset is taken from the high and low wind seasons in attempt to capture large increases in demand deficit while approximating the average demand deficit with a subset of days. We compare these results to the metrics calculated for a set of wind sites that is selected by maximizing the average wind output only, since this is a common approach that is used.

We find that the backward greedy algorithm outperforms the forward greedy algorithm in most cases. For the exact optimization, we are able to significantly decrease the variability for the subset of the data, but when this metric is calculated for the full time horizon using the 10-minute data, the decrease in variability is small. However, for a larger region with lower wind correlations we believe this method would be more effective in reducing variability.

Another potential option for further reducing variability in our study may be to include solar data as well. Although we specifically focus on wind farm siting, there is nothing in the model that would preclude solar from being included among the site options.

One advantage of our methods is that they make no assumptions on the distribution, which Dowds *et al.* [100] emphasized as a shortcoming of many of the studies reviewed. In our case study we use simulated wind sites from the Eastern Wind Data Set [131]. In general, any of these methods could be used in combination with multi-criteria, GIS-based, tools that would determine the initial candidate sites to input to our model.

CHAPTER 5
CONCLUSION

We study three problems from the domains of energy and national security. First, we consider a network interdiction problem in which an adversary seeks to maximize the damage of transporting illicit nuclear material to a selected target while the defender seeks to minimize this damage. The defender selects a set of defense options, subject to a limited budget, in attempt to interdict the adversary. We model the problem as a bi-level program and consider the robust variant where the adversary's probability of success is not exactly known. Although the example we consider is nuclear smuggling through the U.S. supply chain, the power grid is another type of network that is subject to vulnerabilities, so this research may also have indirect applications in the energy domain.

Second, we develop an optimization model to recommend development strategies for the power generation and transmission system in sub-Saharan Africa. We consider four variants on a metric for the fraction of demand met, representing four different policy options. Additionally, rather than assuming 100% of demand will be met by a fixed year we analyze the effect on cost of varying the electrification rate. We test our model on a case study of Rwanda and find that the cost to electrify the entire country uniformly is only slightly greater than the cost to meet the same fraction of demand aggregated across the country. Furthermore, the generation portfolio is very stable even across different electrification rates and the main changes observed are to the transmission system.

Finally, we seek to strategically locate wind farms in order to minimize the impact of wind variability on the rest of the power generation system. We develop two heuristics to select a complementary set of sites with both low demand deficit and variability in this deficit using a year of 10-minute wind data for the Southwest Power Pool. An analysis of the data shows that (after aggregating over each hour of the data) starting from two selected

days, one in the high wind season and one in the low wind season, the majority of the demand deficit and variability is captured within the first 22 days from these starting points. Using these results we solve the exact optimization model with wind data aggregated by the hour across 44 days of the year (22 in each season).

Appendices

APPENDIX A

ARC SHUT-OFF METHOD

As mentioned in Section 2.2.1, a pair of nodes can have multiple arcs between them representing each mitigation option. Let $\mathcal{M}$ be the set of mitigation options. When a specific mitigation option $m \in \mathcal{M}$ is selected, the option m impacts a subset of corridors and a subset of arcs within each corridor that is impacted. We model each possible mitigation option by adding an arc to each corridor for each transit option that it affects.

Recall that without any mitigation options a corridor may already have multiple arcs between the end nodes if multiple transit options exist between these locations. However, to demonstrate how mitigation options are handled consider three node pairs, (i, j), (k, ℓ), (m, n), with only one transit option between each pair. Suppose with the baseline defense in place (i.e. without any additional mitigation options), the probabilities that an adversary successfully traverses each of these corridors are 0.83, 0.75, and 0.85, respectively, as shown in Figure A.1.

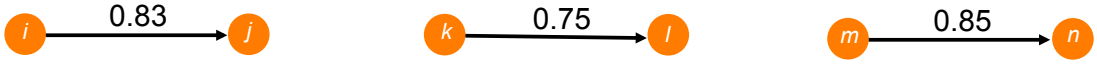

Figure A.1: Three example arcs of an interdiction network with no consideration for impact of mitigation options and a single transit option between each node pair.

Now suppose we have three mitigation options that affect each of the corridors as depicted in Table A.1. A "1" indicates the given mitigation option affects the given corridor. For example, Option 1 impacts corridors (i, j) and (k, ℓ) only. Table A.2 shows the probability, for affected arcs, that an adversary can successfully cross the given corridor when only the specified mitigation option is in place.

Table A.1: Mitigation options and impacted corridors.

Mitigation	(i, j)	(k, ℓ)	(m, n)
Option 1	1	1	0
Option 2	1	0	1
Option 3	1	1	1

Table A.2: Mitigation options and impacted probabilities.

Mitigation	(i, j)	(k, ℓ)	(m, n)
Option 1	0.66	0.68	-
Option 2	0.37	-	0.72
Option 3	0.55	0.45	0.27

We model these mitigation options by adding a set of new arcs to the network, where each arc represents the impact of a specific mitigation option on a corridor. To incorporate the impact probabilities of the three mitigation options given in Table A.2, seven new arcs are added, as depicted in Figure A.2.

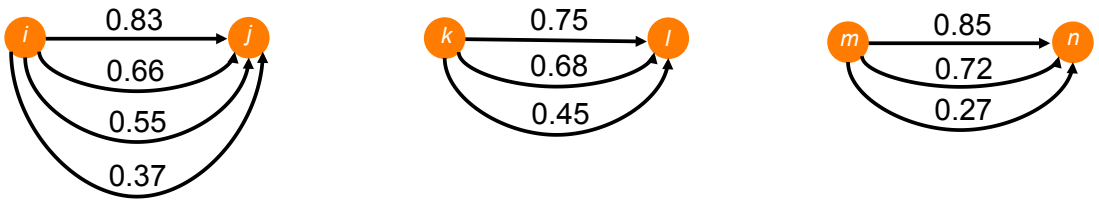

Figure A.2: Three example arcs of an interdiction network augmented to reflect the impact of the three mitigation options.

Observe that the probability that a smuggler successfully traverses one of the new arcs within a given corridor is lower than the success probability of traversing the original arc. Therefore, if all arcs are available, the smuggler will always choose to traverse the original arc, rather than one of the new, lower probability, arcs. When no mitigation option (other than the baseline) affecting a certain corridor is selected we leave all of the arc options for

the corridor available to the adversary, so the original arc will be taken. If, on the other hand, a mitigation option is implemented affecting a certain corridor we shut off all arcs with a higher probability than the probability with the given mitigation option in place. We restrict the adversary from taking these higher probability arcs through Constraints (2.1d) and (2.2d) in the deterministic and robust models, respectively. Because the adversary aims to maximize the probability of successfully smuggling the nuclear material, the adversary will always choose the arc with the greatest probability available with the selected mitigation options in place.

Figure A.3 shows the impacts of implementing three combinations of mitigation options from the options given in Tables A.1 and A.2. Figure A.3(a) depicts the impact of implementing Option 1 only, Figure A.3(b) depicts the impact of implementing Option 2 only, and Figure A.3(c) depicts the combined impact of implementing Options 1 and 2 together. Arcs that are shut off are marked with an "x."

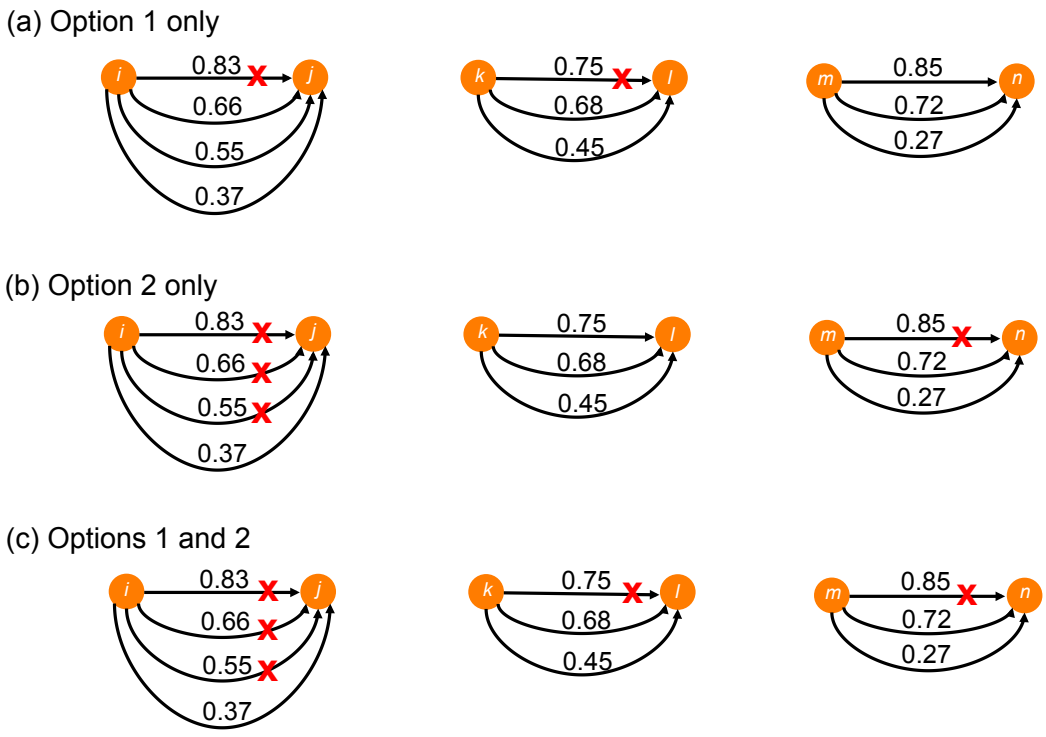

Figure A.3: Shows the impact of implementing three sets of mitigation options: (a) Option 1 only, (b) Option 2 only, and (c) Options 1 and 2 together.

Consider the impact of implementing Option 2 only, as depicted in Figure A.3(b). If Option 2 is selected, then four arcs are shut off, three in corridor (i, j) and one in corridor (m, n). If a smuggler chooses to traverse corridor (i, j) the probability of success is now 0.37, as all higher probability arcs (with values 0.55, 0.66, 0.83) have been disabled. Similarly, the new probability of successfully traversing corridor (m, n) is 0.72, as the original arc with success probability of 0.85 has been disabled. Corridor (k, ℓ) is not affected, so the adversary will choose the original arc, which has probability 0.75. This mitigation to arc shut-off relationship can be concisely represented using a binary table such as Table A.1, which is an example of γ in our model. This framework permits simultaneous consideration of implementing multiple mitigation options.

APPENDIX B

MITIGATION OPTIONS

The mitigation options considered in the case study are shown in Table B.1. We emphasize that these are artificial mitigation options for the sole purpose of testing the model and are not based on actual GNDA data.

Table B.1: Mitigation options considered in case study (continued from previous page). The mitigation options are grouped by transportation type affected. The cost given is the increase (in million USD) from baseline cost per each node at which the mitigation option is deployed. We emphasize that these are artificial mitigation options for the sole purpose of testing the model and are not based on actual GNDA data. Abbreviations used: Situational Awareness (SA); Customs Trade Partnership Against Terrorism (C-TPAT); roll-on and roll-off (RO/RO); electro-optical/infrared (EO/IR); United States Coast Guard (USCG); Customs Border Patrol (CBP).

Mitigation Option	**Cost per Node (M$)**	**Detect evasion prob.**			**Interdiction evasion prob.**	**SA evasion prob.**
		1 IND	**10 IND**	**RDD**		
Air						
1. Baseline	0	0.999	0.999	0.999	0.9	0.9
2. Fixed radiation portal monitors (imaging systems)	50	0.6	0.5	0.4	0.8	0.5
3. Vehicle-based radiation spectometers	20	0.8	0.8	0.7	0.9	0.9
4. Personnel worn radiation dosimeters	2	0.9	0.9	0.8	0.9	0.9
5. Unit Load Device security seals	0.1	0.999	0.999	0.999	0.9	0.8
6. Unit Load Device security sensors	2	0.999	0.999	0.999	0.85	0.5
7. Unit Load Device radiation counters	60	0.999	0.999	0.999	0.8	0.5
8. Air Waybill inspection targeted screening	3	0.999	0.999	0.999	0.5	0.9
9. Mandatory C-TPAT	15	0.999	0.999	0.999	0.9	0.3
Train						
10. Baseline	0	0.9	0.9	0.9	0.999	0.999

11. Fixed radiation portal monitors (imaging systems)	50	0.6	0.5	0.4	0.8	0.5
12. Personnel worn radiation dosimeters	2	0.8	0.8	0.7	0.9	0.95
13. Rail car based radiation counters	60	0.5	0.5	0.4	0.8	0.5
14. Mandatory sealing rail cars	0.1	0.9	0.9	0.9	0.85	0.5
15. Mandatory sealing intermodal maritime containers	0.1	0.9	0.9	0.9	0.85	0.5
16. Rail waybill inspection targeted screening	3	0.9	0.9	0.9	0.5	0.999
17. Mandatory C-TPAT	15	0.9	0.9	0.9	0.999	0.3
18. Joint interagency task force for trains	20	0.9	0.9	0.9	0.3	0.1

Maritime

19. Baseline	0	0.98	0.98	0.98	0.9	0.9
20. C-TPAT for Cruise Ships	15	0.98	0.98	0.98	0.9	0.3
21. Mandatory C-TPAT for maritime cargo	15	0.98	0.98	0.98	0.9	0.3
22. Security sensors for containerized cargo	2	0.98	0.98	0.98	0.85	0.5
23. Security sensors for RO/RO	2	0.98	0.98	0.98	0.85	0.5
24. Radiation counters in intermodal containers	30	0.5	0.5	0.4	0.8	0.5
25. Security seals for RO/RO	0.1	0.98	0.98	0.98	0.9	0.8
26. EO/IR Camera (applies to all maritime domain awareness)	50	0.98	0.98	0.98	0.9	0.3

27. ISF 10+2 Manifest/Stow plan reporting for RO/RO	1	0.98	0.98	0.98	0.9	0.3
28. Joint interagency task force for ships	20	0.98	0.98	0.98	0.9	0.1
29. Marine safety and security teams for cruise ships	0	0.98	0.98	0.98	0.01	0.5
30. Tactical law enforcement teams for maritime interdictions	0	0.98	0.98	0.98	0.01	0.5
31. USCG Patrols underway for cruise ship and cargo vessels	0	0.98	0.98	0.98	0.01	0.5
32. CBP Patrols underway for cruise ship and cargo vessels	0	0.98	0.98	0.98	0.01	0.5
33. Local law enforcement patrols for cruise ship and small vessels	0	0.98	0.98	0.98	0.01	0.5
34. Personal radiation detector for containerized cargo	2	0.9	0.9	0.8	0.9	0.9
35. Personal radiation detector for roll-on and roll-off	2	0.9	0.9	0.8	0.9	0.9
36. Personal radiation detector for cruise ship	2	0.9	0.9	0.8	0.9	0.9
37. Backpack for roll-on and roll-off	5	0.8	0.8	0.7	0.9	0.9
38. Backpack for cruise ship	5	0.8	0.8	0.7	0.9	0.9
39. Non-intrusive inspection of targeted containers for RO/RO	10	0.98	0.98	0.98	0.8	0.6
40. Fixed Radiation portal monitor scanning of cargo for RO/RO	50	0.6	0.5	0.4	0.8	0.5
41. Mobile Radiation portal monitor scanning of cargo for RO/RO	20	0.8	0.8	0.7	0.9	0.9
42. Non-intrusive inspection of targeted cargo for cruise ships	10	0.98	0.98	0.98	0.8	0.6

APPENDIX C

NODE INDICES

Tables C.1 to C.3 show the cities corresponding to each node index. Table C.1 shows the international origins considered. Table C.2 shows the non-target transshipment nodes, and Table C.3 shows the targets considered.

Table C.1: Origin cities (continued from previous page).

Index	**City, Country**	**Index**	**City, Country**
1	Abu Dhabi, United Arab Emirates	36	Lianyungung, China
2	Algerciras Bay, Spain	37	London, Great Britain
3	Ambarli, Turkey	38	Manila, Philippines
4	Amsterdam, Netherlands	39	Marsaxlokk, Malta
5	Antwerp, Belguim	40	Metro Vancouver, Canada
6	Balboa, Panama	41	Monterrey, Mexico
7	Bangkok, Thailand	42	Montreal, Canada
8	Beijing, China	43	Nagoya, Japan
9	Bremen/Bremerhaven, Germany	44	Ningbo-Zhoushan, China
10	Busan, South Korea	45	Osaka, Japan
11	Calgary, Canada	46	Paris, France
12	Colon, Panama	47	Port Kelang, Malaysia
13	Columbo, Sri Lanka	48	Port Said East, Egypt
14	Dalian, China	49	Qingdao, China
15	Doha, Qatar	50	Queretaro, Mexico
16	Dubai, United Arab Emirates	51	Regina, Canada
17	Durban, South Africa	52	Rotterdam, Netherlands

18	Felixstowe, U.K.	53	Salalah, Oman
19	Frankfurt, Germany	54	Santos, Brazil
20	Gioia Tauro, Italy	55	Shanghai, China
21	Guangzhou, China	56	Sharjah, United Arab Emirates
22	Hamburg, Germany	57	Shenzhen, China
23	Hanshin ports, Japan	58	Singapore, Singapore
24	Hermosillo, Mexico	59	Taipei, Taiwan
25	Ho Chi Minh, Vietnam	60	Tanjung Pelepas, Malaysia
26	Hong Kong, Hong Kong	61	Tanjung Perak, Surabaya,
27	Incheon, South Korea		Indonesia
28	Jawaharlal Nehru, India	62	Tanjung Priok, Jakarta,
29	Jebel Ali, Dubai, United Arab		Indonesia
	Emirates	63	Tianjin, China
30	Jeddah, Saudi Arabia	64	Tokyo, Japan
31	Kaohsiung, Taiwan	65	Toronto, Canada
32	Keihin ports, Japan	66	Valencia, Spain
33	Kuala Lumpur, Malaysia	67	Winnipeg, Canada
34	Laem Chabang, Thailand	68	Xiamen, China
35	Leipzig, Germany	69	Yingkou, China

Table C.2: Non-target transshipment nodes (continued from previous page).

Index	City, State	Index	City, State
70	Albany, NY	99	Lubbock, TX
71	Allentown/Bethlehem, PA	100	Marion, OH
72	Amarillo, TX	101	Mobile, AL
73	Anchorage, AK	102	Norfolk, VA

74	Ayer, MA	103	Orlando, FL
75	Billings, MT	104	Panama City, FL
76	Birmingham, AL	105	Pittsburgh, PA
77	Buffalo, NY	106	Port Everglades, FL
78	Charleston, SC	107	Port Hueneme, CA
79	Chester, PA	108	Reno, NV
80	Cincinnati, OH	109	Salt Lake City, UT
81	Decatur, IL	110	San Bernardino, CA
82	Des Moines, IA	111	San Juan, PR
83	Evansville, IN	112	Savannah, GA
84	Fargo, ND	113	Scranton, PA
85	Freeport, TX	114	Spokane, WA
86	Front Royal, VA	115	Springfield, MA
87	Ft. Lauderdale, FL	116	St. Louis, MO
88	Georgetown, KY	117	Stockton, CA
89	Greensboro, NC	118	Syracuse, NY
90	Gulfport, MS	119	Tacoma, WA
91	Harrisburg, PA	120	Tampa, FL
92	Honolulu, HI	121	Toledo, OH
93	Huntsville, AL	122	Waterville, ME
94	Iowa City, IA	123	West Palm Beach, FL
95	Jackson, MS	124	Wilmington, DE
96	Kingsport, TN	125	Wilmington, NC
97	Laredo, TX	126	Worcester, MA
98	Lewiston, ME		

Table C.3: Target nodes.

Index	City, State	Index	City, State	Index	City, State
127	Albuquerque, NM	140	Fresno, CA	153	Nashville, TN
128	Atlanta, GA	141	Houston, TX	154	New Orleans, LA
129	Baltimore, MD	142	Indianapolis, IN	155	New York, NY
130	Boston, MA	143	Jacksonville, FL	156	Oakland, CA
131	Charlotte, NC	144	Kansas City, MO	157	Omaha, NE
132	Chicago, IL	145	Las Vegas, NV	158	Philadelphia, PA
133	Cleveland, OH	146	Long Beach, CA	159	Phoenix, AZ
134	Columbus, OH	147	Los Angeles, CA	160	Portland, OR
135	Dallas, TX	148	Louisville, KY	161	San Antonio, TX
136	Denver, CO	149	Memphis, TN	162	San Diego, CA
137	Detroit, MI	150	Miami, FL	163	San Francisco, CA
138	El Paso, TX	151	Milwaukee, WI	164	Seattle, WA
139	Fort Worth, TX	152	Minneapolis, MN	165	Tucson, AZ

REFERENCES

[1] U.S. Department of Homeland Security, *The global nuclear detection architecture*, Last update October 4, 2015. Accessed at http://www.dhs.gov/global-nuclear-detection-architecture.

[2] The World Bank, *Access to electricity (% of population)*, Accessed April 18, 2017 at http://data.worldbank.org/indicator/EG.ELC.ACCS.ZS?name_desc=false&page=1&view=map, 2017.

[3] C. Mama, "Tackling Africa's power crisis," *African Business*, 2016.

[4] International Energy Agency, "Africa energy outlook: A focus on energy prospects in sub-Saharan Africa," Tech. Rep., 2014, Accessed April 3, 2017 at https://www.iea.org/publications/freepublications/publication/WEO2014_AfricaEnergyOutlook.pdf.

[5] Technical Assistance Facility for the SE4All Initiative, "Technical assistance facility for the Sustainable Energy for All initiative west and central Africa, Rwanda, part 1 - rural electrification strategy [draft report]," 2015.

[6] U.S. Energy Information Administration, *Frequently asked questions: What is U.S. electricity by energy source?* Accessed March 16, 2017 at https://www.eia.gov/tools/faqs/faq.php?id=427&t=3, 2016.

[7] N. O. Bakir, "A decision tree model for evaluating countermeasures to secure cargo at united states southwestern ports of entry," *Decision Analysis*, vol. 5, pp. 230–248, 4 2008.

[8] J. R. W. Merrick and L. A. McLay, "Is screening cargo containers for smuggled nuclear threats worthwhile?" *Decision Analysis*, vol. 7, no. 2, 2010.

[9] R. Gibbons, "Game theory for applied economists," in. Princeton University Press, 1992, ch. 2.1.B Stackelberg Model of Duopoly.

[10] D. Aksen, N. Aras, and N. Piyade, "A bilevel p-median model for the planning and protection of critical facilities," *Journal of Heuristics*, vol. 19, pp. 373–398, 2013.

[11] N. Haphuriwat, V. M. Bier, and H. H. Willis, "Deterring the smuggling of nuclear weapons in container freight through detection and retaliation," *Decision Analysis*, vol. 8, pp. 88–102, 2 2011.

[12] C. Wang and V. M. Bier, "Target-hardening decisions based on uncertain multiattribute terrorist utility," *Decision Analysis*, vol. 8, pp. 286–302, 4 2011.

[13] B. Zeng and Y. An, "Solving bilevel mixed integer program by reformulations and decomposition," Accessed July 3, 2016 at http://www.optimization-online.org/DB_FILE/2014/07/4455.pdf, 2014.

[14] R. K. Wood, "Deterministic network interdiction," *Mathematical and Computer Modelling*, vol. 17, pp. 1–18, 2 1993.

[15] G. Brown, M. Carlyle, J. Salmerón, and K. Wood, "Defending critical infrastructure," *Interfaces*, vol. 36, no. 6, pp. 530–544, 2006.

[16] A. Washburn and K. Wood, "Two-person zero-sum games for network interdiction," *Operations Research*, vol. 43, pp. 243–251, 2 1995.

[17] M. E. Paté-Cornell, "Games, risks, and analytics: Several illustrative cases involving national security and management situations," *Decision Analysis*, vol. 9, pp. 186–203, 2 2012.

[18] X. G. Shan and J. Zhuang, "Modeling credible retaliation threats in deterring the smuggling of nuclear weapons using partial inspection–a three-stage game," *Decision Analysis*, vol. 11, 1 2014.

[19] E. Israeli and R. K. Wood, "Shortest-path network interdiction," *Networks*, vol. 40, pp. 97–111, 2 2002.

[20] M. P. Scaparra and R. L. Church, "A bilevel mixed-integer program for critical infrastructure protection planning," *Computers and Operations Research*, vol. 35, pp. 1905–1923, 6 2008.

[21] D. J. Caswell, R. A. Howard, and M. E. Paté-Cornell, "Analysis of national strategies to counter a countrys nuclear weapons program," *Decision Analysis*, vol. 8, no. 1, pp. 30–45, 2011.

[22] K. Hausken and J. Zhuang, "Governments and terrorists' defense and attack in a T-period game," *Decision Analysis*, vol. 8, pp. 46–70, 1 2011.

[23] M. Hemmati, J. C. Smith, and M. T. Thai, "A cutting-plane algorithm for solving a weighted influence interdiction problem," *Computational Optimization and Applications*, vol. 57, pp. 71–104, 1 2014.

[24] J. S. Borrero, O. A. Prokopyev, and D. Sauré, "Sequential shortest path interdiction with incomplete information," *Decision Analysis*, vol. 13, no. 1, pp. 68–98, 2016.

[25] K. J. Cormican, D. P. Morton, and R. K. Wood, "Stochastic network interdiction," *Operations Research*, vol. 46, 2 1998.

[26] U. Janjarassuk and J. Linderoth, "Reformulation and sampling to solve a stochastic network interdiction problem," *Networks*, vol. 52, pp. 120–132, 3 2008.

[27] D. P. Michalopoulos, J. Barnes, and D. P.Morton, "Prioritized interdiction of nuclear smuggling via tabu search," *Optimization Letters*, vol. 9, pp. 1477–1494, 8 2015.

[28] F. Pan and D. P. Morton, "Minimizing a stochastic maximum-reliability path," *Networks*, vol. 52, pp. 111–119, 3 2008.

[29] N. B. Dimitrov, D. P. Michalopoulos, D. P. Morton, M. V. Nehme, F. Pan, E. Popova, E. A. Schneider, and G. G. Thoreson, "Network deployment of radiation detectors with physics-based detection probability calculations," *Annals of Operations Research*, vol. 187, pp. 207–228, 1 2011.

[30] S. Alizadeh, P. Marcotte, and G. Savard, "Two-stage stochastic bilevel programming over a transportation network," *Transportation Research Part B: Methodological*, vol. 58, pp. 92–105, 2013.

[31] D. Bertsimas and M. Sim, "The price of robustness," *Operations Research*, vol. 52, no. 1, pp. 35–53, 2004.

[32] D. P. Morton, F. Pan, and K. J. Saeger, "Models for nuclear smuggling interdiction," *IIE Transactions*, vol. 39, pp. 3–14, 2007.

[33] National Nuclear Security Administration, *Core program*, Accessed November 28, 2016 at https://nnsa.energy.gov/aboutus/ourprograms/nonproliferation/programoffices/internationalmaterialprotectionandcooperation/-4, 2016.

[34] T. B. Cochran and M. G. McKinzie, "Detecting nuclear smuggling," *Scientific American*, vol. 298, pp. 98–104, 2008.

[35] A. L. Soyster, "Convex programming with set-inclusive constraints and applications to inexact linear programming," *Operations Research*, vol. 21, pp. 1154–1157, 5 1973.

[36] U.S. Census Bureau, Population Division, *Annual estimates of the resident population for incorporated places of 50,000 or more, ranked by july 1, 2014 population: April 1, 2010 to july 1, 2014*, Accessed July 6, 2015 at http://factfinder.census.gov/faces/tableservices/jsf/pages/productview.xhtml?src=bkmk, May 2015.

[37] Airports Council International, *Year to date cargo traffic*, Last update June 22, 2015. Accessed at http://www.aci.aero/Data-Centre/Monthly-Traffic-Data/Freight-Summary/Year-to-date.

[38] Integrated Distribution Services, *Intermodal network map*, Accessed July 6, 2015 at http://www.idstransportation.com/intermodal-network-map, 2015.

[39] World Shipping Council, *Top 50 world container ports*, Accessed July 6, 2015 at http://www.worldshipping.org/about-the-industry/global-trade/top-50-world-container-ports, 2015.

[40] P. Burnson, "Top 30 u.s. ports: Finding the right balance," *Logistics Management*, 2012, Accessed July 6, 2015 at http://www.logisticsmgmt.com/images/site/LM1205_TopPorts.pdf.

[41] J. Alfaro and S. Miller, "Satisfying the rural residential demand in liberia with decentralized renewable energy schemes," *Renewable and Sustainable Energy Reviews*, vol. 30, pp. 903–911, 2014.

[42] A. C. Brent and D. E. Rogers, "Renewable rural electrification: Sustainability assessment of mini-hybrid off-grid technological systems in the African context," *Renewable Energy*, vol. 35, pp. 257–265, 1 2010.

[43] H. Camblonga, J. Sarr, A. Niang, O. Curea, J. Alzola, E. Sylla, and M. Santos, "Micro-grids project, part 1: Analysis of rural electrification with high content of renewable energy sources in Senegal," *Renewable Energy*, vol. 34, pp. 2141–2150, 10 2009.

[44] M. Zeyringer, S. Pachauri, E. Schmid, J. Schmidt, E. Worrell, and U. B. Morawetz, "Analyzing grid extension and stand-alone photovoltaic systems for the cost-effective electrification of Kenya," *Energy for Sustainable Development*, vol. 25, pp. 75–86, 2015.

[45] S. Ohiare, "Expanding electricity access to all in Nigeria: A spatial planning and cost analysis," *Energy, Sustainability and Society*, vol. 5, no. 8, pp. 1–18, 2015.

[46] A. Sanoh, L. Parshall, O. F. Sarr, S. Kum, and V. Modi, "Local and national electricity planning in Senegal: Scenarios and policies," *Energy for Sustainable Development*, vol. 16, no. 1, pp. 13–25, 2012.

[47] E. Ilskoga, B. Kjellstrom, M. Gullberg, M. Katyega, and W. Chambala, "Electrification co-operatives bring new light to rural Tanzania," *Energy Policy*, vol. 33, pp. 1299–1307, 10 2005.

[48] T. Levin and V. M. Thomas, "Least-cost network evaluation of centralized and decentralized contributions to global electrification," *Energy Policy*, vol. 41, pp. 286–302, 2012.

[49] ——, "A mixed-integer optimization model for electricity infrastructure development," *Energy Systems*, vol. 4, 1 2013.

[50] ——, "Utility-maximizing financial contracts for distributed rural electrification," *Energy*, vol. 69, 2014.

[51] H. Ahlborg and L. Hammar, "Drivers and barriers to rural electrification in Tanzania and Mozambique grid-extension, off-grid, and renewable energy technologies," *Renewable Energy*, pp. 117–124, 2014.

[52] A. Castellano, A. Kendall, M. Nikomarov, and T. Swemmer, "Brighter Africa: The growth potential of the sub-Saharan electricity sector," McKinsey & Company, Tech. Rep., 2015.

[53] A. Miketa and B. Merven, "Southern african power pool: Planning and prospects for renewable energy," International Renewable Energy Agency, Tech. Rep., 2013.

[54] M. Bazilian, P. Nussbaumer, H.-H. Rogner, A. Brew-Hammond, V. Foster, S. Pachauri, E. Williams, M. Howells, P. Niyongabo, L. Musaba, B. Ó. Gallachóir, M. Radka, and D. M. Kammen, "Energy access scenarios to 2030 for the power sector in sub-Saharan Africa," *Utilities Policy*, vol. 20, no. 1, pp. 1–16, 2012.

[55] African Development Bank Group, "Rwanda energy sector review and action plan," Tech. Rep., 2013, Accessed April 3, 2017 at https://www.afdb.org/fileadmin/uploads/afdb/Documents/Project-and-Operations/Rwanda_-_Energy_Sector_Review_and_Action_Plan.pdf.

[56] Technical Assistance Facility for the SE4All Initiative, "Technical assistance facility for the Sustainable Energy for All initiative west and central Africa, Rwanda, part 2 - tariff [draft report]," 2015.

[57] ——, "Technical assistance facility for the Sustainable Energy for All initiative west and central Africa, Rwanda, part 3 - action plan [draft report]," 2015.

[58] ——, "Technical assistance facility for the Sustainable Energy for All initiative west and central Africa, Rwanda, part 4 - rural electrification fund [draft report]," 2015.

[59] B. Safari, "A review of energy in Rwanda," *Renewable and Sustainable Energy Reviews*, vol. 14, pp. 524–529, 2010.

[60] A. Sanoh, A. S. Kocaman, S. Kocal, S. Sherpa, and V. Modi, "The economics of clean energy resource development and grid interconnection in Africa," *Renewable Energy*, vol. 62, 598–609 2014.

[61] G Heinrich, M Howells, L Basson, and J Petrie, "Electricity supply industry modelling for multiple objectives under demand growth uncertainty," *Energy*, vol. 32, no. 11, pp. 2210–2229, 2007.

[62] E. Panos, M. Densing, and K. Volkart, "Access to electricity in the World Energy Council's global energy scenarios: An outlook for developing regions until 2030," *Energy Strategy Reviews*, vol. 9, pp. 28–49, 2016.

[63] T. Ekholm, H. Ghoddusi, V. Krey, and K. Riahi, "The effect of financial constraints on energy-climate scenarios," *Energy Policy*, vol. 59, pp. 562–572, 2013.

[64] C. Arndt, R. Davies, S. Gabriel, K. Makrelov, B. Merven, F. Hartley, and J. Thurlow, "A sequential approach to integrated energy modeling in South Africa," *Applied Energy*, vol. 161, pp. 591–599, 2016.

[65] P. Balachandra and V. Chandru, "Supply demand matching in resource constrained electricity systems," *Energy Conversion and Management*, vol. 44, no. 3, pp. 411–437, 2003.

[66] T Mai, E Drury, K Eurek, N Bodington, A Lopez, and A Perry, "Resource planning model: An integrated resource planning and dispatch tool for regional electric systems," National Renewable Energy Laboratory, Tech. Rep., 2013.

[67] United States Department of Labor, Bureau of Labor Statistics, *CPI inflation calculator*, Accessed April 27, 2016 at http://www.bls.gov/data/inflation_calculator.htm.

[68] Map Library, *Rwanda - administrative boundaries*, Accessed April 11, 2017 at http://maplibrary.org/library/stacks/Africa/Rwanda/index.htm.

[69] M. Taylor, K. Daniel, A. Ilas, and E. Y. So, "Renewable power generation costs in 2014," International Renewable Energy Agency, Tech. Rep., 2015.

[70] National Institute of Statistics of Rwanda, *Fourth population and housing census, Rwanda, 2012: Main indicators report (final results)*, 2014.

[71] United Nations, Department of Economic and Social Affairs, Population Division, *World urbanization prospects: The 2014 revision, CD-ROM edition*, Accessed June 9, 2016 at https://esa.un.org/unpd/wup/CD-ROM/, 2014.

[72] Rwanda Utilities Regulatory Authority, Economic Regulation Unit, *Key statistics in electricity sub-sector as of march of the year 2016*, Accessed April 14, 2017 at http:

//www.rura.rw/fileadmin/docs/Energy_Statistics_report_as_of_march_2016.pdf, 2016.

[73] Republic of Rwanda Ministry of Infrastructure, *Sustainable Energy for All rapid assessment and gap analysis Rwanda*, Accessed April 14, 2017 at http://www.se4all.org/sites/default/files/Rwanda_RAGA_EN_Released.pdf, 2014.

[74] ——, *Rural electrification strategy*, Accessed April 13, 2017 at http://www.mininfra.gov.rw/fileadmin/user_upload/aircraft/Rural_Electrification_Strategy.pdf, 2016.

[75] Lahmeyer International and Electrogaz, "Analysis and projection of Rwanda's electricity demand," Tech. Rep., 2004, Accessed April 14, 2017 at http://www.devpartners.gov.rw/fileadmin/templates/docs/EDPRS/Key%20Analytical%20Studies/Sectoral%20Studies/Energy_Demand_Analysis_%26_Projection_2004.pdf.

[76] Latitude.to, *Administrative regions in Rwanda*, Accessed April 5, 2016 at http://latitude.to/map/rw/rwanda/regions.

[77] International Renewable Energy Agency, *IRENA/SANEDI workshop: Renewable energy planning for the Southern African Power Pool*, Electricity generation data file. Accessed November 22, 2016 at www.irena.org/SAPP, 2016.

[78] Eastern Africa Power Pool (EAPP), Ea Energy Analysis, and Energinet.dk, "EAPP regional power system master plan, volume II: Data report," Tech. Rep., 2014, Accessed April 11, 2017 at http://www.ea-energianalyse.dk/reports/1332/1332_eapp_master_plan_2014_volume_2_data_report.pdf.

[79] P. Y. Kerl, W. Zhang, J. B. Moreno-Cruz, A. Nenes, M. J. Realff, A. G. Russell, J. Sokol, and V. M. Thomas, "Supporting information: New approach for optimal electricity planning and dispatching with hourly time-scale air quality and health considerations," *Proceedings of the National Academy of Sciences*, vol. 112, no. 35, pp. 10 884–10 889, 2015.

[80] U.S. Energy Information Administration, *Frequently asked questions: How much carbon dioxide is produced when different fuels are burned?* Accessed April 12, 2017 at https://www.eia.gov/tools/faqs/faq.php?id=73&t=11, 2016.

[81] Food and Agriculture Organization of the United Nations, *Knowledge reference for national forest assessments - modeling for estimation and monitoring*, Accessed April 12, 2017 at http://www.fao.org/forestry/17111/en/, 2005.

[82] Environmental Assessment & Optimization Group, *Opgee: The oil production greenhouse gas emissions estimator*, Accessed April 12, 2017 at https://eao.stanford.edu/research-areas/opgee.

[83] National Renewable Energy Laboratory, *Hydropower results - life cycle assessment review*, Accessed April 12, 2017 at http://www.nrel.gov/analysis/sustain_lca_hydro.html, 2013.

[84] ——, *Crystalline silicon and thin film photovoltaic results - life cycle assessment harmonization*, Accessed April 12, 2017 at http://www.nrel.gov/analysis/sustain_lca_pv.html, 2013.

[85] P. Dwivedi, M. Khanna, R. Bailis, and A. Ghilardi, "Potential greenhouse gas benefits of transatlantic wood pellet trade," *Environmental Research Letters*, vol. 9, pp. 1–11, 2014.

[86] G. Guest, F. Cherubini, and A. H. Strømman, "Global warming potential of carbon dioxide emissions from biomass stored in the anthroposphere and used for bioenergy at end of life," *Journal of Industrial Ecology*, vol. 17, no. 1, pp. 20–30, 2013.

[87] National Energy Technology Laboratory, *Power generation technology comparison from a life cycle perspective*, Accessed April 12, 2017 at https://www.netl.doe.gov/File%20Library/Research/Energy%20Analysis/Life%20Cycle%20Analysis/Technology-Assessment-Compilation-Report.pdf, 2013.

[88] R. Drigo, A. Munyehirwe, V. Nzabanita, and A. Munyampundu, *Final report - update and upgrade of WISDOM Rwanda and woodfuels value chain analysis as a basis for the Rwanda supply master plan for fuelwood and charcoal*, Accessed April 12, 2017 at https://www.unpei.org/sites/default/files/e_library_documents/Rwanda-Economic-Analysis.pdf, 2013.

[89] Republic of Rwanda Ministry of Infrastructure, *Geothermal energy*, Accessed June 17, 2016 at http://www.mininfra.gov.rw/index.php?id=81, 2014.

[90] Rwanda Ministry of Infrastructure and Belgian Development Corporation, *Rwanda hydropower atlas*, Accessed June 22, 2016 at http://www.africa-eu-renewables.org/wp-content/uploads/2015/10/Rwanda-Hydropower-Atlas.png, 2007.

[91] National Renewable Energy Laboratory, *Openei - rwanda: Energy resources*, Accessed June 17, 2016 at http://en.openei.org/wiki/Rwanda.

[92] Energy Private Developers, *Peat to power*, Accessed November 22, 2016 at http://www.epd-rwanda.com/peat-to-power-kigali.html.

[93] J. W. Rosen, "Lake Kivu's great gas gamble," *MIT Technology Review*, vol. 118, no. 3, 2015.

[94] Rwanda Utilities Regulatory Authority, Economic Regulation Unit, *Key statistics in electricity sub-sector as of june of the year 2016*, Accessed June 30, 2017 at

http://www.rura.rw/fileadmin/docs/Energy_Statistics_report_as_of_June_2016.pdf, 2016.

[95] Rwanda Energy Group, *Current electricity generation status*, Accessed April 13, 2017 at http://www.reg.rw/index.php/our-business/generation/465-current-electricity-generation-status, 2017.

[96] Solar Energy Services for Professionals, *Free hchour (2004-2005) - helioclim3v5 time-series of hourly solar irradiance over the horizontal plane*, Accessed June 3, 2015 at http://www.soda-is.com/eng/services/service_invoke/gui.php?xml_descript=hc3v5_invoke_hour_demo.xml&Submit=HC3v5hour.

[97] H. Aburub and W. T. Jewell, "Revised analysis of the cost per kilowatt hour to store electricity," Accessed June 10, 2016 at http://webs.wichita.edu/depttools/depttoolsmemberfiles/T48/Revised_Analysis_of_the_Cost_per_Kilowatt_Hour_to_Store_Electricity.pdf.

[98] B. R. Phillips and R. S. Middleton, "Simwind: A geospatial infrastructure model for optimizing wind power generation and transmission," *Energy Policy*, vol. 43, pp. 291–302, 2012.

[99] U.S. Energy Information Administration, *International energy statistics: Total carbon dioxide emissions from the consumption of energy 2014*, Accessed April 14, 2017 at http://www.eia.gov/beta/international/data/browser/.

[100] J. Dowds, P. Hines, T. Ryan, W. Buchanan, E. Kirby, J. Apt, and P. Jaramillo, "A review of large-scale wind integration studies," *Renewable and Sustainable Energy Reviews*, vol. 49, pp. 768–794, 2015.

[101] C. L. Archer and M. Z. Jacobson, "Supplying baseload power and reducing transmission requirements by interconnecting wind farms," *Journal of Applied Meteorology and Climatology*, vol. 46, no. 11, pp. 1701–1717, 2007.

[102] B. Drake and K. Hubacek, "What to expect from a greater geographic dispersion of wind farms?-a risk portfolio approach," *Energy Policy*, vol. 35, no. 8, pp. 3999–4008, 2007.

[103] W. Katzenstein, E. Fertig, and J. Apt, "The variability of interconnected wind plants," *Energy Policy*, vol. 38, no. 8, pp. 4400–4410, 2010.

[104] W. Katzenstein and J. Apt, "The cost of wind power variability," *Energy Policy*, vol. 51, pp. 233–243, 2012.

[105] F. J. Santos-Alamillos, N. S. Thomaidis, S. Quesada-Ruiz, J. A. Ruiz-Arias, and D. Pozo-Vázquez, "Do current wind farms in Spain take maximum advantage of spa-

tiotemporal balancing of the wind resource?" *Renewable Energy*, vol. 96, pp. 574–582, 2016.

[106] H. Holttinen, P. Meibom, A. Orths, B. Lange, M. O'Malley, J. O. Tande, A. Estanqueiro, E. Gomez, L. Söder, G. Strbac, J. C. Smith, and F. van Hulle, "Impacts of large amounts of wind power on design and operation of power systems, results of IEA collaboration," *Wind Energy*, vol. 14, pp. 179–192, 2011.

[107] L. Gigović, D. Pamučar, D. Božanić, and S. Ljubojević, "Application of the GIS-DANP-MABAC multi-criteria model for selecting the location of wind farms: A case study of Vojvodina, Serbia," *Renewable Energy*, vol. 103, pp. 501–521, 2017.

[108] T. Höfer, Y. Sunak, H. Siddique, and R. Madlener, "Wind farm siting using a spatial analytic hierarchy process approach: A case study of the städteregion aachen," *Applied Energy*, vol. 163, pp. 222–243, 2016.

[109] D. Latinopoulos and K. Kechagia, "A GIS-based multi-criteria evaluation for wind farm site selection. A regional scale application in Greece," *Renewable Energy*, vol. 78, pp. 550–560, 2015.

[110] J. Jangid, A. K. Bera, M. Joseph, V. Singh, T. P. Singh, B. K. Pradhan, and S. Das, "Potential zones identification for harvesting wind energy resources in desert region of India - a multi criteria evaluation approach using remote sensing and GIS," *Renewable and Sustainable Energy Reviews*, vol. 65, pp. 1–10, 2016.

[111] A. Azadeh, S. F. Ghaderi, and M. R. Nasrollahi, "Location optimization of wind plants in iran by an integrated hierarchical data envelopment analysis," *Renewable Energy*, vol. 36, no. 5, pp. 1621–1631, 2011.

[112] G. M. Lewis, "Estimating the value of wind energy using electricity locational marginal price," *Energy Policy*, vol. 38, no. 7, pp. 3221–3231, 2010.

[113] D. C. Hoppock and D. Patiño-Echeverri, "Cost of wind energy: Comparing distant wind resources to local resources in the Midwestern United States," *Environmental Science and Technology*, vol. 44, no. 22, pp. 8758–8765, 2010.

[114] G. Mokryani and P. Siano, "Optimal wind turbines placement within a distribution market environment," *Applied Soft Computing*, vol. 13, no. 10, pp. 4038–4046, 2013.

[115] N. Jain, S. N. Singh, and S. C. Srivastava, "PSO based placement of multiple wind DGs and capacitors utilizing probabilistic load flow model," *Swarm and Evolutionary Computation*, vol. 19, pp. 15–24, 2014.

[116] F. Cassola, M. Burlando, M. Antonelli, and C. F. Ratto, "Optimization of the regional spatial distribution of wind power plants to minimize the variability of wind energy input into power supply systems," *Journal of Applied Meteorology and Climatology*, vol. 47, no. 12, pp. 3099–3116, 2008.

[117] F. Roques, C. Hiroux, and M. Saguan, "Optimal wind power deployment in Europe - a portfolio approach," *Energy Policy*, vol. 38, no. 7, pp. 3245–3256, 2010.

[118] N. S. Thomaidis, F. J. Santos-Alamillos, D. Pozo-Vázquez, and J. Usaola-García, "Optimal management of wind and solar energy resources," *Computers & Operations Research*, vol. 66, pp. 284–291, 2016.

[119] L. Reichenberg, A. Wojciechowski, F. Hedenus, and F. Johnsson, "Geographic aggregation of wind power - an optimization methodology for avoiding low outputs," *Wind Energy*, vol. 20, pp. 19–32, 2017.

[120] O. Grothe and J. Schnieders, "Spatial dependence in wind and optimal wind power allocation: A copula-based analysis," *Energy Policy*, vol. 39, no. 9, pp. 4742–4754, 2011.

[121] L. Reichenberg, F. Johnsson, and M. Odenberger, "Dampening variations in wind power generation - the effect of optimizing geographic location of generating sites," *Wind Energy*, vol. 17, pp. 1631–1643, 2014.

[122] S. H. Madaeni and R. Sioshansi, "The impacts of stochastic programming and demand response on wind integration," *Energy Systems*, vol. 4, no. 2, pp. 109–124, 2013.

[123] M. Z. Jacobson, M. A. Delucchi, M. A. Cameron, and B. A. Frew, "Low-cost solution to the grid reliability problem with 100% penetration of intermittent wind, water, and solar for all purposes," *Proceedings of the National Academy of Sciences*, vol. 112, no. 49, pp. 15 060–15 065, 2015.

[124] R. Sioshansi and P. Denholm, "Benefits of colocating concentrating solar power and wind," *IEEE Transactions on Sustainable Energy*, vol. 4, no. 4, pp. 877–885, 2013.

[125] A. A. Solomon, D. Faiman, and G. Meron, "Grid matching of large-scale wind energy conversion systems, alone and in tandem with large-scale photovoltaic systems: An Israeli case study," *Energy Policy*, vol. 38, no. 11, pp. 7070–7081, 2010.

[126] N. Gupta, "A review on the inclusion of wind generation in power system studies," *Renewable and Sustainable Energy Reviews*, vol. 59, pp. 530–543, 2016.

[127] S. Behera, S. Sahoo, and B. B. Pati, "A review on optimization algorithms and application to wind energy integration to grid," *Renewable and Sustainable Energy Reviews*, vol. 48, pp. 214–227, 2015.

[128] H. Long and Z. Zhang, "A two-echelon wind farm layout planning model," *IEEE Transactions on Sustainable Energy*, vol. 6, no. 3, pp. 863–871, 2015.

[129] P. Mittal, K. Kulkarni, and K. Mitra, "A novel hybrid optimization methodology to optimize the total number and placement of wind turbines," *Renewable Energy*, vol. 86, pp. 133–147, 2016.

[130] Federal Energy Regulatory Commission, *Electric power markets: Southwest power pool (spp)*, Accessed January 26, 2015 at http://www.ferc.gov/market-oversight/mkt-electric/spp.asp#geo, 2013.

[131] N. R. E. Laboratory, *Eastern wind dataset*, Accessed November 18, 2014 at http://www.nrel.gov/electricity/transmission/eastern_wind_methodology.html, 2013.

[132] EnerNex Corporation, *Eastern wind integration and transmission study*, Prepared for The National Renewable Energy Laboratory, Subcontract Report NREL/SR-5500-47078, 2011.

[133] Federal Energy Regulatory Commission, *Form no. 714 - annual electric balancing authority area and planning area report*, Accessed December 9, 2014 at http://www.ferc.gov/docs-filing/forms/form-714/data.asp, 2014.

[134] M. C. Lott, "Wind patterns - and electricity generation - vary across the seasons," *Scientific American*, 2015, Accessed May 16, 2017 at https://blogs.scientificamerican.com/plugged-in/wind-patterns-and-electricity-generation-vary-across-the-seasons/.